Impact of New Physics on $b \to (c,u) l \bar{\nu}_l$ Transitions

ATASI RAY

SCHOOL OF PHYSICS

UNIVERSITY OF HYDERABAD

DECEMBER, 2020

Impact of New Physics on $b \to (c, u)\ell\bar{\nu}_\ell$ transitions

To be submitted in the partial fulfilment for the degree of
DOCTOR OF PHILOSOPHY IN PHYSICS

BY

ATASI RAY

16PHPH01

Under the supervision of
Prof. RUKMANI MOHANTA

School of Physics

University of Hyderabad

Hyderabad 500 046, INDIA

December 2020

DECLARATION

I hereby declare that, this thesis titled **Impact of New Physics on $b \to (c, u)\ell\bar{\nu}_\ell$ transitions** submitted by me, under the guidance and supervision of **Prof. Rukmani Mohanta**, is a bonafide research work and is free from plagiarism. I also declare that it has not been submitted previously, in part or in full to this University or any other University or Institution, for the award of any degree or diploma. I hereby agree that my thesis can be deposited in Shodhganga/INFLIBNET.

A report on plagiarism statistics from the University Librarian is enclosed.

Atasi Ray

Hyderabad
Date: 29.12.2020

(Atasi Ray)
Reg. No.: 16PHPH01

CERTIFICATE

This is to certify that the thesis entitled **Impact of New Physics on $b \to (c, u)\ell\bar{\nu}_\ell$ transitions** submitted by Atasi Ray bearing registration number 16PHPH01 in partial fulfilment of the requirements for award of Doctor of Philosophy in the School of Physics is a bonafide work carried out by her under my supervision and guidance.

This thesis is free from plagiarism and has not been submitted previously in part or in full to this or any other University or Institution for award of any degree or diploma.

Further, the student has the following publications before the submission of the thesis for adjudication.

1) S. Sahoo, A. Ray, and R. Mohanta, Physical Review D **96**, 115017 (2017), (ISSN No: 2470-0029 (online)), Chapter 2.

2) A. Ray, S. Sahoo, and R. Mohanta, Physical Review D **99**, 015015 (2019), (ISSN No: 2470-0029 (online)), Chapter 3.

3) A. Ray, S. Sahoo, and R. Mohanta, Eur. Phys. J. C **79**, 670 (2019), (ISSN No: 1434-6052 (online)), Chapter 4.

Further, the student has passed the following courses towards fulfilment of coursework requirement for Ph.D:

Course Code	Name	Credits	Pass/Fail
PY601	Research Methodology	4	Pass
PY602	Advanced Quantum Mechanics	4	Pass
PY60305	Advanced Experimental Techniques	4	Pass
PY60309	Advanced Mathematical Methods	4	Pass

Rukmani Mohanta

Prof. Rukmani Mohanta
Thesis Supervisor
School of Physics
University of Hyderabad

Prof. Ashok Chatterjee
Dean
School of Physics
University of Hyderabad

DEAN
School of Physics
University of Hyderabad
HYDERABAD - 500 046.

Date: 29.12.2020

Dr. Rukmani Mohanta
Professor
School of Physics
UNIVERSITY OF HYDERABAD
Central University P.O.
Hyderabad-500 046.

Acknowledgements

I would like to express my deep gratitude to many people for their continuous support and encouragement throughout my research career.

First of all i would like to convey my heartly gratefulness to my supervisor, Prof. Rukmani Mohanta for taking me in her group and giving her invaluable guidance. It would be impossible to count all the ways that she has helped me in my career. I am humbled to have such a great mentor and teacher who motivated and supported me when ever i was down. She always inspired us with her punctuality, thoughtfulness, patience and hard work. Besides being the best supervisor one can ever have she was always there to guide us to be a better and responsible person. I am out of words to express my heartly gratitude to her.

I am grateful to my doctoral committee members Prof. E. Harikumar and Dr. Soma Sanyal for their constant motivation and suggestions which help to improve my work and presentation skill. I would like to thank Prof. Ashok Chatterjee, Dean , SOP and our former dean Prof. Rajender Singh and Prof.V. Sheshubai for academic support. My special thanks to our former Dean Prof. Bindu A. Bambah, for her encouragement and motivation to pursue research in high energy physics. I am fortunate enough to interact with Prof. Surajit Dhara, Prof. S. Srinath , Prof. James Raju, Prof. P.K. Suresh, Prof. Nirmalkumar Viswanathan during my course work which was a great motivation for my research. I would also like to thank Dr. Barilang Mawlang, Prof. P. Anantha Laxmi, Prof. Ashok Vudayagiri, and all the faculty members of SOP for their suggestions, support and encouragement.

I am deeply grateful to my collaborator Dr. Suchismita Sahoo for her cooperation, guidance and valuable discussions.

I would like to thank all the non-teaching staff of our School. My special thank goes to Mr. T. Abraham, Mr. Sudarshan and Mrs. Deepika, Mrs. Shailaja, Mr. Prashad for their help in the academic activities.

I acknowledge the Science and Engineering Research Board (SERB), Government of India for the financial support during my research period. In this context, I would like to convey my gratitude to my supervisor for giving me this opportunity.

I would pay my special regards to my teachers (from School to University) for their encouragement,support and for blessing me with their knowledge at different stages of my academic life.

I wish to show my appreciation to my labmates Dr. Shiva Rama Krishna Singirala, Rudra, Mitesh, Aishwarya, Dinesh for their cooperation and discussions. My special thanks to Mitesh and Rudra for their constant support, motivation and helping me out to develop my computer skill. I am also thankful to my friends Pooja, Dinesh, Vinod, Sharif, Praveen, Akshay and seniors Dr. Soram Robertson Singh, Dr. Anupama Swain, Mrs. Atiya Farheen and Miss. Nisha Goutam for their support and care. It is a humbling experience to acknowledge my friends Sthitaprajna, Sasmita, Trupti, Suprabhat, Subhranshu, Rekha, Anand, Tanmay, Itishreee, Lokeshwari, Somya and my junior Swayamsikha who encouraged and helped me at different phases of my life.

Finally my deep gratitude to my family for their unconditional love, understanding, giving me freedom to choose my own career and supporting me at every stage of my life. I am forever indebted to my parents Mr. Gouranga Charan Ray and Mrs. Kalpana Jena for giving me opportunities to make me who i am with their love , moral values and teaching to be a better human being. I am grateful to my elder brother Romio Ray for his motivation and for being there as a friend. I would also like to thank my relatives specially my brother-in-law Mr. Subrat Kumar Ray and cousin Dr. Jashashree Ray for motivating me to pursue Ph.D..

Abstract

In recent times the study of lepton non universality (LNU) and other observables associated with the angular distribution of semileptonic B decays has attracted lots of attention. The observed (2-4) σ deviation in the experimental values of various LNU parameters associated with several semileptonic B meson decays mediated by $b \to (c, s)$ quark level transitions as well as in the angular observable (P_5') in $\bar{B} \to \bar{K}^* \mu^+ \mu^-$ decay process from their corresponding standard model (SM) predictions boost the particle physics community to focus their attention to understand the reason behind these anomalies. Studying these anomalies helps to probe the nature of new physics (NP) beyond the SM. Similar to $b \to (c, s)$ quark level transition one can also study the possibility of observing various related associated with $b \to u$ quark level transition. Taking into account $b \to u\ell\bar{\nu}_\ell$ transition a deviation of $\sim 1\sigma$ has been observed in the experimental measurement of $R_\pi^\ell = \frac{\tau_{B^0}}{\tau_{B^-}} \frac{\mathrm{BR}(B^- \to \tau^- \bar{\nu}_\tau)}{\mathrm{BR}(B^0 \to \pi^+ \ell^- \bar{\nu}_\ell)}|_{Expt} = 0.699 \pm 0.156$ from its SM prediction $R_\pi^\ell|_{\mathrm{SM}} = 0.583 \pm 0.055$, where $\ell = e, \mu$. This may be considered as a possible hint for the presence of NP. In this aspect, we perform a model independent investigation of various semileptonic decay processes involving $b \to (u, c)\ell\bar{\nu}_\ell$ transitions.

We investigate the effect of NP in $B \to P(V)\ell\bar{\nu}_\ell$ decay process in a model independent way where $P = (K, \pi, \eta')$ and $V = (K^*, \rho)$ are pseudo-scalar and vector mesons respectively.We consider the most general effective Lagrangian containing additional Wilson coefficients to the SM and constrain the parameter space of these coefficients from the observed experimental values of branching ratios of $B_u^+ \to \ell^+ \nu_\ell$ and $B^- \to \pi^0 \mu^- \bar{\nu}_\mu$. We show the effect of these new parameters in the branching ratio, forward backward asymmetry and LNU parameters associated with $B \to (P, V)\ell\bar{\nu}_\ell$ decay processes.

Also we present a model independent investigation of semi-leptonic Λ_b decays. Here we consider the effect of additional vector, scalar and tensor type of new couplings in addition to the SM Lagrangian and constrain the parameter space of these new couplings from the experimentally measured values of branching ratios of $B_{c,u} \to \tau^+ \nu_\tau$ and $B \to \pi\tau\nu_\tau$ decay processes. Within the constrained parameter space of these new coefficients we calculate the branching ratio and other parameters sensitive towards NP such as the LNU parameters, forward-backward asymmetry, hadron and lepton polarization asymmetry and convexity parameter associated with $\Lambda_b \to (\Lambda_c, p)\ell\bar{\nu}_\ell$ decay processes which are mediated by $b \to (c, u)\ell\bar{\nu}_\ell$ transitions.

Again we look over the effect of NP on $B^* \to P\ell\bar{\nu}_\ell$ decay process where P is a pseudo-scalar meson. We take into account $B_{d,s}^* \to D, D_s, \pi, K$ decay process which are mediated by $b \to (c, s)$ quark level transitions. We obtain the constrained parameter space of the new couplings by χ^2 fitting of $\mathrm{BR}(B_u^+ \to \tau^+ \nu_\tau)$, $\mathrm{BR}(B \to \pi\tau\nu_\tau)$ and R_π^ℓ observables

for $b \to u\tau^-\bar{\nu}_\tau$ transitions. The parameter space of the new couplings associated with $b \to c\tau^-\bar{\nu}_\tau$ transition are constrained from the experimental values of branching ratio of $B_c^+ \to \tau^+\nu_\tau$, R_{D^*} and $R_{J/\psi}$. In the allowed parameter space of these new couplings we show the q^2 variation of differential branching ratio, LNU parameter, forward backward asymmetry and convexity parameter in presence of individual new couplings. We also calculate the numerical values of these parameters in presence of individual new couplings.

Contents

List of Figures

List of Tables

Dedicated to my Parents

Chapter 1

Introduction

This chapter contains a brief introduction of the Standard Model. Starting from the well established Lagrangian, it contains a general overview on the CKM matrix, the unitarity triangle and a brief discussion on the drawbacks of SM. The chapter also includes an introduction to Flavor Physics and CP violation signifying the study of B Physics and the required effective Hamiltonian formalism to study several B meson decays. We conclude this chapter with having a look on various anomalies associated with different B decays.

1.1 The Standard Model

The Standard Model (SM) of particle physics is the most successful theory which describes very well the fundamental particles and forces of nature. It is based on the gauge symmetry group $G_{\rm SM} \equiv SU(3)_C \times SU(2)_L \times U(1)_Y$ [1–3], where the group $SU(3)_C$ is associated with the strong interaction, whereas $SU(2)_L \times U(1)_Y$ deals with the electroweak interactions. The SM has three fermion generations consisting of five representations of $G_{\rm SM}$ which are expressed as follows,

- $Q^I_{Li}(3,2)_{+1/6}$: Left-handed quarks which are triplet under $SU(3)_C$, doublet under $SU(2)_L$ having hypercharge 1/6.
- $U^I_{Ri}(3,1)_{+2/3}$: Right-handed up type quarks which are triplet under $SU(3)_C$, singlet under $SU(2)_L$ with hypercharge 2/3.
- $D^I_{Ri}(3,1)_{-1/3}$: Right-handed down type quarks which are triplet under $SU(3)_C$, singlet under $SU(2)_L$ with hypercharge $-1/3$.

- $L^I_{Li}(1,2)_{-1/2}$: Left-handed leptons which are singlet under $SU(3)_C$ and doublet under $SU(2)_L$ having hypercharge $-1/2$.
- $E^I_{Ri}(1,1)_{-1}$: Right-handed charged leptons which are singlet under $SU(3)_C$, singlet under $SU(2)_L$ having hypercharge -1.
- In addition, there is a scalar representation $\phi(1,2)_{+1/2}$ which transforms as a singlet under $SU(3)_C$, doublet under $SU(2)_L$ with hypercharge $Y = 1/2$.

The SM gauge symmetry is spontaneously broken to $G_{\rm SM} \to SU(3)_C \times U(1)_{\rm EM}$ as a consequence of the scalar ϕ attaining a non-zero vacuum expectation value (VEV) [4–6],

$$\langle \phi \rangle = \begin{pmatrix} 0 \\ v/\sqrt{2} \end{pmatrix}.$$

Quarks and leptons which are considered as basic the building blocks of nature are arranged in three generations with increasing masses and identical quantum numbers. Quarks are spin-1/2 particles having fractional charges. The three quark generations comprising of six quarks, namely up (u), down (d), charm (c), strange (s), top (t) and bottom (b) are represented as

$$\begin{pmatrix} u \\ d \end{pmatrix}, \quad \begin{pmatrix} c \\ s \end{pmatrix}, \quad \begin{pmatrix} t \\ b \end{pmatrix}. \tag{1.1}$$

The up-type of quarks have charge 2/3 whereas the down-type of quarks have charge $-1/3$. All the quarks are assigned with three color quantum numbers namely red (R), blue (B) and green (G) and corresponding anti-colors ($\overline{R}, \overline{B}, \overline{G}$) in order to satisfy Pauli exclusion principle. Quarks can not exist freely in nature and always combined to form bound states in such a way that the resultant particle is colour neutral. There are also three generations of leptons which are given as,

$$\begin{pmatrix} e \\ \nu_e \end{pmatrix}, \quad \begin{pmatrix} \mu \\ \nu_\mu \end{pmatrix}, \quad \begin{pmatrix} \tau \\ \nu_\tau \end{pmatrix}. \tag{1.2}$$

The neutrinos are massless within the SM. All the lepton generations are assigned with lepton numbers L_i which must be conserved within the SM. Being spin 1/2 particles, quarks and leptons are categorized as fermions which obey Fermi-Dirac statistics and hence, Pauli-exclusion principle. For all the particles, corresponding anti-particles exist with same quantum numbers as the particle and opposite charge and internal quantum numbers. In general, all the subatomic particles are categorized to leptons and hadrons (quark bound states). Hadrons are further classified into baryons which are bound states of three quarks and mesons which are comprised of a quark and an anti-quark.

All these subatomic particles interact through three fundamental forces, which are strong, electromagnetic and weak interaction mediated by vector gauge bosons. Gravitational force which is another fundamental interaction is not considered in subatomic level as it is effective only at larger massive scale. Gluons (g) and photon (γ) are the mediators of strong and electromagnetic interactions while weak interaction takes place by the exchange of $W^{\pm}$ and Z^0 bosons. The particle content of SM got a complete picture with the discovery of the scalar Higgs boson on 4^{th} July 2012 by the LHC collaboration, which is responsible for the generation of all particle masses through Higgs mechanism [4–6].

The SM effective Lagrangian which is gauge invariant, and is defined as follows containing three terms [7],

$$\mathcal{L}_{\text{SM}} = \mathcal{L}_{\text{kinetic}} + \mathcal{L}_{\text{Higgs}} + \mathcal{L}_{\text{Yukawa}}. \tag{1.3}$$

1. **Kinetic term:**

   For gauge invariance the partial derivative in the kinetic term is replaced with the covariant derivative,

   $$D^{\mu} = \partial^{\mu} + ig_s G_a^{\mu} L_a + igW_b^{\mu} T_b + ig' B^{\mu} Y. \tag{1.4}$$

   Here G_a^{μ} are the eight gluon fields, W_b^{μ} and B^{μ} represent the three weak gauge bosons and the single hyper-charge boson respectively. L_a refer to $SU(3)$ generators which are expressed in terms 3×3 Gell-Mann matrices as $\frac{1}{2}\lambda_a$ for triplets and 0 for singlets, T_b are the $SU(2)$ generators which are 2×2 Pauli matrices ($\frac{1}{2}\tau_b$) for doublets and 0 for singlets and Y is the $U(1)_Y$ charge. g, g' and g_s are the gauge coupling parameters for $SU(2)_L$, $U(1)_Y$ and $SU(3)_C$, respectively. Now we can write the kinetic part of the Lagrangian for left-handed quarks as,

   $$\mathcal{L}_{\text{kinetic}}(Q_L) = i\bar{Q}_{Li}^I \gamma_{\mu} \Big(\partial^{\mu} + \frac{i}{2} g_s G_a^{\mu} \lambda_a + \frac{i}{2} g W_b^{\mu} \tau_b + \frac{i}{6} g' B^{\mu} \Big) Q_{Li}^I \, . \tag{1.5}$$

   For left handed leptons,

   $$\mathcal{L}_{\text{kinetic}}(L_L) = i\bar{L}_{Li}^I \gamma_{\mu} \Big(\partial^{\mu} + \frac{i}{2} g W_b^{\mu} \tau_b - \frac{i}{2} g' B^{\mu} \Big) L_{Li}^I \, . \tag{1.6}$$

2. **Higgs term:** The scalar self interaction is described by the Higgs potential involving the Higgs field given as,

   $$\mathcal{L}_{\text{Higgs}} = \mu^2 \phi^{\dagger} \phi - \lambda (\phi^{\dagger} \phi)^2 \tag{1.7}$$

3. **Yukawa term:** Yukawa interaction refers to the interaction between a scalar field and the Dirac bilinear fields. The Yukawa part of the SM Lagrangian is further divided into leptonic and quark parts. The lepton Yukawa Interaction is,

$$-\mathcal{L}^{\text{lepton}}_{\text{Yukawa}} = Y^{e}_{ij}\bar{L}^{I}_{Li}\phi E^{I}_{Rj} + \text{h.c.}.$$

The three physical parameters involved in this term are chosen to be the three charged lepton masses. The quark masses arise in the quark Yukawa interaction given by,

$$-\mathcal{L}^{\text{quark}}_{\text{Yukawa}} = Y^{d}_{ij}\bar{Q}^{I}_{Li}\phi D^{I}_{Rj} + Y^{u}_{ij}\bar{Q}^{I}_{Li}\tilde{\phi}U^{I}_{Rj} + \text{h.c.},$$

where $\tilde{\phi} = i\tau\phi^{*}$.

1.1.1 The CKM matrix and Unitarity triangle

Flavour physics basically describes the interaction between various flavours. The left handed and right handed quarks are arranged in $SU(2)_L$ doublets and $SU(2)_R$ singlets respectively in the SM as,

$$\begin{aligned} Q_j &= \begin{pmatrix} u_L \\ d_L \end{pmatrix}, \quad \begin{pmatrix} c_L \\ s_L \end{pmatrix}, \quad \begin{pmatrix} t_L \\ b_L \end{pmatrix} \\ U_j &= u_R, c_R, t_R \qquad\qquad D_j = d_R, s_R, b_R. \end{aligned} \tag{1.8}$$

The down-type quark flavor and mass eigenstates are related by the equation,

$$\begin{pmatrix} d' \\ s' \\ b' \end{pmatrix} = V_{CKM} \begin{pmatrix} d \\ s \\ b \end{pmatrix}. \tag{1.9}$$

where V_{CKM} is the well known CKM matrix [8, 9] represented as,

$$V_{CKM} = \begin{pmatrix} V_{ud} & V_{us} & V_{ub} \\ V_{cd} & V_{cs} & V_{cb} \\ V_{td} & V_{ts} & V_{tb} \end{pmatrix}. \tag{1.10}$$

The CKM matrix can be represented in standard parametrisation [10] as,

$$V_{CKM} = \begin{pmatrix} c_{12}c_{13} & s_{12}c_{13} & s_{13}e^{-i\delta} \\ -s_{12}c_{23} - c_{12}s_{23}s_{13}e^{i\delta} & c_{12}c_{23} - s_{12}s_{23}s_{13}e^{i\delta} & s_{23}c_{13} \\ s_{12}s_{23} - c_{12}c_{23}s_{13}e^{i\delta} & -c_{12}s_{23} - s_{12}c_{23}s_{13}e^{i\delta} & c_{23}c_{13} \end{pmatrix}. \tag{1.11}$$

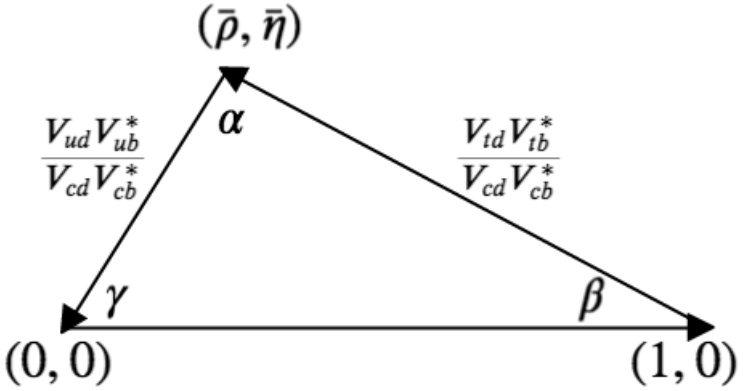

FIGURE 1.1: Unitarity triangle

Here c_{ij} correspond to $\cos\theta_{ij}$ and s_{ij} are $\sin\theta_{ij}$ with θ_{ij} as the mixing parameters while δ represents the Kobayashi-Maskwa phase.

The CKM matrix can be represented in the Wolfenstin parametrization ($\mathcal{O}(\lambda^3)$) [11] as,

$$V_{CKM} = \begin{pmatrix} 1-\frac{\lambda^2}{2} & \lambda & A\lambda^3(\rho - i\eta) \\ -\lambda & 1-\frac{\lambda^2}{2} & A\lambda^2 \\ A\lambda^3(1-\rho-i\eta) & -A\lambda^2 & 1 \end{pmatrix},$$

where λ, A, ρ and η are the mixing parameters. λ is of the order of 0.22 is the expansion parameter and η stands for the CP violating phase.

Being a 3×3 unitary matrix, the CKM matrix gives nine relations among the matrix elements. One of the main orthogonal relation between the CKM matrix elements is,

$$V_{ud}V_{ub}^* + V_{cd}V_{cb}^* + V_{td}V_{tb}^* = 0. \tag{1.12}$$

This can be represented by a triangle in the complex plane, known as the unitarity triangle, which is shown in Fig. 1.1.

One of the most interesting fact about this triangle is the area of this unitarity triangle is related to the CP violating observable as, $A_\triangle = \frac{J_{CP}}{2}$, where J_{CP} is known as the Jarlskog invariant [12], which can be obtained from the following relation,

$$\mathcal{I}m(V_{ij}V_{kl}V_{il}^*V_{kj}^*) = J_{CP}\sum_{m,n=1}^{3}\epsilon_{ikm}\epsilon_{jln}.$$

In explicit form $J_{CP} = c_{12}c_{23}c_{13}^2 s_{12}s_{23}s_{13}\sin\delta \approx \lambda^6 A^2\eta$.

1.1.2 CP violation

- Under Charge conjugation a particle transforms into its antiparticle.

$$C : \psi \rightarrow i(\bar{\psi}\gamma^0\gamma^2)^T. \tag{1.13}$$

- Under Parity, a left handed fermion field transforms in to a right handed one.

$$P : \psi(r,t) \rightarrow \gamma^0\psi(-r,t). \tag{1.14}$$

Weak interaction violates both C and P as it treats left and right handed quarks differently. Under combined CP, a left handed particle transforms to its antiparticle, which is right-handed. The neutral current interactions are invariant under CP which are mediated by gluons, photon and Z^0 bosons.

In charged current interactions,

$$\begin{aligned}\mathcal{L}_{c.c.} &= \frac{g}{\sqrt{2}}V_{ik}\bar{u}_{Li}\gamma_\mu W^{\mu+}d_{Lk} + h.c. \\ &\xrightarrow{CP} \frac{g}{\sqrt{2}}V_{ik}\bar{d}_{Lk}\gamma_\mu W^{\mu+}u_{Li} + \frac{g}{\sqrt{2}}V^*_{ik}\bar{u}_{Li}\gamma_\mu W^{\mu+}d_{Lk} \\ &= \frac{g}{\sqrt{2}}V^*_{ik}\bar{u}_{Li}\gamma_\mu W^{\mu+}d_{Lk} + \text{h.c.}.\end{aligned} \tag{1.15}$$

The CP symmetry is violated due to the presence of non vanishing complex phase in the CKM matrix. Physical measure of CP violation is given by the Jarlskog invariant whose experimental value is $J_{CP} \simeq 3 \times 10^{-5}$.

1.1.3 Drawbacks of the SM

Although SM is considered as the fundamental theory of particle physics, it is still unable to shed light on some sectors in the understanding of our universe which are still remained as mysteries for science so far. The baryon asymmetry of the universe, origin of the neutrino mass (neutrino oscillation), dark matter and dark energy content of the universe, hierarchy problem, etc., are beyond the scope of the SM.

1. Neutrino oscillation is the phenomenon where a neutrino of a specific family change into another neutrino of different family. SM is unable to describe this phenomenon so far.

2. In a fundamental theory, Higgs mass ($m_h = 125$ GeV) and the gravitational scale ($M_{\text{Planck}} \sim \sqrt{G} \sim 10^{19}$ GeV), can be expected to be of the same order. But

$m_h/M_{\text{Planck}} \sim 10^{-17}$. So there arises a question that why there is a huge difference between these two scales, which is generally known as the hierarchy problem.

3. Relating the energy density of free space time (Λ) with the Planck scale, we can see $\left(\frac{\Lambda}{M_{\text{Planck}}}\right)^4 \sim 10^{-120} \ll 1$. The question of why this ratio is such a small number is well known as the cosmological constant problem which is still unsolved in fundamental physics.

4. Considering the constituent of our universe, 4% of our universe consists of the visible matter, 22% of it is dark matter and rest 74% consists of dark energy. But there is no suitable candidate of dark matter within the SM, which is the major part of our Universe.

1.2 Introduction to B Physics

B Physics or beauty physics deals with the study of various B meson decay processes. According to Big bang Theory, which describes the creation of our Universe, same amount of matter and antimatter were created during the formation of our universe. If the universe contains equal amount of matter and antimatter then they should annihilate and produce energy resulting an energy dominated Universe. But the current scenario of our Universe is matter dominant. According to Andrei Sakharov [13], CP violation (CPV) is one of the ingredients to describe the matter antimatter asymmetry of our Universe. In 1964 CP violation was first observed in neutral K meson system [14] but the order of CPV is very less in K sector ($\mathcal{O}(10^{-3})$). Whereas the order of CPV is $\mathcal{O}(1)$ in B meson system, which makes the study of B physics quite interesting. Hence the study of B sector is more relevant to understand the matter dominance of our Universe. Additionally, due to comparative high mass of B meson, it has quite large number of decay channels to study.

1.2.1 Effective Hamiltonian

The SM effective Hamiltonian for $|\Delta B| = 1$ processes can be written as,

$$\mathcal{H}_{eff} = \frac{G_F}{\sqrt{2}} \sum_i V^i_{CKM} C_i(\mu) Q_i, \tag{1.16}$$

where C_i's are the Wilson coefficients, G_F is the Fermi constant and Q_i are the local four-fermion operators.

The six classes of operators are represented as,

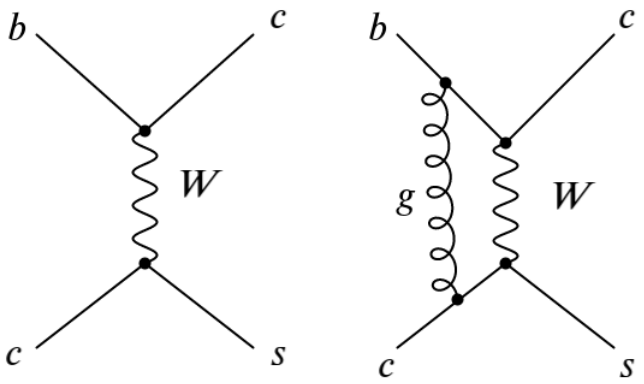

FIGURE 1.2: Tree level diagram for $b \to c\bar{c}s$ decay process.

- **Current-current:**

$$\begin{aligned} Q_1 &= (\bar{c}_\alpha b_\beta)_{V-A}(\bar{s}_\beta c_\alpha)_{V-A} \ , \\ Q_2 &= (\bar{c}b)_{V-A}(\bar{s}c)_{V-A} \ , \end{aligned} \tag{1.17}$$

  where $(\bar{q}_1 q_2)_{V-A} \equiv \bar{q}_1 \gamma^\mu (1-\gamma_5) q_2$.

- **QCD Penguins:**

$$\begin{aligned} Q_3 &= (\bar{s}b)_{V-A} \sum_{q=u,d,s,c,b} (\bar{q}q)_{V-A} \ , \\ Q_4 &= (\bar{s}_\alpha b_\beta)_{V-A} \sum_{q=u,d,s,c,b} (\bar{q}_\beta q_\alpha)_{V-A} \ , \\ Q_5 &= (\bar{s}b)_{V-A} \sum_{q=u,d,s,c,b} (\bar{q}q)_{V+A} \ , \\ Q_6 &= (\bar{s}_\alpha b_\beta)_{V-A} \sum_{q=u,d,s,c,b} (\bar{q}_\beta q_\alpha)_{V+A} \ . \end{aligned} \tag{1.18}$$

- **Electroweak Penguins:**

$$\begin{aligned} Q_7 &= \frac{3}{2}(\bar{s}b)_{V-A} \sum_{q=u,d,s,c,b} e_q (\bar{q}q)_{V+A} \ , \\ Q_8 &= \frac{3}{2}(\bar{s}_\alpha b_\beta)_{V-A} \sum_{q=u,d,s,c,b} e_q (\bar{q}_\beta q_\alpha)_{V+A} \ , \\ Q_9 &= \frac{3}{2}(\bar{s}b)_{V-A} \sum_{q=u,d,s,c,b} e_q (\bar{q}q)_{V-A} \ , \\ Q_{10} &= \frac{3}{2}(\bar{s}_\alpha b_\beta)_{V-A} \sum_{q=u,d,s,c,b} e_q (\bar{q}_\beta q_\alpha)_{V-A} \ . \end{aligned} \tag{1.19}$$

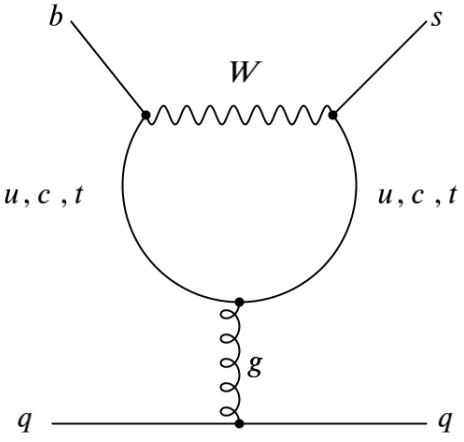

FIGURE 1.3: Feynman diagram for QCD penguin describing $b \to sq\bar{q}$ processes.

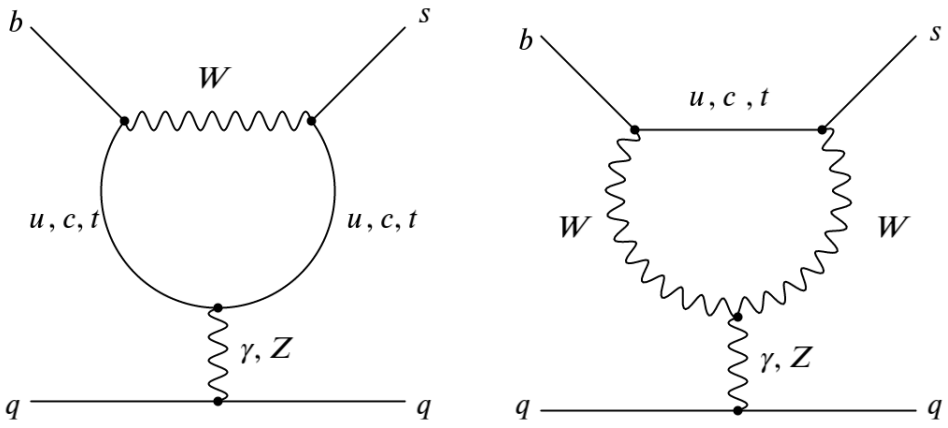

FIGURE 1.4: Electroweak penguin diagrams for $b \to sq\bar{q}$ processes.

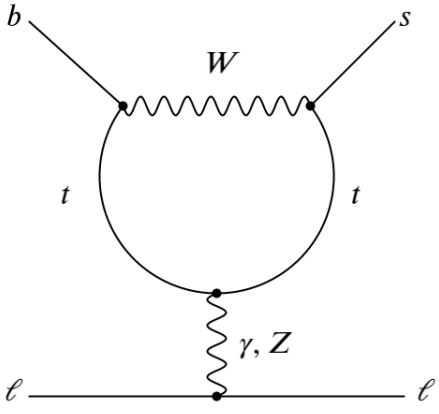

FIGURE 1.5: Electroweak penguin diagram for $b \to s\ell\ell$ transition.

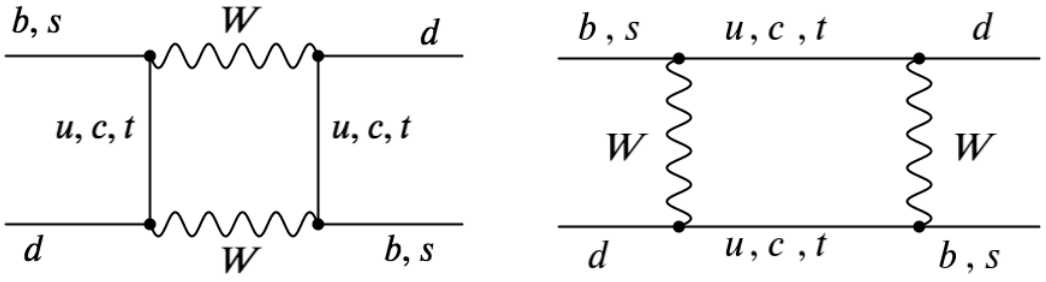

FIGURE 1.6: Box diagrams for $B_{d,s} - \bar{B}_{d,s}$ mixing.

- **Magnetic Penguins:**

$$Q_{7\gamma} = \frac{e}{8\pi^2} m_b \bar{s}_\alpha \sigma^{\mu\nu}(1+\gamma_5) b_\alpha F_{\mu\nu} \ ,$$
$$Q_{8G} = \frac{e}{8\pi^2} m_b \bar{s}_\alpha \sigma^{\mu\nu}(1+\gamma_5) b_\alpha T^a_{\alpha\beta} G^a_{\mu\nu} \ . \tag{1.20}$$

- $|\triangle \mathbf{S}| = \mathbf{2}$ **and** $|\triangle \mathbf{B}| = \mathbf{2}$ **operators:**

$$Q(|\triangle S| = 2) = (\bar{s}d)_{V-A}(\bar{s}d)_{V-A} \ ,$$
$$Q(|\triangle B| = 2) = (\bar{b}d)_{V-A}(\bar{b}d)_{V-A} \ . \tag{1.21}$$

The Feynman diagrams for various processes due to all these operators are displayed in Figs. 1.2-1.6.

1.2.2 Recent anomalies in B-sector

Recently several anomalies have been observed by BaBar, Bell and LHCb experiments in various rare semileptonic B meson decays driven by the flavour changing neutral current (FCNC) $b \to s\ell\ell$ and flavour changing charged current (FCCC) $b \to c\ell\nu_\ell$ transitions.

- The angular observable P_5' of $\bar{B} \to \bar{K}^* \mu^+ \mu^-$ and the branching ratios of $\bar{B} \to \bar{K}^* \mu^+ \mu^-$ and $B_s \to \phi \mu^+ \mu^-$ [15] show nearly 3σ deviations from their corresponding SM predictions.

- The recently measured value of lepton non universality (LNU) parameter $R_K = \frac{\mathrm{BR}\left(B^+ \to K^+ \mu^+ \mu^-\right)}{\mathrm{BR}(B^+ \to K^+ e^+ e^-)} = 0.846^{+0.060+0.016}_{-0.054-0.014}$ in the bin $q^2 \in [1.1, 6]$ by LHCb experiment [16] shows 2.5σ deviation from its predicted SM value, $R_K^{SM} = 1.0003 \pm 0.0001$.

- Similarly the measured values of $R_{K^*} = \frac{\mathrm{BR}\left(\bar{B} \to \bar{K}^* \mu^+ \mu^-\right)}{\mathrm{BR}\left(\bar{B} \to \bar{K}^* e^+ e^-\right)}$ in the low-q^2 bins $q^2 \in [0.045, 1.1]$ and $q^2 \in [1.1, 6]$: $R_{K^*}|_{q^2 \in [0.045, 1.1]} = 0.52^{+0.036}_{-0.026} \pm 0.05$, $R_{K^*}|_{q^2 \in [1.1,6]} =$

$0.96^{+0.45}_{-0.29} \pm 0.11$ [17], show respectively 2.2σ and 2.4σ deviations from their SM predictions.

- In case of FCCC transition the LNU parameters $R_D = \frac{\mathrm{BR}\left(\bar{B}\to\bar{D}\tau\bar{\nu}_\tau\right)}{\mathrm{BR}\left(\bar{B}\to\bar{D}l\bar{\nu}_l\right)}$, $R_{D^*} = \frac{\mathrm{BR}\left(\bar{B}\to\bar{D}^*\tau\bar{\nu}_\tau\right)}{\mathrm{BR}\left(\bar{B}\to\bar{D}^*l\bar{\nu}_l\right)}$ [18] display respectively 1.9σ and 3.3σ deviations from their corresponding SM predictions.

- The measured value of LNU parameter $R_{J/\psi} = \frac{\mathrm{Br}(B_c\to J/\psi\tau\bar{\nu}_\tau)}{\mathrm{Br}(B_c\to J/\psi\ell\bar{\nu}_\ell)} = 0.71 \pm 0.17 \pm 0.18$ [19], also shows nearly 2σ deviation from its SM prediction .

The SM and Experimental measured values of these LNU parameters are listed in Table-1.1.

TABLE 1.1: Values of various LNU observables.

LNU Observable	Measured value	SM prediction	Deviation
$R_K\vert_{q^2\in[1.1,6]\ \mathrm{GeV}^2}$	$0.846^{+0.060+0.016}_{-0.054-0.014}$ [16]	1.0003 ± 0.0001 [20]	2.5σ
$R_{K^*}\vert_{q^2\in[0.045,1.1]\ \mathrm{GeV}^2}$	$0.660^{+0.110}_{-0.070} \pm 0.024$ [17]	0.92 ± 0.02 [21]	2.2σ
$R_{K^*}\vert_{q^2\in[1.1,6]\ \mathrm{GeV}^2}$	$0.685^{+0.113}_{-0.007} \pm 0.047$ [17]	1.00 ± 0.01 [21]	2.4σ
R_D	$0.340 \pm 0.027 \pm 0.013$ [18]	0.299 ± 0.003 [22]	1.9σ
R_{D^*}	$0.295 \pm 0.011 \pm 0.008$ [18]	0.258 ± 0.005 [23]	3.3σ
$R_{J/\psi}$	$0.71 \pm 0.17 \pm 0.184$ [19]	0.289 ± 0.01 [24]	2σ

In this aspect we would like to study the possible impact of new physics in LNU observables and other asymmetries associated with $b \to c, u$ quark level transitions.

1.3 Thesis overview

Chapter-1 presents a brief introduction to the SM of particle physics. Along with the particle content of the SM we present the effective Lagrangian, CKM matrix and the unitarity triangle. This chapter also contains an introduction to Flavor Physics and CP violation. Highlighting the importance of Beauty Physics, this chapter is concluded with the discussion on recently observed anomalies by various B-experiments. Chapter-2 presents a study of semileptonic $b \to ul\bar{\nu}_l$ decay processes in model independent framework. This chapter contains the study of B meson decaying to a pseudoscalar and vector meson. In our analysis we take into account $P = K, \pi, \eta'$ and $V = K^*, \rho$ and show the variation of different observables sensitive to NP in presence of various new Wilson coefficients. Chapter-3 comprises of the study of $\Lambda_b \to (\Lambda_c, p)\ell\bar{\nu}_\ell$ decays mediated by $b \to (c, u)\ell\bar{\nu}_\ell$ transition in the frame of NP with the contribution of additional complex

Wilson coefficients. A study of $B^* \to P\ell\bar{\nu}_\ell$ decay processes is explored in chapter-4 where P is a pseudo scalar meson. This study is based on a model independent investigation. We summarize our findings in chapter-5.

Chapter 2

Analysis of semileptonic $b \to u l \bar{\nu}_l$ decay processes in model independent approach

LHCb and both the B factories Belle and BaBar have studied various B decays associated with $b \to c l \nu_l$ and $b \to s \ell \ell^-$ quark level transitions. They also reported various anomalies associated with different B meson decay processes. There are a few striking deviations in the experimental values of lepton non universality observables associated with $b \to (c, s)$ transitions and in the angular observables associated with $\bar{B} \to \bar{K^*} \mu^+ \mu^-$ decay process, from their corresponding SM predictions. Therefore, it is interesting to investigate analogous observables in different B decays associated with $b \to u l \bar{\nu}_l$ transitions. In this chapter, we focus on the model independent analysis of various decay processes associated with $b \to u l \bar{\nu}_l$ transitions. We mainly explore the semileptonic decay channels where B meson is decaying to pseudoscalar mesons (π, K, η') and vector mesons (K^*, ρ).

2.1 General effective Lagrangian for $b \to u l \bar{\nu}_l$ transitions

The most general effective Lagrangian for $b \to u l \bar{\nu}_l$ process is given by [25]

$$\begin{aligned} \mathcal{L}_{\text{eff}} &= -\frac{4\,G_F}{\sqrt{2}}\,V_{ub}\Big\{(1+V_L)\,\bar{l}_L\,\gamma_\mu\,\nu_L\,\bar{u}_L\,\gamma^\mu\,b_L + V_R\,\bar{l}_L\,\gamma_\mu\,\nu_L\,\bar{u}_R\,\gamma^\mu\,b_R \\ &\quad + S_L\,\bar{l}_R\,\nu_L\,\bar{u}_R\,b_L + S_R\,\bar{l}_R\,\nu_L\,\bar{u}_L\,b_R + T_L\,\bar{l}_R\,\sigma_{\mu\nu}\,\nu_L\,\bar{u}_R\,\sigma^{\mu\nu}\,b_L\Big\} + \text{h.c.}\,, \end{aligned} \tag{2.1}$$

where G_F is the Fermi constant, V_{ub} is the Cabibbo-Kobayashi-Maskawa (CKM) matrix element and $q_{L(R)} = L(R)q$ are the chiral quark fields with $L(R) = (1 \mp \gamma_5)/2$ as the projection operator. Here $V_{L,R}$, $S_{L,R}$ and T_L are the vector, scalar and tensor new physics couplings associated with the left-handed neutrinos, which are zero in the SM. The constraint on the new coefficients obtained from the leptonic $B_u^+ \to l^+\nu_l$ processes are discussed in the subsection below.

2.1.1 Constraints on new couplings from rare leptonic $B_u^+ \to l^+\nu_l$ processes

The rare leptonic $B_u^+ \to l^+\nu_l$ processes are mediated by the quark-level transitions $b \to u$ and are theoretically very clean. The only non-perturbative quantity involved in these processes is the decay constant of B_u meson. Including the new coefficients from Eqn. (2.1), the branching ratios of $B_u^+ \to l^+\nu_l$ processes in the presence of NP are given by [26]

$$\begin{aligned} \mathrm{BR}(B_u^+ \to l^+\nu_l) &= \frac{G_F^2 M_{B_u} m_l^2}{8\pi}\Big(1 - \frac{m_l^2}{M_{B_u}^2}\Big)^2 f_{B_u}^2 \left|V_{ub}\right|^2 \tau_{B_u^+} \\ &\times \left|(1 + V_L - V_R) - \frac{M_{B_u}^2}{m_l(m_b + m_u)}(S_L - S_R)\right|^2, \end{aligned} \tag{2.2}$$

where M_{B_u} (f_{B_u}) is the mass (decay constant) of B_u meson and m_l is the lepton mass. In our analysis, all the particle masses and the life time of B_u^+ meson are taken from [27]. The decay constant of B_u meson is taken as $f_{B_u} = 190.5$ (4.2) MeV [28], and for the CKM matrix element, we use the Wolfenstein parametrization [11], with the values $A = 0.811 \pm 0.026$, $\lambda = 0.22506 \pm 0.00050$, $\bar{\rho} = 0.124^{+0.019}_{-0.018}$ and $\bar{\eta} = 0.356 \pm 0.011$ [27]. Using these values, the obtained branching fractions of $B_u^+ \to l^+\nu_l$ processes in the SM are given as

$$\begin{aligned} \mathrm{BR}(B_u^+ \to e^+\nu_e)|^{\mathrm{SM}} &= (8.9 \pm 0.23) \times 10^{-12}, \\ \mathrm{BR}(B_u^+ \to \mu^+\nu_\mu)|^{\mathrm{SM}} &= (3.83 \pm 0.1) \times 10^{-7}, \\ \mathrm{BR}(B_u^+ \to \tau^+\nu_\tau)|^{\mathrm{SM}} &= (8.48 \pm 0.28) \times 10^{-5}, \end{aligned} \tag{2.3}$$

and the corresponding experimental values are [27]

$$\begin{aligned} \mathrm{BR}(B_u^+ \to e^+\nu_e)|^{\mathrm{Expt}} &< 9.8 \times 10^{-7}, \\ \mathrm{BR}(B_u^+ \to \mu^+\nu_\mu)|^{\mathrm{Expt}} &< 1.0 \times 10^{-6}, \\ \mathrm{BR}(B_u^+ \to \tau^+\nu_\tau)|^{\mathrm{Expt}} &= (1.09 \pm 0.24) \times 10^{-4}. \end{aligned} \tag{2.4}$$

Since $B_u^+ \to l^+\nu_l$ processes do not receive any contribution from tensor coupling, we ignore the effect of tensor operator in this work. In our analysis, we consider the new coefficients $V_{L,R}$, $S_{L,R}$ as complex. For simplicity, we consider the presence of only one coefficient at a time and constrain its real and imaginary parts by comparing the predicted SM branching fractions of $B_u^+ \to l^+\nu_l$ processes with the corresponding experimental results. For $B_u^+ \to \tau^+\nu_\tau$, we compare with the 1σ range of observed data. In Fig. 2.1, we show the constraints on the real and imaginary parts of the V_L coefficient obtained from the $B_u^+ \to e^+\nu_e$ (top-left panel), $B_u^+ \to \mu^+\nu_\mu$ (top-right panel) and $B_u^+ \to \tau^+\nu_\tau$ (bottom panel) processes. Analogously, the allowed ranges of the real and imaginary parts of S_L coefficient derived from the $B_u^+ \to e^+\nu_e$ (top-left panel), $B_u^+ \to \mu^+\nu_\mu$ (top-right panel) and $B_u^+ \to \tau^+\nu_\tau$ (bottom panel) processes are shown in Fig. 2.2. The constraint on the imaginary part of the V_R (S_R) coefficient is same as V_L (S_L) coefficient and the corresponding real part is related by $\mathrm{Re}[V_R]$ ($\mathrm{Re}[S_R]$) $= -\mathrm{Re}[V_L]$ ($\mathrm{Re}[S_L]$). It should be noted that the bounds obtained from $B_u^+ \to e^+\nu_e(\mu^+\nu_\mu)$ process are comparatively weak as only the upper limits on the branching ratios of these processes exist. Furthermore, the bounds on new coefficients obtained from $B_u^+ \to e^+\nu_e$ process are too weak to make reasonable predictions for the observables associated with $b \to ue^+\nu_e$ decay modes. Therefore, we only present the results for semileptonic B decays with $\mu(\tau)$ in the final state.

2.2 $B \to Pl\bar{\nu}_l$ processes

In this section, we discuss the rare $B \to Pl\bar{\nu}_l$ processes, where $P = \pi, K, \eta^{(\prime)}$. The matrix elements of various hadronic currents between the initial B meson and the final pseudoscalar meson P, can be parametrized in terms of two form factors F_0, F_1 [29, 30] as

$$\langle P(k)|\bar{u}\gamma_\mu\, b|B(p_B)\rangle = F_1(q^2)\Big[(p_B+k)_\mu - \frac{M_B^2 - M_P^2}{q^2}q_\mu\Big] + F_0(q^2)\frac{M_B^2 - M_P^2}{q^2}q_\mu\ , \quad (2.5)$$

where p_B and k are respectively the four momenta of the B and P mesons and $q = p_B - k$ is the momentum transfer. Now using the above form factors, the double differential decay distribution of $B \to Pl\nu_l$ processes in terms of the helicity amplitudes H_0, H_t and

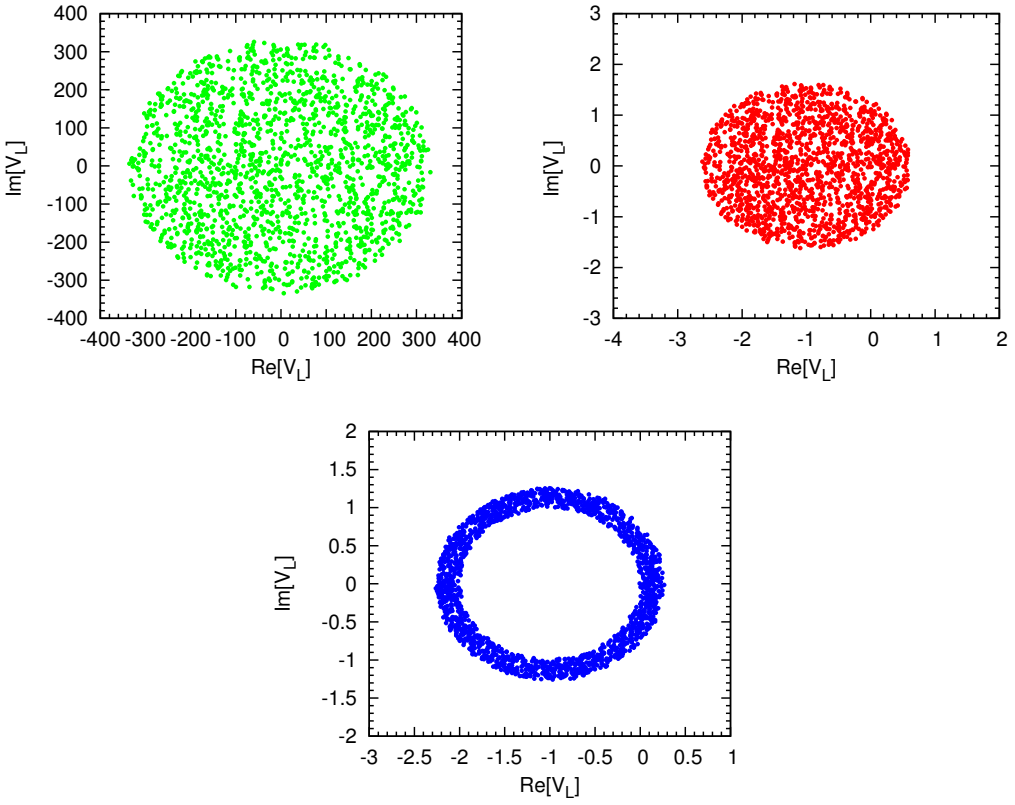

FIGURE 2.1: Allowed parameter space for the real and imaginary parts of V_L parameter obtained from $B_u^+ \to e^+\nu_e$ (top-left panel), $B_u^+ \to \mu^+\nu_\mu$ (top-right panel) and $B_u^+ \to \tau^+\nu_\tau$ (bottom panel).

H_S are given by [30]

$$\begin{aligned}\frac{d\Gamma(B \to Pl\bar{\nu}_l)}{dq^2} &= \frac{G_F^2|V_{ub}|^2}{192\pi^3 M_B^3} q^2 \sqrt{\lambda_P(q^2)} \left(1 - \frac{m_l^2}{q^2}\right)^2 \\ &\times \left\{ \left|1 + V_L + V_R\right|^2 \left[\left(1 + \frac{m_l^2}{2q^2}\right) H_0^2 + \frac{3}{2}\frac{m_l^2}{q^2} H_t^2 \right] + \frac{3}{2}|S_L + S_R|^2 H_S^2 \right. \\ &+ \left. 3\mathrm{Re}\left[(1 + V_L + V_R)(S_L^* + S_R^*)\right] \frac{m_l}{\sqrt{q^2}} H_S H_t \right\}, \end{aligned} \tag{2.6}$$

where

$$\lambda_P(q^2) = \lambda(M_B^2, M_P^2, q^2) = M_B^4 + M_P^4 + q^4 - 2(M_B^2 M_P^2 + M_P^2 q^2 + M_B^2 q^2)\,, \tag{2.7}$$

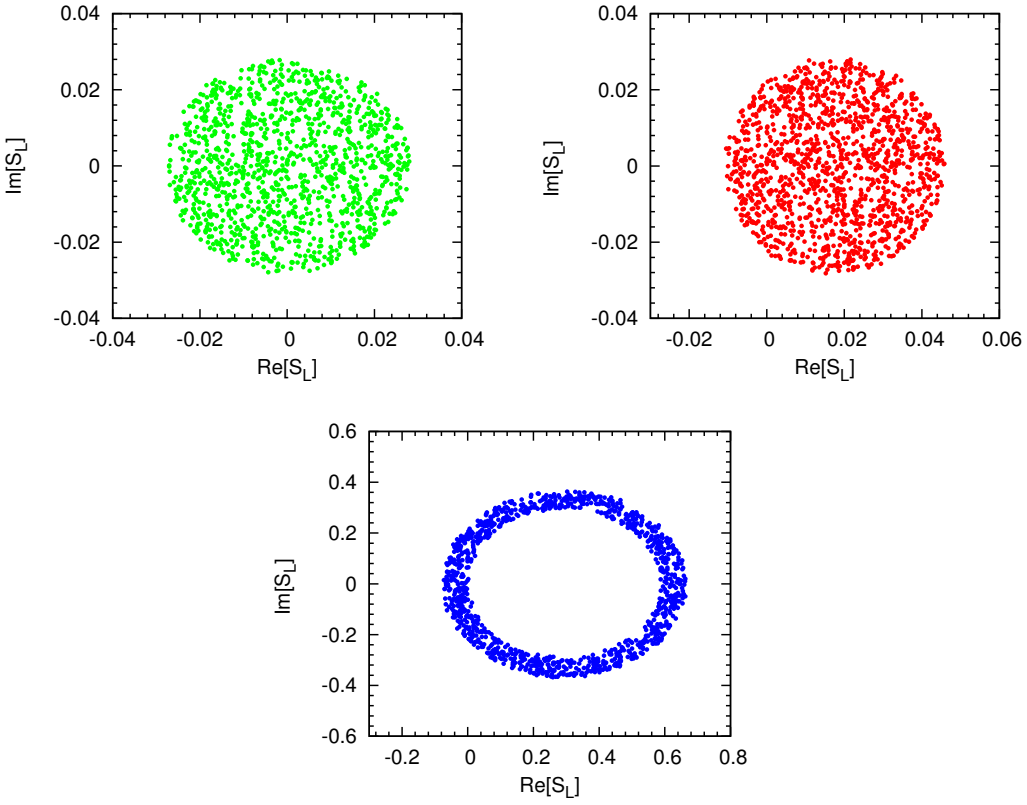

FIGURE 2.2: Constraint on the real and imaginary parts of the S_L parameter obtained from $B_u^+ \to e^+\nu_e$ (top-left panel), $B_u^+ \to \mu^+\nu_\mu$ (top-right panel) and $B_u^+ \to \tau^+\nu_\tau$ (bottom panel).

and the helicity amplitudes ($H_{0,t,S}$) in terms of the form factors ($F_{0,1}$) are given as

$$\begin{aligned} H_0(q^2) &= \sqrt{\frac{\lambda_P(q^2)}{q^2}} F_1(q^2), \\ H_t(q^2) &= \frac{M_B^2 - M_P^2}{\sqrt{q^2}} F_0(q^2), \\ H_S(q^2) &= \frac{M_B^2 - M_P^2}{m_b - m_u} F_0(q^2). \end{aligned} \tag{2.8}$$

Here M_P is the mass of the P meson and m_b (m_u) is the mass of the b (u) quark.

The forward-backward asymmetry, which is an interesting observable to look for NP, defined as

$$A_{FB}(q^2) = \frac{\int_0^1 \frac{d\Gamma}{dq^2 d\cos\theta} d\cos\theta - \int_{-1}^0 \frac{d\Gamma}{dq^2 d\cos\theta} d\cos\theta}{d\Gamma/dq^2}. \tag{2.9}$$

Besides the branching ratio and forward-backward asymmetry, another important observable is the LNU ratio. Similar to $R_{D^{(*)}}$ observables, we define the LNU parameter

for $B \to Pl\nu_l$ processes as

$$R_P^{\tau\mu} = \frac{\mathrm{BR}(B \to P\tau\bar{\nu}_\tau)}{\mathrm{BR}(B \to P\mu\bar{\nu}_\mu)} \,, \tag{2.10}$$

in order to scrutinize the violation of lepton universality effect in $b \to ul\nu_l$ decays. In Ref. [22], the authors have studied the lepton universality violating ratio $\mathrm{BR}(B \to P\tau\bar{\nu}_\tau)/\mathrm{BR}(B \to Pl\bar{\nu}_l)$, where $l = e, \mu$. Since the constraints on new coefficients obtained from $B_u^+ \to e^+\nu_e$ process are too weak, it would not be possible to predict reasonably constrained result for the $\mathrm{BR}(B \to P\tau\bar{\nu}_\tau)/\mathrm{BR}(B \to Pe\bar{\nu}_e)$ ratio. Therefore, we only consider the $\mathrm{BR}(B \to P\tau\bar{\nu}_\tau)/\mathrm{BR}(B \to P\mu\bar{\nu}_\mu)$ observable in our analysis.

In order to explore few other observables which are sensitive to NP in the $b \to ul\bar{\nu}_l$ processes, we define the parameter $R_{PP'}^l$ as ratio of branching fractions of $B \to Pl^-\bar{\nu}_l$ to $B \to P'l^-\bar{\nu}_l$ processes

$$R_{PP'}^l = \frac{\mathrm{BR}(B \to Pl^-\bar{\nu}_l)}{\mathrm{BR}(B \to P'l^-\bar{\nu}_l)} \,. \tag{2.11}$$

These processes differ only in the spectator quark content and hence, any deviation from SM prediction, if observed would hint towards the existence of NP.

After setting the stage, we now proceed for numerical analysis. We consider all the particle masses and the life time of B meson from the Ref. [27]. To make predictions for the various observables or to extract information about potentially new short distance physics, one should have sufficient knowledge on the associated hadronic form factors. For the form factors of $\bar{B}_s \to K^+l^-\bar{\nu}_l$ processes, we consider the perturbative QCD (PQCD) calculation [31, 32] based on the k_T factorization [33] at next-to-leading order (NLO) in α_s [34], which gives

$$\begin{aligned} F_1^{B_s\to K}(q^2) &= F_1^{B_s\to K}(0)\left(\frac{1}{(1-q^2/M_{B_s}^2)} + \frac{a_1 q^2/M_{B_s}^2}{(1-q^2/M_{B_s}^2)(1-b_1 q^2/M_{B_s}^2)}\right), \\ F_0^{B_s\to K}(q^2) &= \frac{F_0^{B_s\to K}(0)}{(1-a_0 q^2/M_{B_s}^2 + b_0 q^4/M_{B_s}^4)} \,, \end{aligned} \tag{2.12}$$

where M_{B_s} is the mass of B_s meson and the values of the parameters $a_{0,1}$, $b_{0,1}$ and $F_{0,1}^{B_s\to K}$ are listed in Table 2.1.

For $B \to \pi$ form factors, we use the light cone sum rule (LCSR) results as input for a z-series parametrization which yield the q^2 shape in the whole semileptonic region of

TABLE 2.1: Numerical values of the $B_s \to K$ form factors in the PQCD approach [31].

Parameters	PQCD
$F_0(0)$	$0.26^{+0.04}_{-0.03} \pm 0.02$
a_0	$0.54 \pm 0.00 \pm 0.05$
b_0	$-0.15 \pm 0.00 \pm 0.00$
$F_1(0)$	$0.26 \pm 0.035 \pm 0.02$
a_1	$0.57 \pm 0.01 \pm 0.02$
b_1	$0.50 \pm 0.01 \pm 0.05$

$B \to \pi l \nu_l$ processes. The q^2 dependence of the form factors is parametrized as [35]

$$F_1(q^2) = \frac{F_1(0)}{\left(1 - \frac{q^2}{M_{B^*2}}\right)} \Bigg\{ 1 + \sum_{k=1}^{N-1} b_k \Big(z(q^2,t_0)^k - z(0,t_0)^k - (-1)^{N-k} \frac{k}{N} \Big[z(q^2,t_0)^N - z(0,t_0)^N \Big] \Big) \Bigg\},$$

$$F_0(q^2) = F_0(0) \left\{ 1 + \sum_{k=1}^{N} b_k^0 \Big(z(q^2,t_0)^k - z(0,t_0)^k \Big) \right\}, \tag{2.13}$$

where $N = 2$ for $F_1(q^2)$ form factor and for $F_0(q^2)$ form factor, $N = 1$. Here the function $z(q^2, t_0)$ is defined as [36]

$$z(q^2,t_0) = \frac{\sqrt{(M_B + M_\pi)^2 - q^2} - \sqrt{(M_B + M_\pi)^2 - t_0}}{\sqrt{(M_B + M_\pi)^2 - q^2} + \sqrt{(M_B + M_\pi)^2 - t_0}}\,, \tag{2.14}$$

where $t_0 = (M_B + M_\pi)^2 - 2\sqrt{M_B\, M_\pi}\sqrt{(M_B + M_\pi)^2 - q^2_{\rm min}}$ is the auxiliary parameter. Here the values of various parameters involved are $F_1(0) = F_0(0) = 0.281 \pm 0.028$, $b_1 = -1.62 \pm 0.70$ and $b_1^0 = -3.98 \pm 0.97$ [35].

The $B^- \to \eta^{(\prime)} l^- \bar{\nu}_l$ processes are also mediated by the flavour changing charged current (FCCC) transitions $b \to u$. For the study of these processes, we use $SU(3)_F$ flavour symmetry to relate the form factors of $F_1^{B\to\eta^{(\prime)}}$ to $F_1^{B\to\pi}$. We choose the scheme as discussed in [37–40], and consider

$$|\eta\rangle = \cos\phi|\eta_q\rangle - \sin\phi|\eta_s\rangle,$$
$$|\eta'\rangle = \sin\phi|\eta_q\rangle + \cos\phi|\eta_s\rangle, \tag{2.15}$$

for the $\eta - \eta'$ mixing, where $|\eta_q\rangle = (u\bar{u} + d\bar{d})/\sqrt{2}$, $\eta_s = s\bar{s}$ and ϕ is the fitted mixing angle ($\phi = 39.3^\circ$) [39, 41]. With these input parameters in hand, we now proceed to discuss four different new physics scenarios and their effect on $b \to ul\nu_l$ processes.

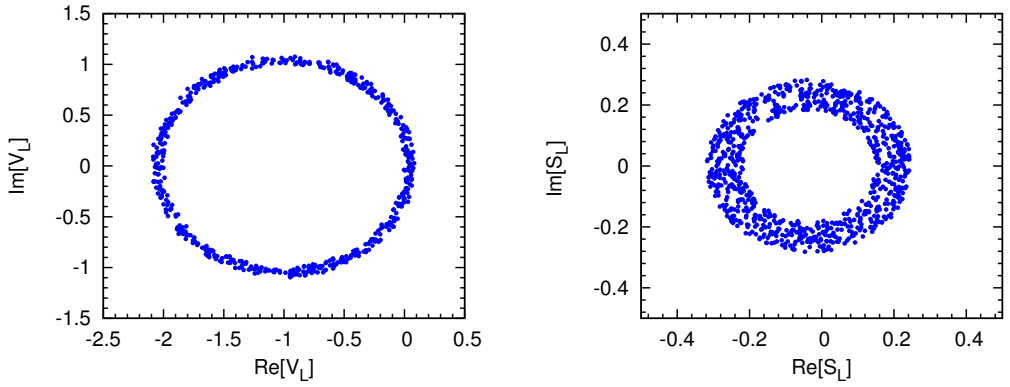

FIGURE 2.3: Constraint on the real and imaginary parts of the V_L (left panel) and S_L (right panel) parameters obtained from $B_u^- \to \pi^0 \mu \bar{\nu}_\mu$ process.

2.2.1 Case A: Effect of V_L only

In this case, we assume that only the new V_L coefficient is present in addition to SM contribution, in the effective Lagrangian (2.1). From Eqn. (2.6) it should be noted that as the NP has the same structure as the SM, the SM decay rate gets modified by the factor $|1 + V_L|^2$. The constraints on the real and imaginary parts of V_L coefficient for $b \to u\tau\bar{\nu}_\tau$ are obtained from the branching ratio of $B_u^+ \to \tau^+ \nu_\tau$ process as discussed in section II. From the bottom panel of Fig. 2.1, one can notice that the constraint on V_L is $|V_L| \leq 2.5$, obtained from $B_u \to \tau\bar{\nu}_\tau$ process. In our analysis, we consider the values for real and imaginary parts of V_L, which give the maximum and minimum values of the branching ratio within the 1σ limit. Thus, imposing the extrema conditions, the allowed parameters are found as $(\mathrm{Re}[V_L], \mathrm{Im}[V_L])^{\max} = (0.130, 0.761)$ and $(\mathrm{Re}[V_L], \mathrm{Im}[V_L])^{\min} = (-0.929, 0.841)$. For $b \to u\mu\bar{\nu}_\mu$ transition as only the upper limit of $B_u \to \mu\bar{\nu}_\mu$ is known, it will not provide any strict bound on the NP coefficient V_L. Therefore, to avoid overestimation of the predicted values of various physical observables, we consider the branching ratio of $B^- \to \pi^0 \mu^- \bar{\nu}_\mu$ process. Comparing the SM predicted value $\mathrm{BR}(B^- \to \pi^0 \mu^- \bar{\nu}_\mu)^{\mathrm{SM}} = (7.15 \pm 0.55) \times 10^{-5}$ with the 1σ range of corresponding measured value $\mathrm{BR}(B^- \to \pi^0 \mu^- \bar{\nu}_\mu)^{\mathrm{Expt}} = (7.80 \pm 0.27) \times 10^{-5}$, we obtain the maximum and minimum values of the V_L parameter as $(\mathrm{Re}[V_L], \mathrm{Im}[V_L])^{\max} = (-0.233, 0.769)$ and $(\mathrm{Re}[V_L], \mathrm{Im}[V_L])^{\min} = (-0.833, 0.968)$. The corresponding allowed parameter space is shown in the left panel of Fig. 2.3.

Using the allowed constrained values, we show the plots for the variation of branching fractions of various $B \to P\mu^- \bar{\nu}_\mu$ processes with respect to q^2 in Fig. 2.4, both in the SM and in NP scenario. Here the plot for $\bar{B}_s \to K^+ \mu^- \bar{\nu}_\mu$ process is represented in the top-left panel, the top-right panel is for the branching ratio of $\bar{B}^0 \to \pi^+ \mu^- \bar{\nu}_\mu$, the bottom-left plot is for $B^- \to \eta \mu^- \bar{\nu}_\mu$ process and the branching ratio of $B^- \to \eta' \mu^- \bar{\nu}_\mu$

process is presented in the bottom-right panel. In these figures, the red bands are due

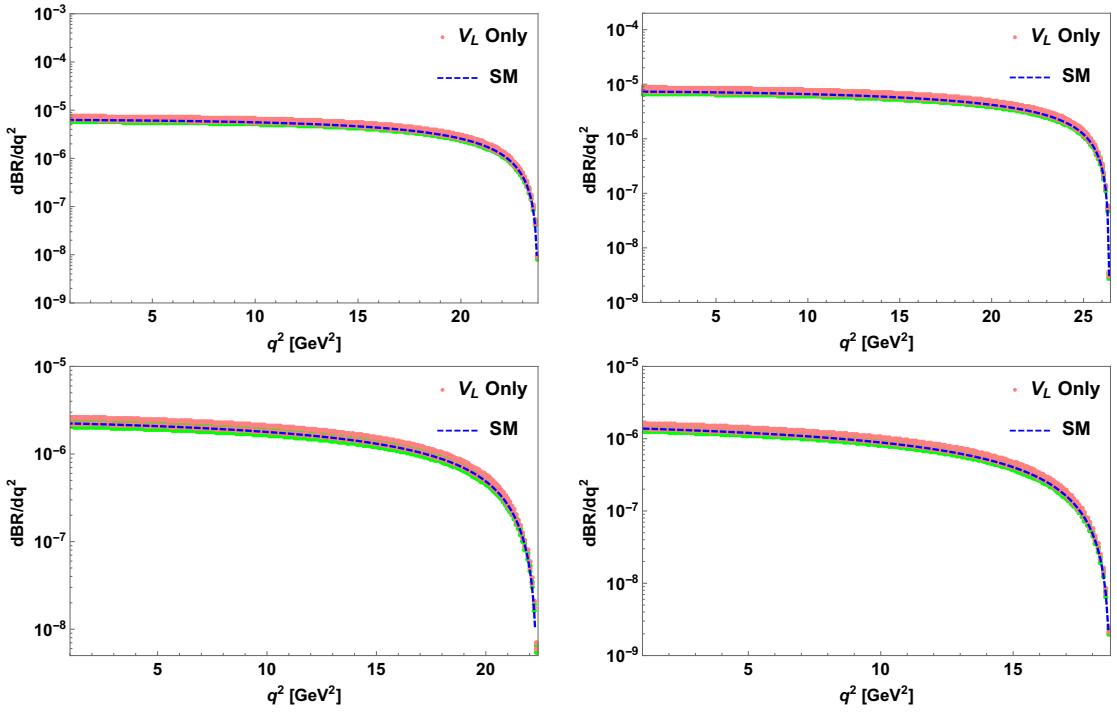

FIGURE 2.4: The q^2 variation of branching ratios of $\bar{B}_s \to K^+\mu^-\bar{\nu}_\mu$ (top-left panel), $\bar{B}^0 \to \pi^+\mu^-\nu_\mu$ (top-right panel), $B^- \to \eta\mu^-\bar{\nu}_\mu$ (bottom-left panel) and $B^- \to \eta'\mu^-\bar{\nu}_\mu$ (bottom-right panel) processes for the NP contribution coming from only V_L coupling. Here the contributions due to the V_L coupling are represented by red bands. The blue dashed lines are for the SM contributions and the green bands are due to the contributions coming from the theoretical uncertainties.

to the contribution coming from V_L new physics parameter in addition to SM and the blue dashed lines are due to SM. The green bands are the corresponding SM theoretical uncertainties, which arise due to the uncertainties in the SM input parameters such as CKM elements and form factors. Analogous plots for the variation of the branching ratios of $\bar{B}_s \to K^+\tau^-\bar{\nu}_\tau$ (top-left panel), $\bar{B}^0 \to \pi^+\tau^-\bar{\nu}_\tau$ (top-right panel), $B^- \to \eta\tau^-\bar{\nu}_\tau$ (bottom-left panel) and $B^- \to \eta'\tau^-\bar{\nu}_\tau$ (bottom-right panel) processes are shown in Fig. 2.5. The integrated values of the branching ratios for these processes are given in Table 2.2. Due to the inclusion of new V_L coefficient, we found certain deviation in the branching ratios of $B \to P\tau\bar{\nu}_\tau$ processes from the SM values, whereas the deviation in the branching ratios of $B \to P\mu\bar{\nu}_\mu$ processes are relatively small. Our predicted results for $B \to (\pi, \eta^{(\prime)})l\nu_l$ processes are consistent with the existing experimental data [27]

$$\begin{aligned}
&\mathrm{BR}(B^+ \to \eta l^+\nu_l)^{\mathrm{Expt}} = (3.8 \pm 0.6) \times 10^{-5},\\
&\mathrm{BR}(B^0 \to \pi^- l^+\nu_l)^{\mathrm{Expt}} = (1.45 \pm 0.05) \times 10^{-4},\\
&\mathrm{BR}(B^+ \to \eta' l^+\nu_l)^{\mathrm{Expt}} = (2.3 \pm 0.8) \times 10^{-5},\\
&\mathrm{BR}(B^0 \to \pi^-\tau^+\nu_\tau)^{\mathrm{Expt}} < 2.5 \times 10^{-4}.
\end{aligned} \tag{2.16}$$

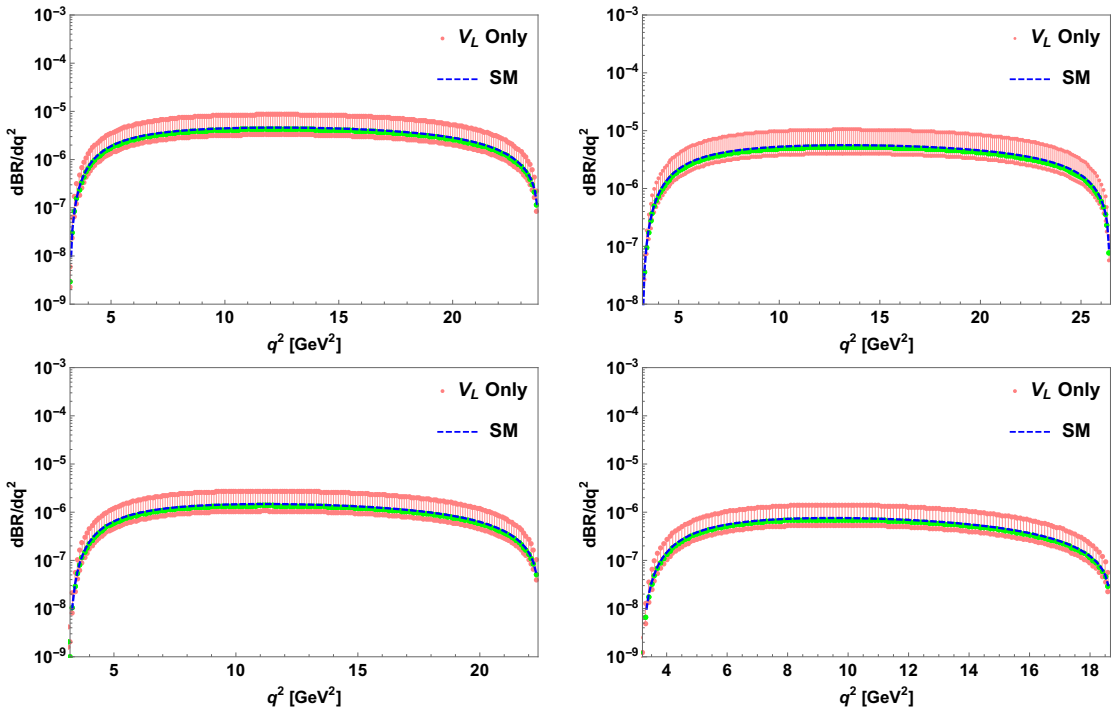

FIGURE 2.5: The q^2 variation of the branching ratios of $\bar{B}_s \to K^+\tau^-\bar{\nu}_\tau$ (top-left panel), $\bar{B}^0 \to \pi^+\tau^-\nu_\tau$ (top-right panel), $B^- \to \eta\tau^-\bar{\nu}_\tau$ (bottom-left panel) and $B^- \to \eta'\tau^-\bar{\nu}_\tau$ (bottom-right panel) processes for the NP contribution due to V_L coupling.

Since the V_L contribution has the same structure as SM, the forward-backward asymmetry parameter of $B \to P\mu^-\bar{\nu}_\mu$ ($\tau^-\bar{\nu}_\tau$) processes do not deviate from their SM values, and the corresponding integrated values (integrated over the whole q^2 range) are presented in Table 2.2. In Fig. 2.6, we show the plots for the LNU parameters of $\bar{B}_{(s)} \to Pl\bar{\nu}_l$ processes, $R_K^{\tau\mu}$ (top-left panel), $R_\pi^{\tau\mu}$ (top-right panel), $R_\eta^{\tau\mu}$ (bottom-left panel) and $R_{\eta'}^{\tau\mu}$ (bottom-right panel). Including only V_L coupling, we also compute the $R_{\pi K}^l$, $R_{\pi\eta}^l$ and $R_{\pi\eta'}^l$ parameters, however, no deviation has been found from their corresponding SM result. The numerical values of these parameters are listed in Table 2.3.

2.2.2 Case B: Effect of V_R only

Here we consider the effect of only V_R coefficient in addition to the SM contribution. The constraints obtained on real and imaginary parts of V_R coupling from $B_u \to \tau\nu$ process are related to that of V_L as $\mathrm{Re}[V_R] = -\mathrm{Re}[V_L]$ and $\mathrm{Im}[V_R] = \mathrm{Im}[V_L]$, and thus, allowed parameter space for V_R is same as that of V_L with a sign flip for the real parts. The minimum and maximum values of the V_R parameters are obtained using the extrema conditions as $(\mathrm{Re}[V_R], \mathrm{Im}[V_R])^{\max} = (-0.242, -0.561)$ and $(\mathrm{Re}[V_R], \mathrm{Im}[V_R])^{\min} = (0.259, -0.406)$. However, the constraints on V_R obtained from $B^- \to \pi^0\mu^-\bar{\nu}_\mu$ for $b \to u\mu\bar{\nu}_\mu$ transition are same as V_L. Thus, the predicted branching ratios for $B \to P\mu\bar{\nu}_\mu$ processes in the presence of V_R coupling are same as those with V_L coupling. Using the

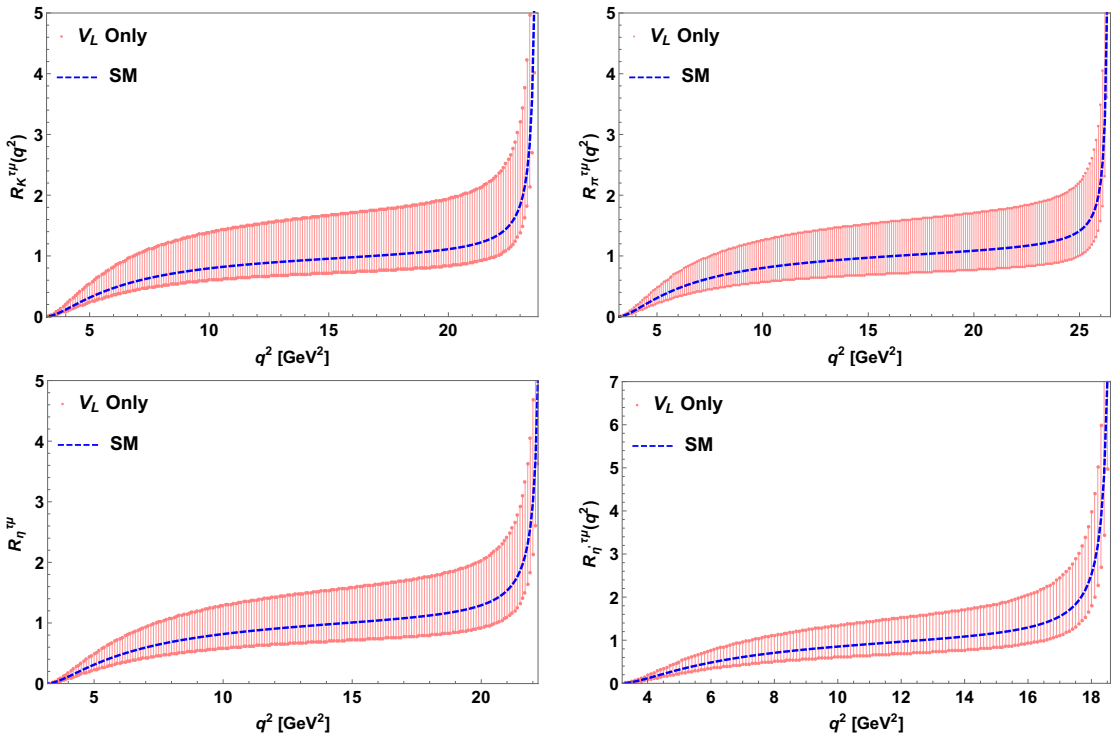

FIGURE 2.6: The plots for the LNU parameters $R_K^{\tau\mu}(q^2)$ (top-left panel), $R_\pi^{\tau\mu}(q^2)$ (top-right panel), $R_\eta^{\tau\mu}(q^2)$ (bottom-left panel) and $R_{\eta'}^{\tau\mu}(q^2)$ (bottom-right panel) for the NP contribution due to V_L coupling.

allowed values of the couplings, the plots for the branching ratios of $\bar{B}_s \to K^+\tau^-\bar{\nu}_\tau$ (top-left panel), $\bar{B}^0 \to \pi^+\tau^-\bar{\nu}_\tau$ (top-right panel), $B^- \to \eta\tau^-\bar{\nu}_\tau$ (bottom-left panel) and $B^- \to \eta'\tau^-\bar{\nu}_\tau$ (bottom-right panel) processes in the presence of V_R coupling are shown in Fig. 2.7. In these plots, the cyan bands are obtained by using the allowed parameter space of V_R. The predicted integrated values of branching ratios of these processes are listed in Table 2.2. Like the previous case, the forward-backward asymmetry parameters are also not affected due to V_R coupling. In Fig. 2.8, we present the plots for the LNU parameters $R_K^{\tau\mu}(q^2)$ (top-left panel), $R_\pi^{\tau\mu}(q^2)$ (top-right panel), $R_\eta^{\tau\mu}(q^2)$ (bottom-left panel) and $R_{\eta'}^{\tau\mu}(q^2)$ (bottom-right panel). In the presence of V_R coupling, the parameters $R_{\pi K}^l$, $R_{\pi\eta^{(\prime)}}^l$ don't have any deviation from their corresponding SM predictions. In Table 2.3, we present the numerical values of these parameters.

2.2.3 Case C: Effect of S_L only

In this subsection, we wish to see the effect of only S_L coupling on various observables associated with $B \to Pl\bar{\nu}_l$ processes. For $b \to u\tau\nu_\tau$ transition, using the extrema conditions, we obtain the maxima and minima of S_L parameter as $(\mathrm{Re}[S_L], \mathrm{Im}[S_L])^{\max} = (-0.1063, -0.0063)$ and $(\mathrm{Re}[S_L], \mathrm{Im}[S_L])^{\min} = (0.5397, 0.0244)$, from the allowed parameter space in the bottom panel of Fig. 2.2. Analogously, for $b \to u\mu\bar{\nu}_\mu$, the extrema values

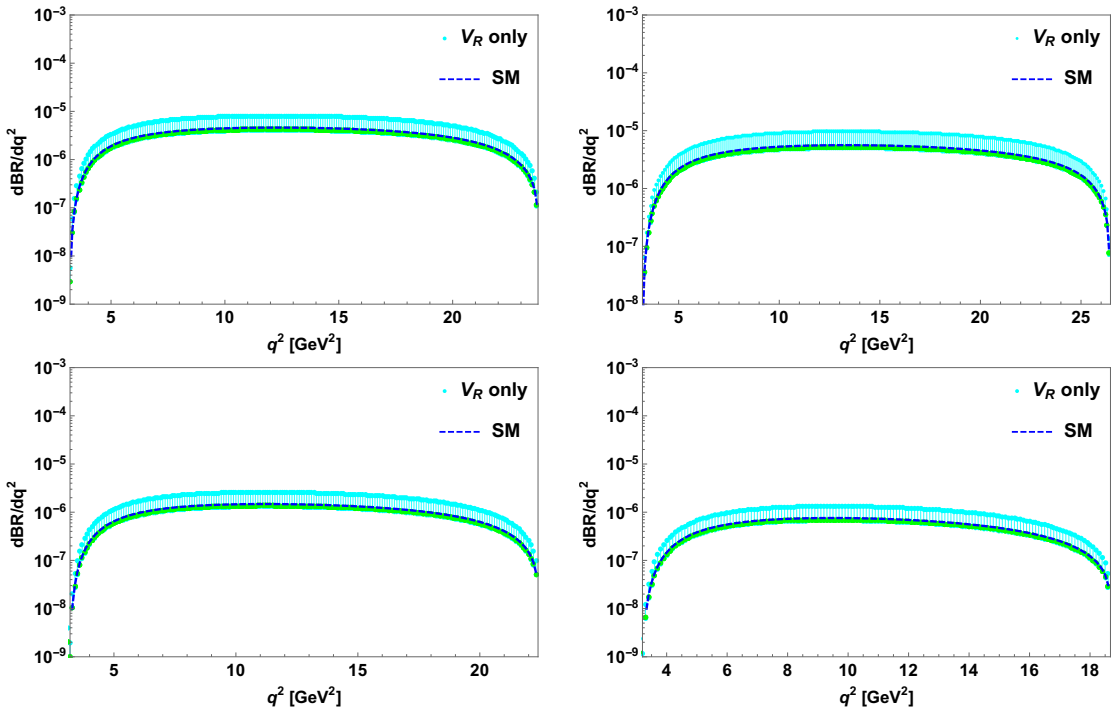

FIGURE 2.7: The plots for the branching ratios of $B_s \to K^+\tau^-\bar{\nu}_\tau$ (top-left panel), $\bar{B}^0 \to \pi^+\tau^-\bar{\nu}_\tau$ (top-right panel), $B^- \to \eta\tau^-\bar{\nu}_\tau$ (bottom-left panel) and $B^- \to \eta'\tau^-\bar{\nu}_\tau$ (bottom-right panel) processes for the NP contribution of only V_R coupling. Here the cyan bands are for the V_R NP coupling contributions.

of S_L are found to be $(\mathrm{Re}[S_L], \mathrm{Im}[S_L])^{\max} = (-0.163, 0.252)$ and $(\mathrm{Re}[S_L], \mathrm{Im}[S_L])^{\min} = (0.017, 0.176)$ and the corresponding 1σ range of allowed parameter space is shown in the right panel of Fig. 2.3. Including the additional contributions from S_L coupling, the obtained branching ratios for various processes are listed in Table 2.4. It is observed that the branching ratios of $\bar{B}_{(s)} \to P^+\tau^-\bar{\nu}_\tau$ processes comparatively deviate more than the corresponding processes with muon in the final state.

Fig. 2.9 represents the q^2 variation of the forward-backwad asymmetry of $\bar{B}_s \to K^+\mu^-\bar{\nu}_\mu$ (top-left panel), $\bar{B}^0 \to \pi^+\mu^-\bar{\nu}_\mu$ (top-right panel), $B^- \to \eta\mu^-\bar{\nu}_\mu$ (bottom-left panel) and $B^- \to \eta'\mu^-\bar{\nu}_\mu$ (bottom-right panel) processes for only S_L coupling. The corresponding plots for $\bar{B}_{(s)} \to P\tau\bar{\nu}_\tau$ processes are given in Fig. 2.10. Due to the additional S_L contribution, the forward-backward asymmetry parameters of these processes deviate significantly from SM. The corresponding integrated values are presented in Table 2.4. Fig. 2.11 represents the plots for the LNU parameters $R_K^{\tau\mu}(q^2)$ (top-left panel), $R_\pi^{\tau\mu}(q^2)$ (top-right panel), $R_\eta^{\tau\mu}(q^2)$ (bottom-left panel) and $R_{\eta'}^{\tau\mu}(q^2)$ (bottom-right panel) verses q^2. The variation of $R_{\pi K}^{\tau}$, $R_{\pi\eta^{(\prime)}}^{\tau}$ parameters with respect to q^2 are shown in Fig. 2.12. In Table 2.5, we give the numerical values of these parameters.

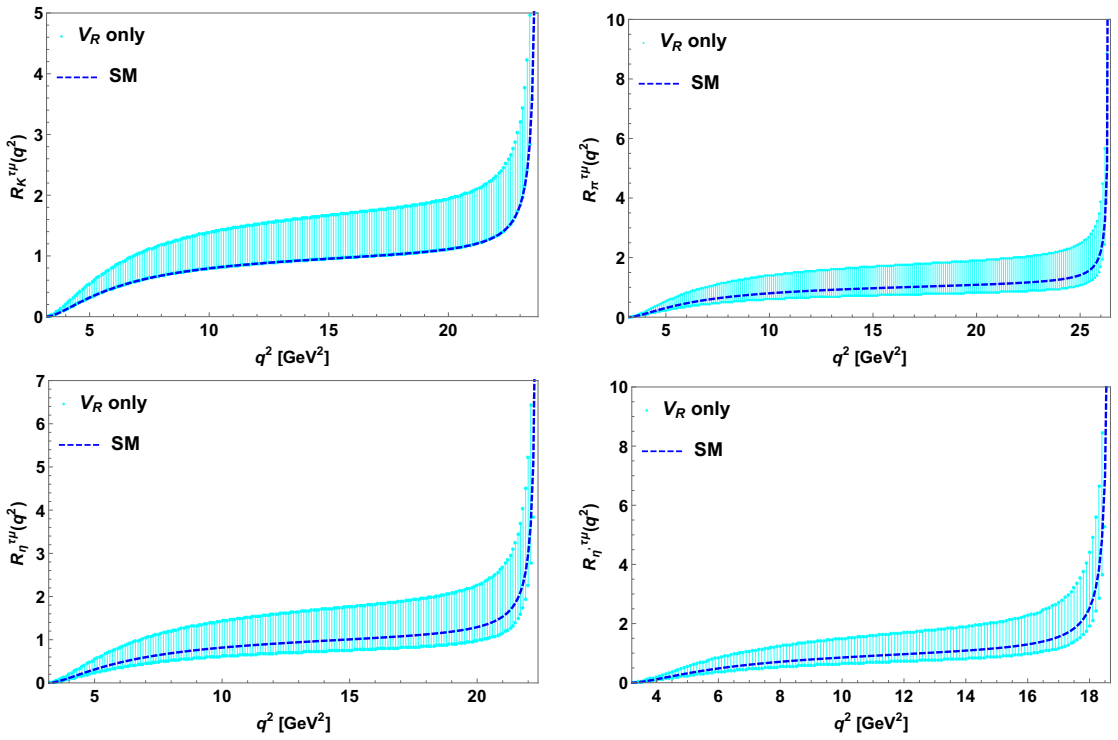

FIGURE 2.8: The plots for the LNU parameters $R_K^{\tau\mu}(q^2)$ (top-left panel), $R_\pi^{\tau\mu}(q^2)$ (top-right panel), $R_\eta^{\tau\mu}(q^2)$ (bottom-left panel) and $R_{\eta'}^{\tau\mu}(q^2)$ (bottom-right panel).

2.2.4 Case D: Effect of S_R only

Here we perform an analysis of $B \to Pl^-\bar{\nu}_l$ processes with the additional S_R coupling. As discussed in section 2.1.1, the real part of S_R coupling differs from the real part of S_L by a negative sign while their imaginary parts are same. The minimum and maximum values of S_R parameter are found as $(\mathrm{Re}[S_R], \mathrm{Im}[S_R])^{\max} = (0.003, 0.268)$ and $(\mathrm{Re}[S_R], \mathrm{Im}[S_R])^{\min} = (-0.54, -0.03)$ for $b \to u\tau\bar{\nu}_\tau$ process. For $b \to u\mu\nu_\mu$ the constraints on S_R couplings are same as S_L. Using these value the q^2 variation of the forward-backward asymmetries for $B^- \to P^0\tau^-\bar{\nu}_\tau$ processes are shown in Fig. 2.13. The branching ratios and forward-backward asymmetries of these processes are presented in Table 2.4. Fig. 2.14 represents the variation of the LNU parameters ($R_{K,\pi,\eta,\eta'}^{\tau\mu}$) due to only S_R coupling. The variation of $R_{PP'}^{\tau}$ parameters are similar to those with S_L coupling. Table 2.5 contains the numerical values of these parameters.

The rare semileptonic $B_s \to Kl\bar{\nu}_l$ and $B \to \pi l\bar{\nu}_l$ processes are investigated in Refs. [31, 42]. The analysis of $B \to \pi l\bar{\nu}_l$ processes using the light cone QCD sume rule approach [31] and 2HDM [43] are also studied in the literature. In Ref. [44–46], $B \to \eta^{(\prime)} l\bar{\nu}_l$ processes are studied by using various model-dependent approaches. The model independent analysis of $b \to ul\bar{\nu}_l$ processes can be found in [47]. Our predicted SM values of the branching ratios of $\bar{B}_{(s)} \to P^+l^-\bar{\nu}_l$ processes are found to be consistent

TABLE 2.2: The predicted branching ratios and forward-backward asymmetries of $\bar{B}_{(s)} \to Pl\bar{\nu}_l$ processes, where $P = K, \pi, \eta^{(\prime)}$ and $l = \mu, \tau$ in the SM and in the presence of $V_{L,R}$ NP couplings.

Observables	SM values	Values for V_L	Values for V_R
$\text{BR}(\bar{B}_s \to K^+\mu^-\bar{\nu}_\mu)$	$(1.03 \pm 0.08) \times 10^{-4}$	$(1.03 - 1.22) \times 10^{-4}$	$(1.03 - 1.22) \times 10^{-4}$
$\text{BR}(\bar{B}_s \to K^+\tau^-\bar{\nu}_\tau)$	$(6.7 \pm 0.54) \times 10^{-5}$	$(0.48 - 1.24) \times 10^{-4}$	$(0.6 - 1.17) \times 10^{-4}$
$\langle A_{FB}^{\mu} \rangle$	$(2.98 \pm 0.24) \times 10^{-3}$	2.98×10^{-3}	2.98×10^{-3}
$\langle A_{FB}^{\tau} \rangle$	0.275 ± 0.022	0.275	0.275
$\text{BR}(\bar{B} \to \pi^+\mu^-\bar{\nu}_\mu)$	$(1.35 \pm 0.1) \times 10^{-4}$	$(1.35 - 1.59) \times 10^{-4}$	$(1.35 - 1.59) \times 10^{-4}$
$\text{BR}(\bar{B} \to \pi^+\tau^-\bar{\nu}_\tau)$	$(9.4 \pm 0.75) \times 10^{-5}$	$(0.67 - 1.75) \times 10^{-4}$	$(0.82 - 1.62) \times 10^{-4}$
$\langle A_{FB}^{\mu} \rangle$	$(2.94 \pm 0.235) \times 10^{-3}$	2.94×10^{-3}	2.94×10^{-3}
$\langle A_{FB}^{\tau} \rangle$	(0.27 ± 0.021)	0.27	0.27
$\text{BR}(B^- \to \eta\mu^-\bar{\nu}_\mu)$	$(3.14 \pm 0.25) \times 10^{-5}$	$(3.143 - 3.7) \times 10^{-5}$	$(3.143 - 3.7) \times 10^{-5}$
$\text{BR}(B^- \to \eta\tau^-\bar{\nu}_\tau)$	$(1.96 \pm 0.16) \times 10^{-5}$	$(1.4 - 3.64) \times 10^{-5}$	$(1.75 - 3.43) \times 10^{-5}$
$\langle A_{FB}^{\mu} \rangle$	$(3.45 \pm 0.276) \times 10^{-3}$	3.45×10^{-3}	3.45×10^{-3}
$\langle A_{FB}^{\tau} \rangle$	(0.292 ± 0.023)	0.292	0.292
$\text{BR}(B^- \to \eta'\mu^-\bar{\nu}_\mu)$	$(1.45 \pm 0.12) \times 10^{-5}$	$(1.45 - 1.7) \times 10^{-5}$	$(1.45 - 1.7) \times 10^{-5}$
$\text{BR}(B^- \to \eta'\tau^-\bar{\nu}_\tau)$	$(7.81 \pm 0.06) \times 10^{-6}$	$(0.56 - 1.45) \times 10^{-5}$	$(0.695 - 1.37) \times 10^{-5}$
$\langle A_{FB}^{\mu} \rangle$	$(4.1 \pm 0.33) \times 10^{-3}$	4.1×10^{-3}	4.1×10^{-3}
$\langle A_{FB}^{\tau} \rangle$	(0.317 ± 0.026)	0.317	0.317

TABLE 2.3: The predicted values of various parameters ($R_P^{\tau\mu}$ and $R_{PP'}^{l}$) of $\bar{B}_{(s)} \to Pl\bar{\nu}_l$ processes in the SM and in the presence of $V_{L,R}$ NP couplings.

Observables	Values in the SM	Values for V_L coupling	Values for V_R coupling
$R_K^{\tau\mu}$	0.649	$0.46 - 1.02$	$0.489 - 1.13$
$R_\pi^{\tau\mu}$	0.7	$0.497 - 1.1$	$0.528 - 1.22$
$R_\eta^{\tau\mu}$	0.624	$0.45 - 0.982$	$0.47 - 1.09$
$R_{\eta'}^{\tau\mu}$	0.54	$0.385 - 0.85$	$0.408 - 0.946$
$R_{\pi K}^{\mu}$	1.31	$1.3 - 1.31$	$1.3 - 1.31$
$R_{\pi\eta}^{\mu}$	4.3	4.3	4.3
$R_{\pi\eta'}^{\mu}$	9.3	$9.3 - 9.35$	$9.3 - 9.35$
$R_{\pi K}^{\tau}$	1.4	$1.4 - 1.41$	$1.373 - 1.39$
$R_{\pi\eta}^{\tau}$	4.8	$4.785 - 4.808$	$4.709 - 4.723$
$R_{\pi\eta'}^{\tau}$	12.0	$11.96 - 12.1$	$11.82 - 11.86$

with the predicted results in the literature, though due to updated input parameters, the central values of the branching ratios of these processes have slight deviations.

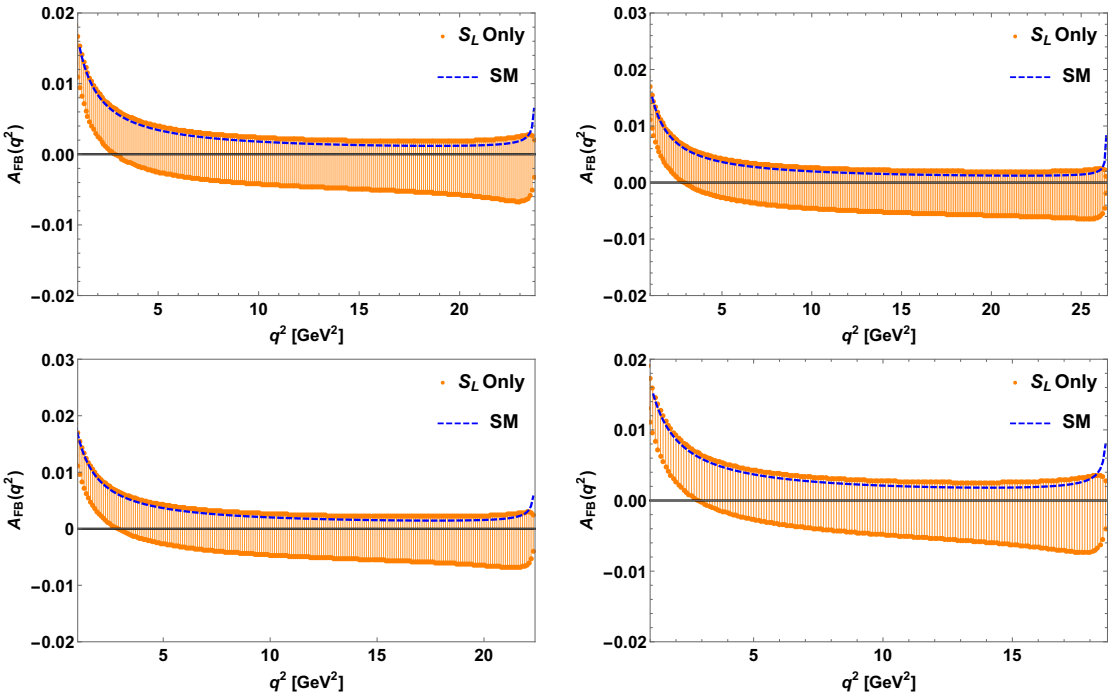

FIGURE 2.9: The plots for the q^2 variation of forward-backward asymmetry of $\bar{B}_s \to K^+\mu^-\bar{\nu}_\mu$ (top-left panel), $\bar{B}^0 \to \pi^+\mu^-\bar{\nu}_\mu$ (top-right panel), $B^- \to \eta\mu^-\bar{\nu}_\mu$ (bottom-left panel) and $B^- \to \eta'\mu^-\bar{\nu}_\mu$ (bottom-right panel) processes.

2.3 $B \to V l \bar{\nu}_l$ processes

In this section, we study the $B \to V l \bar{\nu}_l$ processes, where $V = K^*, \rho$. The hadronic matrix element of the $B \to V l \bar{\nu}_l$ processes can be parametrized as [30]

$$\begin{aligned}
\left\langle V(k,\varepsilon)|\bar{u}\gamma_\mu b|\bar{B}(p_B)\right\rangle &= -i\epsilon_{\mu\nu\rho\sigma}\varepsilon^{\nu *}p_B^\rho k^\sigma \frac{2V(q^2)}{M_B+M_V}\,, \\
\left\langle V(k,\varepsilon)|\bar{u}\gamma_\mu\gamma_5 b|\bar{B}(p_B)\right\rangle &= \varepsilon^{\mu *}\left(M_B+M_V\right)A_1(q^2) - (p_B+k)_\mu\,(\varepsilon^*\cdot q)\frac{A_2(q^2)}{M_B+M_V} \\
&- q_\mu(\varepsilon^*\cdot q)\frac{2M_V}{q^2}\left[A_3(q^2)-A_0(q^2)\right], \qquad (2.17)
\end{aligned}$$

where

$$A_3(q^2) = \frac{M_B+M_V}{2M_V}A_1(q^2) - \frac{M_B-M_V}{2M_V}A_2(q^2)\,. \qquad (2.18)$$

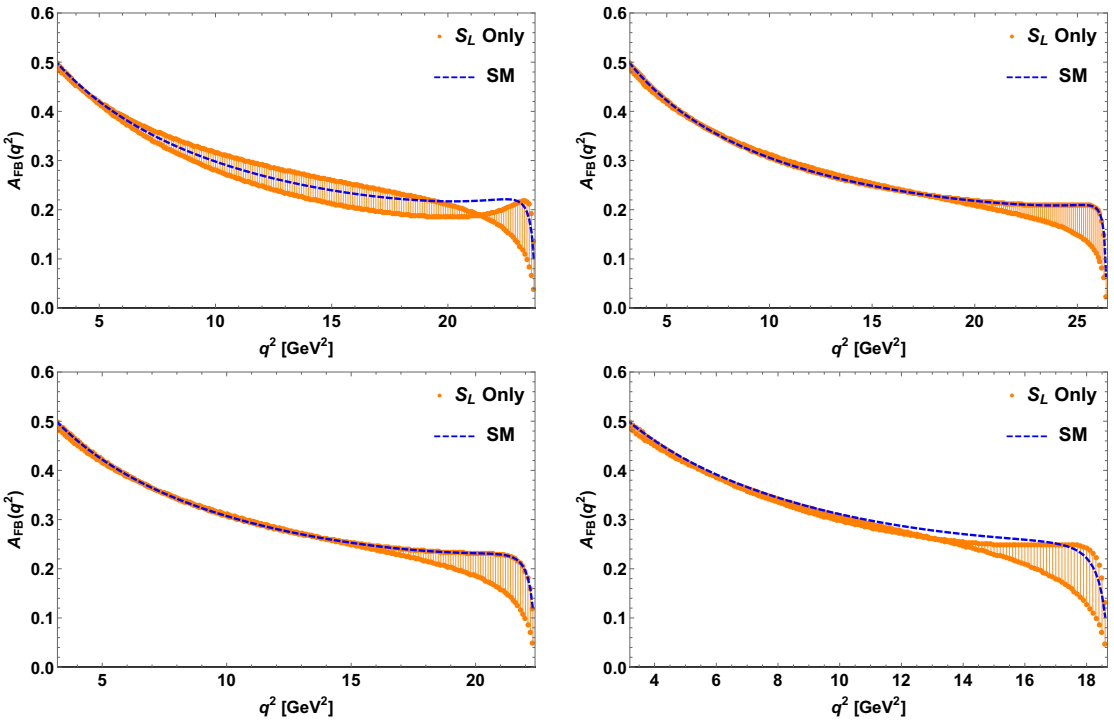

FIGURE 2.10: The plots for the q^2 variation of forward-backward asymmetry of $\bar{B}_s \to K^+\tau^-\bar{\nu}_\tau$ (top-left panel), $\bar{B}^0 \to \pi^+\tau^-\bar{\nu}_\tau$ (top-right panel), $B^- \to \eta\tau^-\bar{\nu}_\tau$ (bottom-left panel) and $B^- \to \eta'\tau^-\bar{\nu}_\tau$ (bottom-right panel) processes.

The differential decay rate of $B \to Vl\nu_l$ processes with respect to q^2 is given by [30]

$$\begin{aligned}
\frac{d\Gamma(B \to Vl\bar{\nu}_l)}{dq^2} &= \frac{G_F^2|V_{ub}|^2}{192\pi^3 M_B^3} q^2 \sqrt{\lambda_V(q^2)} \left(1 - \frac{m_l^2}{q^2}\right)^2 \Bigg\{ (|1+V_L|^2 + |V_R|^2) \\
&\times \left[\left(1 + \frac{m_l^2}{2q^2}\right)(H_{V,+}^2 + H_{V,-}^2 + H_{V,0}^2) + \frac{3}{2}\frac{m_l^2}{q^2} H_{V,t}^2\right] \\
&- 2\mathrm{Re}[(1+V_L)V_R^*] \left[\left(1 + \frac{m_l^2}{2q^2}\right)(H_{V,0}^2 + 2H_{V,+}H_{V,-}) + \frac{3}{2}\frac{m_l^2}{q^2} H_{V,t}^2\right] \\
&+ \frac{3}{2}|S_L - S_R|^2 H_S^2 \\
&+ 3\mathrm{Re}[(1 + V_L - V_R)(S_L^* - S_R^*)] \frac{m_l}{\sqrt{q^2}} H_S H_{V,t} \Bigg\}, \qquad (2.19)
\end{aligned}$$

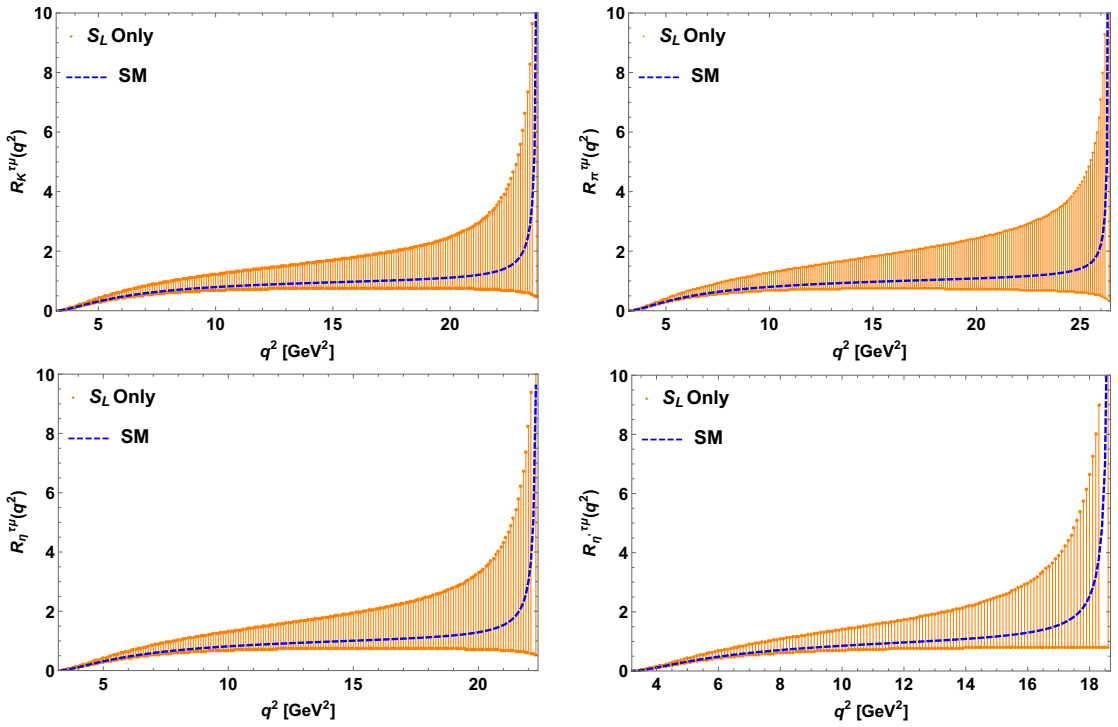

FIGURE 2.11: The plots for the LNU parameters $R_K^{\tau\mu}(q^2)$ (top-left panel), $R_\pi^{\tau\mu}(q^2)$ (top-right panel), $R_\eta^{\tau\mu}(q^2)$ (bottom-left panel) and $R_{\eta'}^{\tau\mu}(q^2)$ (bottom-right panel) due to S_L coupling.

where $\lambda_V = \lambda(M_B^2, M_V^2, q^2)$ and the hadronic amplitudes in terms of the form factors are given as

$$
\begin{aligned}
H_{V,\pm}(q^2) &= (M_B + M_V)\, A_1(q^2) \mp \frac{\sqrt{\lambda_V(q^2)}}{M_B + M_V} V(q^2), \\
H_{V,0}(q^2) &= \frac{M_B + M_V}{2M_V\sqrt{q^2}} \Big[-\left(M_B^2 - M_V^2 - q^2\right) A_1(q^2) + \frac{\lambda_V(q^2)}{(M_B + M_V)^2} A_2(q^2) \Big], \\
H_{V,t}(q^2) &= -\sqrt{\frac{\lambda_V(q^2)}{q^2}} A_0(q^2), \\
H_S(q^2) &= -H_{S_2}^0(q^2) \simeq -\frac{\sqrt{\lambda_V(q^2)}}{m_b + m_u} A_0(q^2).
\end{aligned} \tag{2.20}
$$

For the momentum transfer dependence of the form factors, we consider the most intuitive and the simplest parametrization of the $B_{(s)} \to (K^*)\rho$ form factors, $(V(q^2), A_{0,1,2}(q^2))$ from Ref. [48]. The masses of all the particles are taken from [27]. Using these input values and the bounds on V_L coupling obtained from $B_u^+ \to \tau^+\nu_\tau$ and $B^- \to \pi^0\mu^-\bar{\nu}_\mu$ processes (discussed in sections 2.1.1 and 2.2.1), we show the plots for the q^2 variation of branching ratios for $\bar{B}_s \to K^{*+}\mu^-\bar{\nu}_\mu$ (top-left panel) and $\bar{B}_s \to K^{*+}\tau^-\bar{\nu}_\tau$ (top-right panel) processes in the presence of V_L in Fig. 2.15. The corresponding plots in the bottom panel of this figure are for V_R coupling. In the presence of V_R coupling, we found reasonable deviation of the branching ratios from the SM predictions, whereas V_L

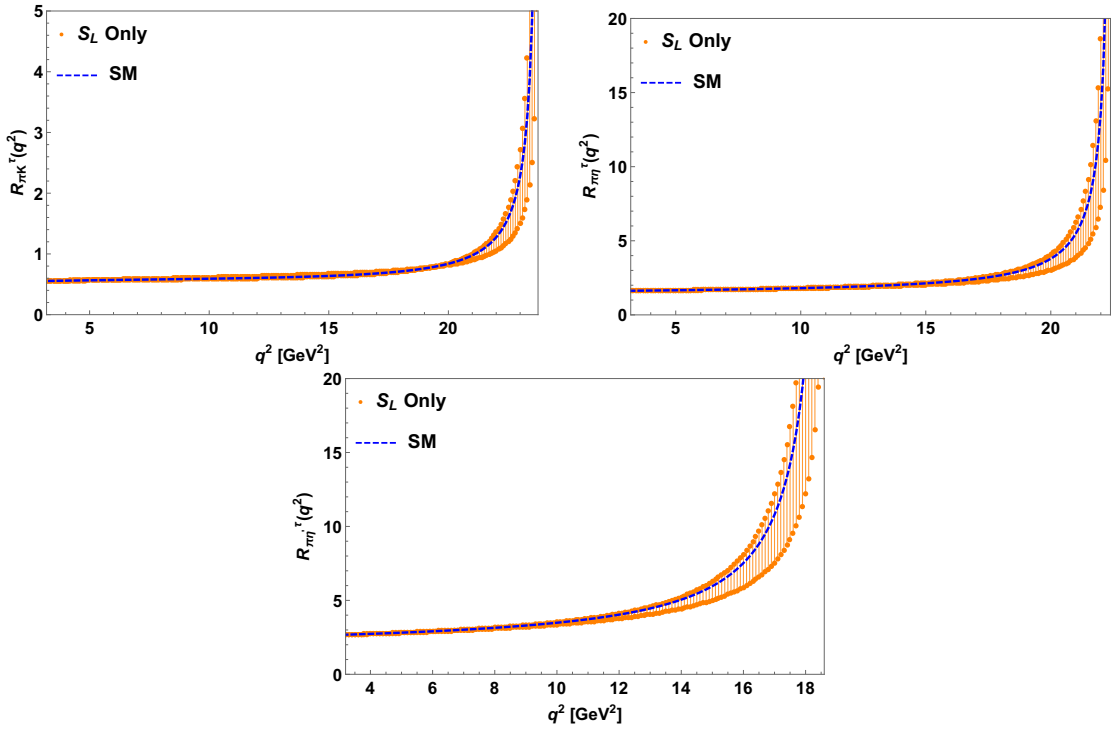

FIGURE 2.12: The plots for $R^{\tau}_{\pi K}(q^2)$ (top-left panel), $R^{\tau}_{\pi\eta}(q^2)$ (top-right panel) and $R^{\tau}_{\pi\eta'}(q^2)$ (bottom panel) parameters.

affects mainly $\bar{B}_s \to K^{*+}\tau^-\bar{\nu}_\tau$ process. In the top-left panel of Fig. 2.16, we show the q^2 variation of forward-backward asymmetries of $B_s \to K^{*+}\mu^-\bar{\nu}_\mu$ processes for V_R coupling. The forward-backward asymmetry of $B_s \to K^{*+}\tau^-\bar{\nu}_\tau$ processes for V_R (top-right panel), S_L (bottom-left panel) and S_R (bottom-right panel) couplings are presented in Fig. 2.16. We found significant deviation in the forward-backward asymmetry parameters from SM values due to the additional V_R and $S_{L,R}$ couplings. The presence of V_L coupling does not affect the forward-backward asymmetry parameters. As seen from the figure, due to $S_{L,R}$ couplings, the forward-backward asymmetry of $\bar{B}_s \to K^{*+}\tau^-\bar{\nu}_\tau$ process receives significant deviation from its SM values, whereas the deviation is negligible for $\bar{B}_s \to K^{*+}\mu^-\bar{\nu}_\mu$ process. The integrated values of the branching ratios and the forward-backward asymmetries for $V_{L,R}$ and $S_{L,R}$ couplings are presented in Table 2.6 and 2.7 respectively. In Fig. 2.17, we present the plots for the $R^{\tau\mu}_{K^*}(q^2)$ parameters for V_L (top-left panel), V_R (top-right panel), S_L (bottom-left panel) and S_R (bottom-right panel) couplings and the corresponding integrated values are presented in Table 2.8.

The q^2 variation of the branching ratios of $\bar{B} \to \rho^+ l^- \bar{\nu}_l$ processes for $V_{L,R}$ couplings are presented in Fig. 2.18. In the presence of $S_{L,R}$ couplings, the branching ratios of $\bar{B} \to \rho^+ l^- \bar{\nu}_l$ processes have negligible deviation from the SM predictions. The predicted values of the branching ratios of these processes are given in Table VI and VII respectively.

TABLE 2.4: Same as Table 2.2 in the presence of $S_{L,R}$ NP couplings.

Observables	Values for S_L coupling	Values for S_R coupling
$\mathrm{BR}(B_s \to K^+\mu^-\bar{\nu}_\mu)$	$(1.1 - 1.15) \times 10^{-4}$	$(1.1 - 1.15) \times 10^{-4}$
$\mathrm{BR}(B_s \to K^+\tau^-\bar{\nu}_\tau)$	$(0.62 - 1.29) \times 10^{-4}$	$(4.97 - 7.4) \times 10^{-5}$
$\langle A_{FB}^{\mu} \rangle$	$(-3.32 \to 3.52) \times 10^{-3}$	$(-3.32 \to 3.52) \times 10^{-3}$
$\langle A_{FB}^{\tau} \rangle$	$0.255 - 0.272$	$0.058 - 0.26$
$\mathrm{BR}(\bar{B} \to \pi^+\mu^-\bar{\nu}_\mu)$	$(1.39 - 1.49) \times 10^{-4}$	$(1.39 - 1.49) \times 10^{-4}$
$\mathrm{BR}(\bar{B} \to \pi^+\tau^-\bar{\nu}_\tau)$	$(0.82 - 1.93) \times 10^{-4}$	$(0.66 - 1.02) \times 10^{-4}$
$\langle A_{FB}^{\mu} \rangle$	$(-3.86 \to 3.51) \times 10^{-3}$	$(-3.86 \to 3.51) \times 10^{-3}$
$\langle A_{FB}^{\tau} \rangle$	$0.25 - 0.27$	$0.0264 - 0.2468$
$\mathrm{BR}(B^- \to \eta^0\mu^-\bar{\nu}_\mu)$	$(3.28 - 3.44) \times 10^{-5}$	$(3.28 - 3.44) \times 10^{-5}$
$\mathrm{BR}(B^- \to \eta^0\tau^-\bar{\nu}_\tau)$	$(1.74 - 3.82) \times 10^{-5}$	$(1.32 - 2.12) \times 10^{-5}$
$\langle A_{FB}^{\mu} \rangle$	$(-3.39 \to 4.0) \times 10^{-3}$	$(-3.39 \to 4.0) \times 10^{-3}$
$\langle A_{FB}^{\tau} \rangle$	$0.27 - 0.277$	$0.085 - 0.272$
$\mathrm{BR}(B^- \to \eta'^0\mu^-\bar{\nu}_\mu)$	$(1.49 - 1.55) \times 10^{-5}$	$(1.49 - 1.55) \times 10^{-5}$
$\mathrm{BR}(B^- \to \eta'^0\tau^-\bar{\nu}_\tau)$	$(0.7 - 1.46) \times 10^{-5}$	$(5.0 - 8.33) \times 10^{-6}$
$\langle A_{FB}^{\mu} \rangle$	$(-2.82 \to 4.68) \times 10^{-3}$	$(-2.92 \to 4.68) \times 10^{-3}$
$\langle A_{FB}^{\tau} \rangle$	$0.287 - 0.31$	$0.153 - 0.298$

TABLE 2.5: Same as Table 2.3 in the presence of $S_{L,R}$ NP couplings.

Observables	Values for S_L coupling	Values for S_R coupling
$R_K^{\tau\mu}$	$0.537 - 1.17$	$0.45 - 0.645$
$R_\pi^{\tau\mu}$	$0.55 - 1.38$	$0.47 - 0.685$
$R_\eta^{\tau\mu}$	$0.5 - 1.16$	$0.4 - 0.62$
$R_{\eta'}^{\tau\mu}$	$0.448 - 0.976$	$0.33 - 0.538$
$R_{\pi K}^{\mu}$	$1.263 - 1.3$	$1.263 - 1.3$
$R_{\pi\eta}^{\mu}$	$4.238 - 4.33$	$4.238 - 4.33$
$R_{\pi\eta'}^{\mu}$	$9.329 - 9.61$	$9.329 - 9.61$
$R_{\pi K}^{\tau}$	$1.32 - 1.5$	$1.328 - 1.378$
$R_{\pi\eta}^{\tau}$	$4.71 - 5.05$	$4.81 - 5.0$
$R_{\pi\eta'}^{\tau}$	$11.71 - 13.22$	$12.45 - 13.2$

The experimental branching ratio of $B^+ \to \rho^0 l^+ \nu_l$ process is [27]

$$\mathrm{BR}(B^+ \to \rho^0 l^+ \nu_l)^{\mathrm{Expt}} = (1.58 \pm 0.11) \times 10^{-4}. \tag{2.21}$$

Our predicted results for $B^- \to \rho^0\mu^-\bar{\nu}_\mu$ process is consistent with the above experimental data (though a part of the allowed parameter space of $V_{L,R}$ and $S_{L,R}$ give values on the higher side of the observed central value). The forward-backward asymmetry plots for $\bar{B} \to \rho^+ l^- \bar{\nu}_l$ are presented in Fig. 2.19 and the corresponding numerical values are given in Table 2.6 and 2.7. Fig. 2.20 represents the plots of LNU parameter $R_\rho^{\tau\mu}(q^2)$ for V_L (top-left panel), V_R (top-right panel), S_L (bottom-left panel) and S_R (bottom-right panel) couplings. In Fig. 2.21, we show the variation of the parameter $R_{\rho K^*}^{\tau}(q^2)$ with

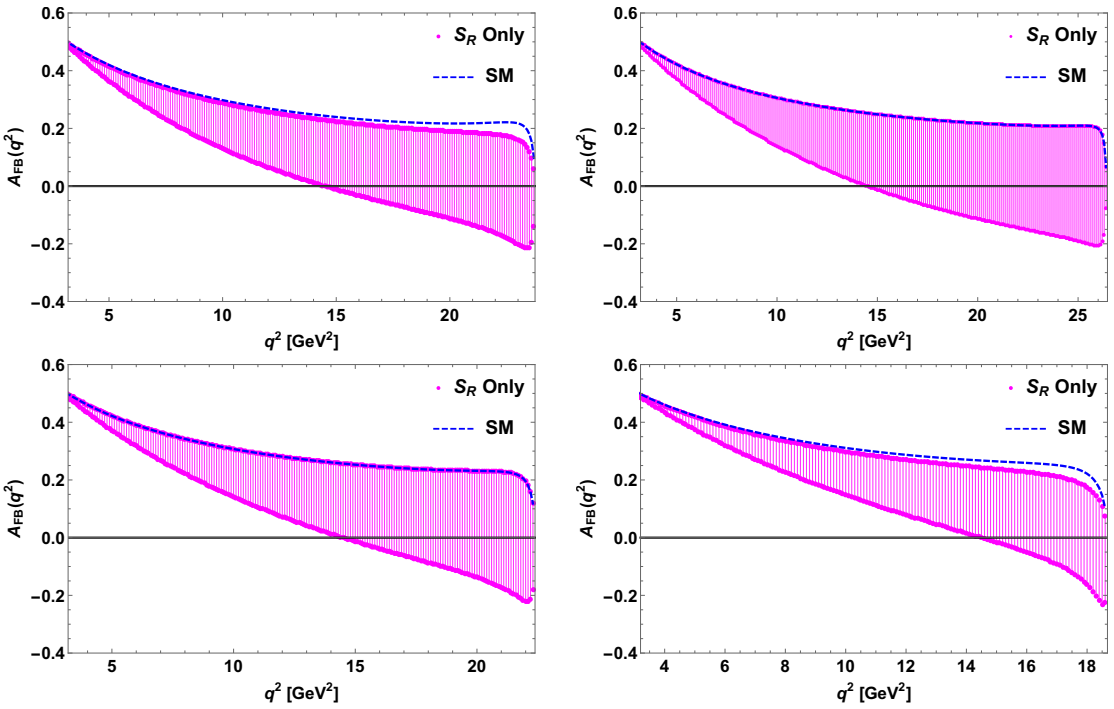

FIGURE 2.13: The plots for the q^2 variation of forward-backward asymmetry of $\bar{B}_s \to K^+\tau^-\bar{\nu}_\tau$ (top-left panel), $\bar{B}^0 \to \pi^+\tau^-\bar{\nu}_\tau$ (top-right panel), $B^- \to \eta\tau^-\bar{\nu}_\tau$ (bottom-left panel) and $B^- \to \eta'\tau^-\bar{\nu}_\tau$ (bottom-right panel) processes.

TABLE 2.6: The predicted branching ratios, forward-backward asymmetries of $\bar{B}_{(s)} \to V^+l^-\bar{\nu}_l$ processes, where $V = K^*, \rho$ and $l = \mu, \tau$ in the SM and for the case of $V_{L,R}$ NP couplings.

Observables	SM prediction	For V_L	For V_R
$\text{BR}(B_s \to K^{*+}\mu^-\bar{\nu}_\mu)$	(3.97 ± 0.32) $\times 10^{-4}$	$(3.97 - 4.68)$ $\times 10^{-4}$	$(3.97 - 8.05)$ $\times 10^{-4}$
$\text{BR}(B_s \to K^{*+}\tau^-\bar{\nu}_\tau)$	(2.16 ± 0.173) $\times 10^{-4}$	$(1.54 - 4.0)$ $\times 10^{-4}$	$(1.92 - 3.8)$ $\times 10^{-4}$
$\langle A_{FB}^{\mu} \rangle$	-0.293 ± 0.023	-0.293	$-0.293 \to -0.052$
$\langle A_{FB}^{\tau} \rangle$	-0.146 ± 0.012	-0.146	$-0.138 \to 0.037$
$\text{BR}(B^- \to \rho^0\mu^-\bar{\nu}_\mu)$	(1.56 ± 0.124) $\times 10^{-4}$	$(1.56 - 1.85)$ $\times 10^{-4}$	$(1.56 - 3.0)$ $\times 10^{-4}$
$\text{BR}(B^- \to \rho^0\tau^-\bar{\nu}_\tau)$	(8.97 ± 0.71) $\times 10^{-5}$	$(0.64 - 1.67)$ $\times 10^{-4}$	$(0.8 - 1.52)$ $\times 10^{-4}$
$\langle A_{FB}^{\mu} \rangle$	-0.362 ± 0.028	-0.362	$-0.362 \to -0.065$
$\langle A_{FB}^{\tau} \rangle$	-0.184 ± 0.015	-0.184	$-0.168 \to 0.024$

respect to q^2 for only S_L (left panel) and S_R (right panel) couplings. The integrated values of these parameters are given in Table 2.8. The additional $V_{L,R}$ couplings don't affect the $R^l_{\rho K^*}$ parameters.

In the literature, the $B \to Vl\nu_l$ processes are investigated in both model-dependent and independent ways [49, 50]. Our findings on these processes are consistent with these

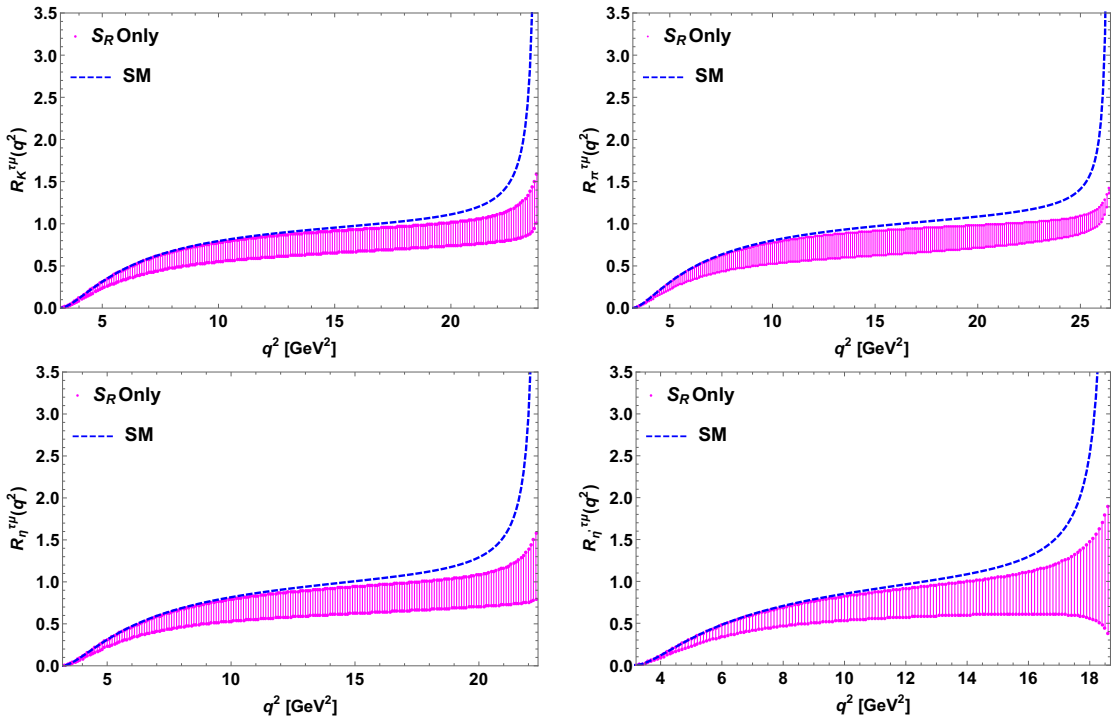

FIGURE 2.14: The plots for the LNU parameters $R_K^{\tau\mu}(q^2)$ (top-left panel), $R_\pi^{\tau\mu}(q^2)$ (top-right panel), $R_\eta^{\tau\mu}(q^2)$ (bottom-left panel) and $R_{\eta'}^{\tau\mu}(q^2)$ (bottom-right panel) due to S_R coupling.

TABLE 2.7: Same as Table 2.6 in the presence of $S_{L,R}$ couplings.

Observables	For S_L coupling	Values for S_R coupling
$\text{BR}(B_s \to K^{*+}\mu^-\bar{\nu}_\mu)$	$(3.97-4.0)\times 10^{-4}$	$(3.97-4.0)\times 10^{-4}$
$\text{BR}(B_s \to K^{*+}\tau^-\bar{\nu}_\tau)$	$(2.1-2.58)\times 10^{-4}$	$(1.99-2.2)\times 10^{-4}$
$\langle A_{FB}^{\mu}\rangle$	$-0.293 \to -0.291$	$-0.293 \to -0.286$
$\langle A_{FB}^{\tau}\rangle$	$-0.169 \to -0.043$	$-0.144 \to -0.056$
$\text{BR}(B^- \to \rho^0\mu^-\bar{\nu}_\mu)$	$(1.57-1.6)\times 10^{-4}$	$(1.57-1.6)\times 10^{-4}$
$\text{BR}(B^- \to \rho^0\tau^-\bar{\nu}_\tau)$	$(0.87-1.12)\times 10^{-4}$	$(8-9.2)\times 10^{-5}$
$\langle A_{FB}^{\mu}\rangle$	$-0.36 \to -0.35$	$-0.36 \to -0.35$
$\langle A_{FB}^{\tau}\rangle$	$-0.21 \to -0.07$	$-0.32 \to -0.18$

predictions.

2.4 Chapter summary

In this chapter we considered the most general effective Lagrangian associated with $B \to (P,V) l \bar{\nu}_l$ decay processes containing additional scalar and vector type of NP couplings in addition to the SM. We constrain the parameter space of these new couplings associated with $b \to u(e,\mu,\tau)$ transitions. within the allowed parameter space of these new couplings we have calculated the differential branching ratio, LNU parameters and

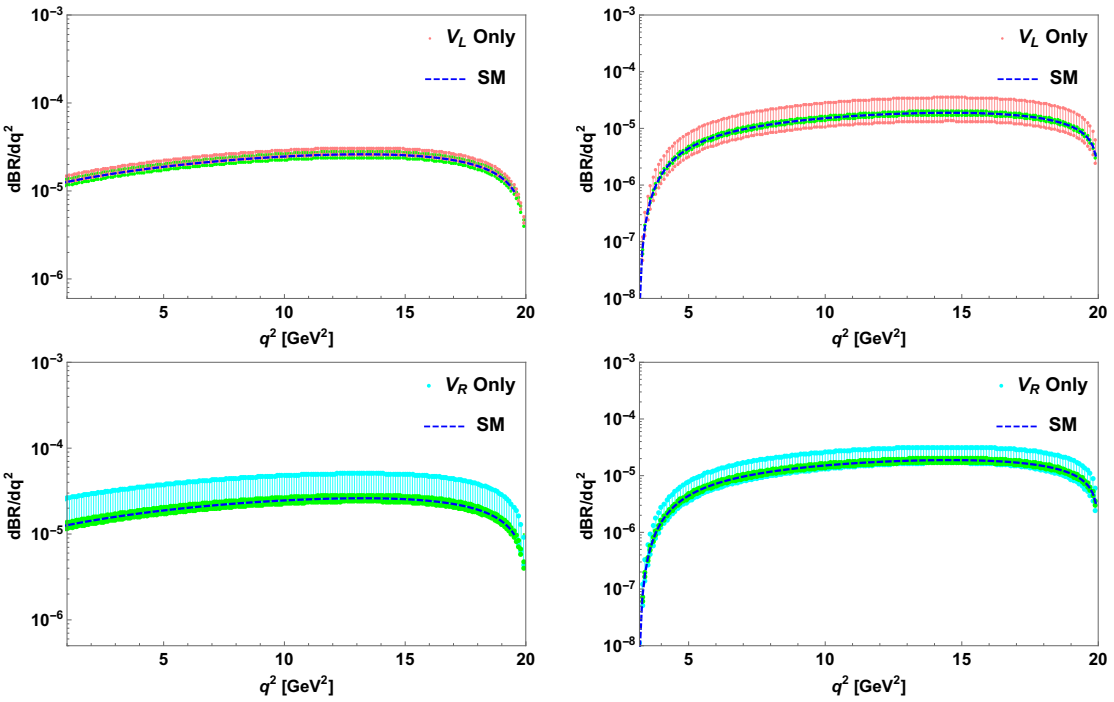

FIGURE 2.15: The plots in the top panel represent the q^2 variation of the branching ratios of $\bar{B}_s \to K^{*+}\mu^-\bar{\nu}_\mu$ (top-left panel) and $\bar{B}_s \to K^{*+}\tau^-\bar{\nu}_\tau$ (top-right panel) processes for only V_L coupling. The corresponding plots for only V_R coupling are shown in the bottom panel.

TABLE 2.8: Values of $R^{\tau\mu}_{K^*}$, $R^{\tau\mu}_{\rho}$, $R^{\mu}_{\rho K^*}$ and $R^{\tau}_{\rho K^*}$ parameters for different cases of NP couplings.

Model	$R^{\tau\mu}_{K^*}$	$R^{\tau\mu}_{\rho}$	$R^{\mu}_{\rho K^*}$	$R^{\tau}_{\rho K^*}$
SM	0.544	0.573	0.393	0.415
V_L	$0.388 - 0.856$	$0.41 - 0.9$	$0.393 - 0.395$	$0.415 - 0.42$
V_R	$0.47 - 0.474$	$0.5 - 0.51$	$0.373 - 0.393$	$0.4 - 0.42$
S_L	$0.522 - 0.646$	$0.542 - 0.712$	$0.393 - 0.4$	$0.414 - 0.434$
S_R	$0.497 - 0.544$	$0.5 - 0.573$	$0.393 - 0.4$	$0.4 - 0.42$

forward backward asymmetry of the considered decay processes. We also present the plots showing the q^2 variation of these parameters associated with several decay processes. In our analysis we show the observed deviation of these parameters from their SM predicted values in presence of individual NP couplings and we got a significant deviation of the considered observables in presence of NP.

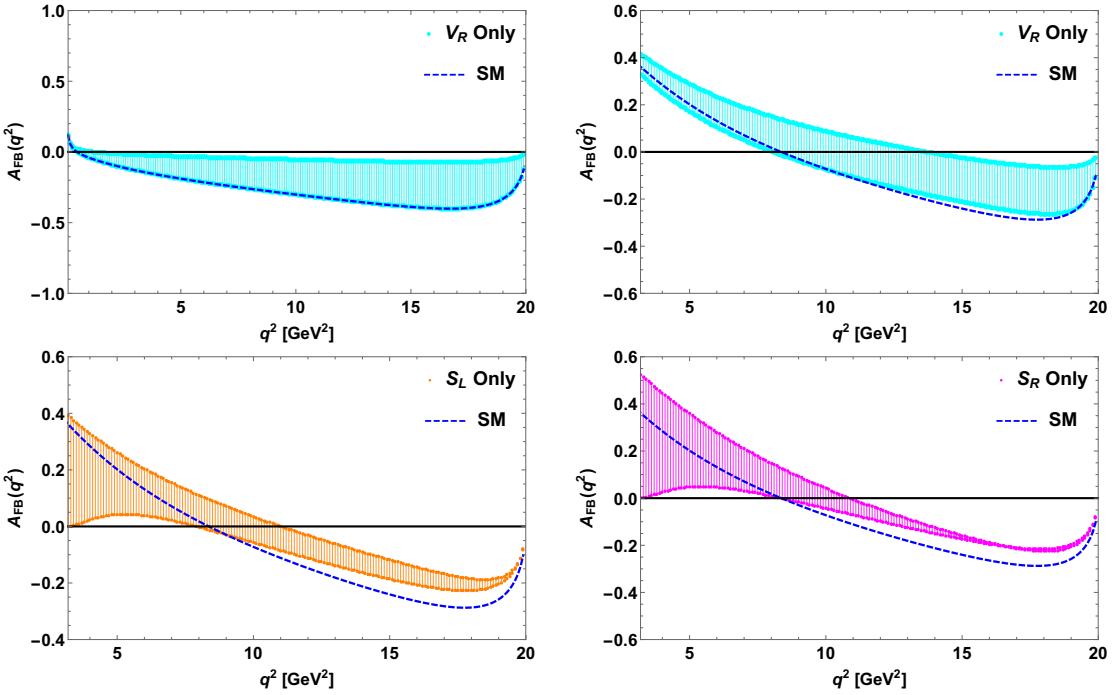

FIGURE 2.16: The plots for the q^2 variations of the forward-backward asymmetry of $\bar{B}_s \to K^{*+}\tau^-\bar{\nu}_\tau$ processes for only V_R (top-right panel), S_L (bottom-left panel) and S_R (bottom-right panel) couplings. The top-left panel represents the plots for the forward-backward asymmetry of $\bar{B}_s \to K^{*+}\mu^-\bar{\nu}_\mu$ processes for only V_R coupling.

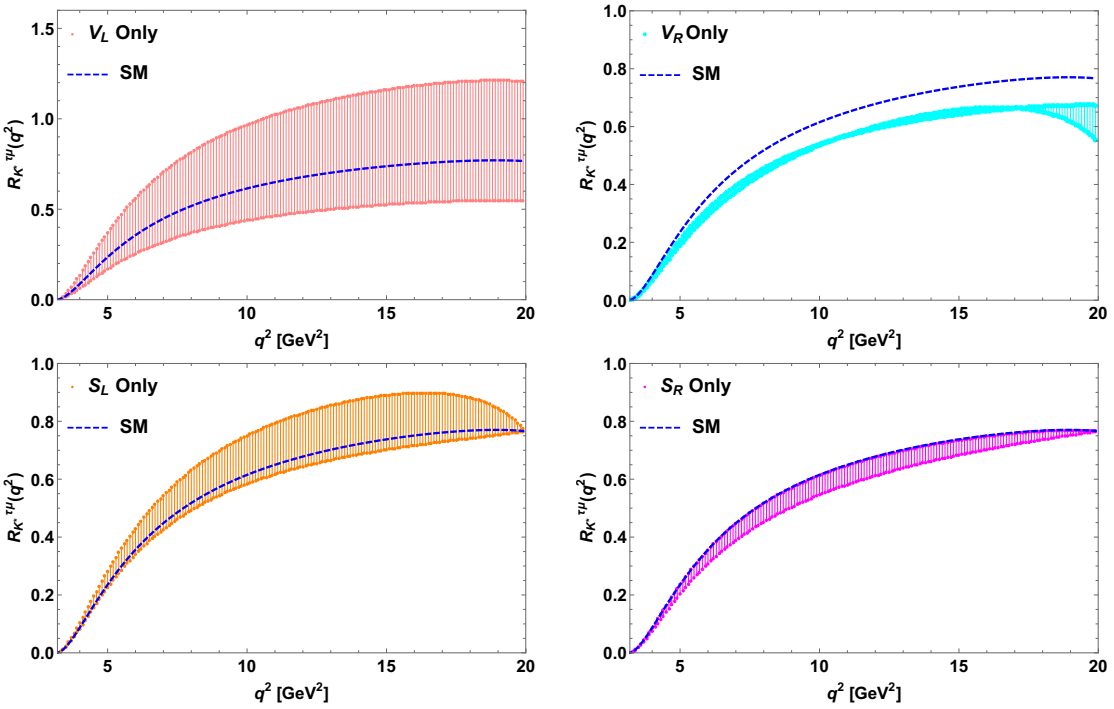

FIGURE 2.17: The plots for $R_{K^*}^{\tau\mu}(q^2)$ parameters verses q^2 for only V_L (top-left panel), V_R (top-right panel), S_L (bottom-left panel) and S_R (bottom-right panel) couplings.

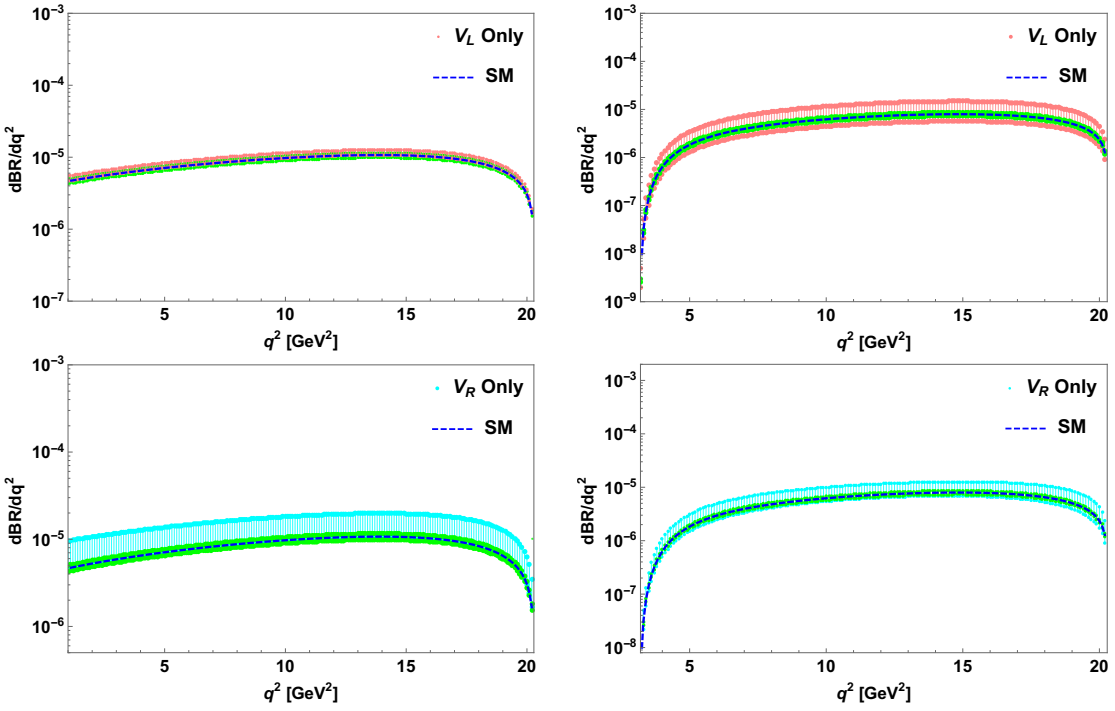

FIGURE 2.18: Same as Fig. 2.15 for $B^- \to \rho^0 l^- \bar{\nu}_l$ processes.

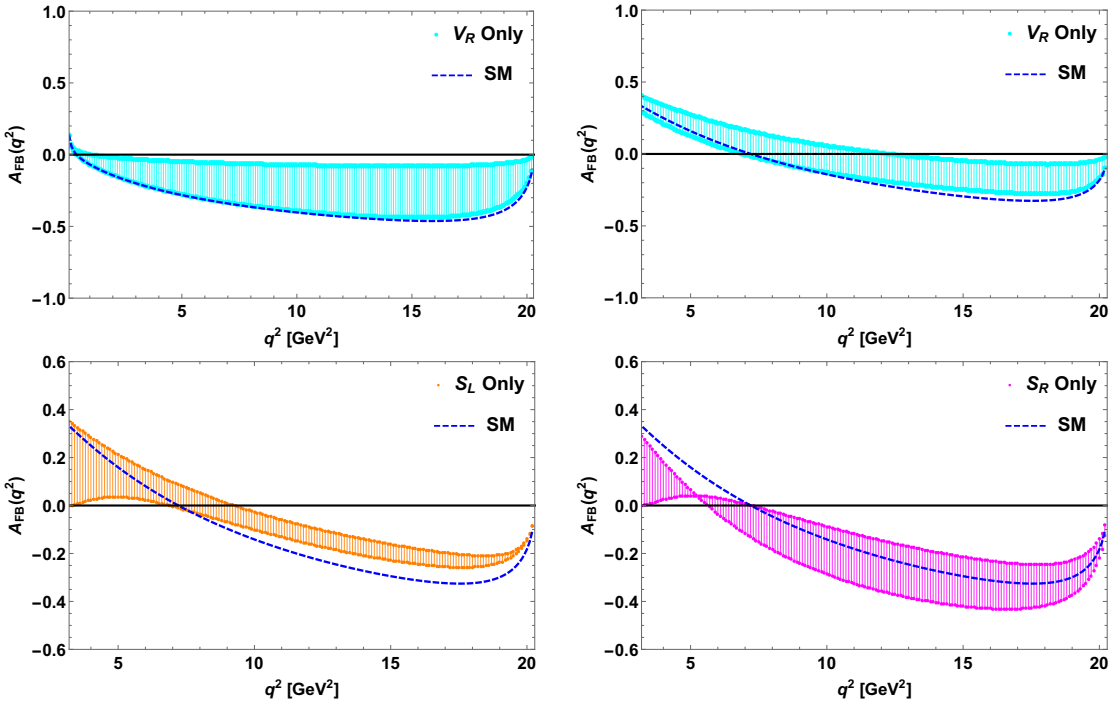

FIGURE 2.19: Same as Fig. 2.16 for $B^- \to \rho^0 l^- \bar{\nu}_l$ processes.

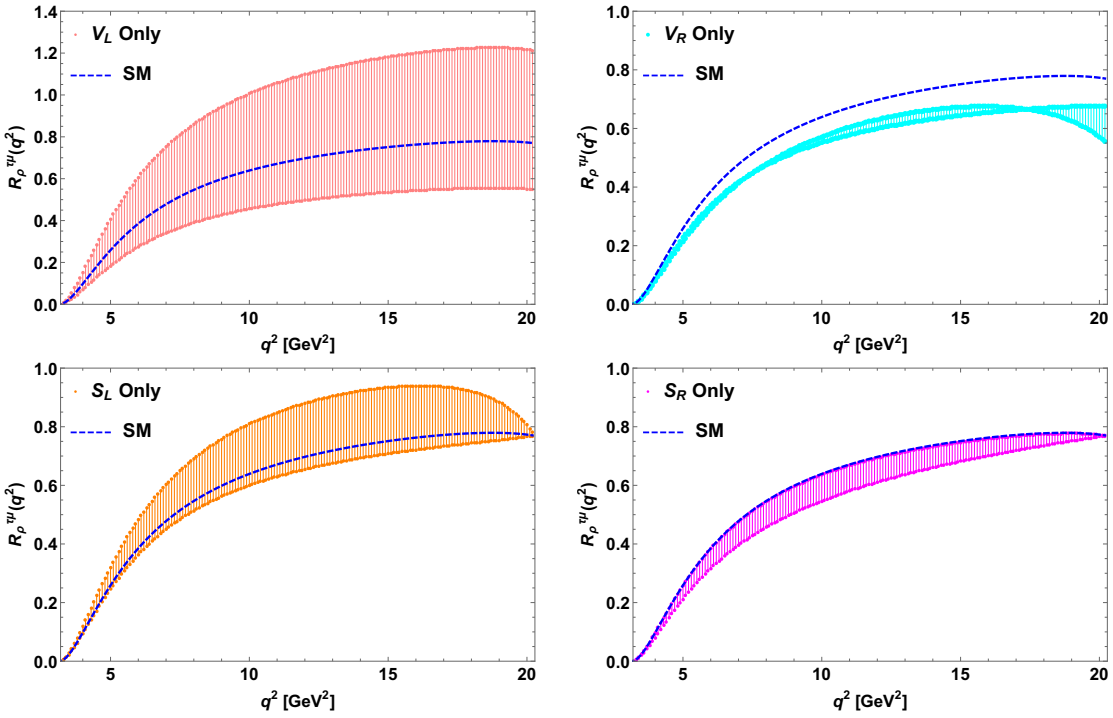

FIGURE 2.20: Same as Fig. 2.17 for $B^- \to \rho^0 l^- \bar{\nu}_l$ processes.

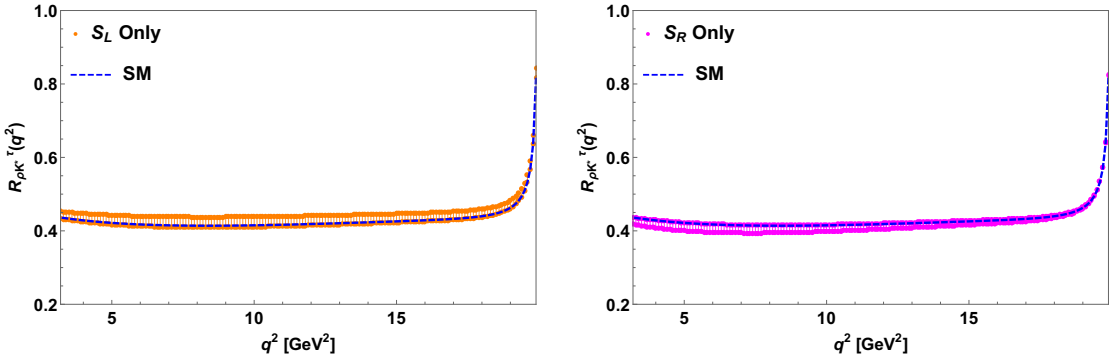

FIGURE 2.21: The plots for $R^{\tau}_{\rho K^*}(q^2)$ parameters verses q^2 for only S_L (left panel) and S_R (right panel) couplings.

Chapter 3

Model independent study of semileptonic Λ_b decays

The number of Λ_b baryon is a major amount (20%) of the total production of hadrons in LHCb[51, 52], making the study of Λ_b fascinating at the present time. The $b \to ql\bar{\nu}_l$ ($q = u, c$) quark level transitions can be probed in both B and Λ_b decays. Similar to B decays we can also look over the presence of lepton universality violation in the corresponding semileptonic baryon decays $\Lambda_b \to (\Lambda_c, p)l\bar{\nu}_l$ to authenticate the results from B sector and thus, to explore the structure of NP. The heavy-heavy and heavy-light semileptonic decays of baryons can serve as an additional source for the determination of the Cabbibo-Kobayashi-Maskawa (CKM) matrix elements V_{qb} [27, 53–55]. In the literature [56–68], the baryonic decay modes mediated by $b \to (u, c)l\bar{\nu}_l$ quark level transitions are studied both in model dependent and independent approaches. The analysis of $\Lambda_b \to \Lambda_c\tau\bar{\nu}_\tau$ decay in the context of SM and various NP couplings has been performed in [58]. In Ref. [60], the SM hadron and lepton polarization asymmetries are computed in the covariant confined quark model. The precise lattice QCD calculation of $\Lambda_b \to (\Lambda_c, p)$ form factors and the investigation of semileptonic baryonic $b \to (u, c)l\bar{\nu}_l$ processes are performed in [61]. Ref. [67] investigates the impact of five possible new physics interactions, adopting five different form factors of $\Lambda_b \to \Lambda_c\tau\bar{\nu}_\tau$ decay mode. Considering various real NP couplings, the differential decay distributions, forward-backward asymmetries and the ratios of branching fractions of these baryonic decay modes are investigated in [62]. In this work, we intend to analyse the effect of complex new couplings on $\Lambda_b \to (\Lambda_c, p)l\bar{\nu}_l$ decay processes in a model independent way. The main goal of this work is to check the possible existence of lepton universality violation in baryonic decays. The new coefficients are constrained by using the branching ratios of $B_{u,c} \to \tau\bar{\nu}_\tau$, $B \to \pi\tau\bar{\nu}_\tau$ processes and the experimental data on $R_{D^{(*)}}, R_{J/\psi}, R^l_\pi$ ratios. We then compute the branching ratios, forward-backward asymmetries, lepton

and hadron polarization asymmetries of these baryonic decay modes. We also check the LNU parameters by using the constrained new couplings. The main difference between our approach and the previous analyses in [58, 65] is that, we investigate the impact of individual complex new couplings on all the angular observables including the lepton and hadron polarization asymmetries. We use the updated experimental limits on $R_{D^{(*)}}$, R_π^l ratios including new $R_{J/\psi}$ parameter to constrain the allowed parameter space.

3.1 Theoretical framework

The most general effective Lagrangian associated with $B_1 \to B_2 l \bar{\nu}_l$ decay processes, where $B_1 = \Lambda_b,\ B_2 = \Lambda_c, p$ mediated by the quark level transition $b \to q l \bar{\nu}_l,\ (q = u, c)$ is given by [25, 69]

$$\begin{aligned}\mathcal{L}_{\text{eff}} &= -\frac{4\,G_F}{\sqrt{2}}\,V_{qb}\Big\{(1+V_L)\,\bar{l}_L\,\gamma_\mu\,\nu_L\,\bar{q}_L\,\gamma^\mu\,b_L + V_R\,\bar{l}_L\,\gamma_\mu\,\nu_L\,\bar{q}_R\,\gamma^\mu\,b_R \\ &\quad + S_L\,\bar{l}_R\,\nu_L\,\bar{q}_R\,b_L + S_R\,\bar{l}_R\,\nu_L\,\bar{q}_L\,b_R + T_L\,\bar{l}_R\,\sigma_{\mu\nu}\,\nu_L\,\bar{q}_R\,\sigma^{\mu\nu}\,b_L\Big\} + \text{h.c.}\,, \quad (3.1)\end{aligned}$$

where G_F denotes the Fermi constant, V_{qb} are the CKM matrix elements and $q(l)_{L,R} = P_{L,R}\,q(l)$ are the chiral quark(lepton) fields with $P_{L,R} = (1 \mp \gamma_5)/2$ as the projection operators. Here $V_{L,R}, S_{L,R}, T_L$ represent the vector, scalar and tensor type NP couplings, which are zero in the SM.

In the presence of NP, the double differential decay distribution for $B_1 \to B_2 l \bar{\nu}_l$ processes with respect to q^2 and $\cos\theta_l$ (θ_l is the angle between the directions of parent B_1 baryon and the l^- in the dilepton rest frame) is given as [58, 66]

$$\begin{aligned}\frac{d^2\Gamma}{dq^2 d\cos(\theta_l)} &= N\left(1-\frac{m_l^2}{q^2}\right)^2\Big[A_1 + \frac{m_l^2}{q^2}A_2 + 2A_3 + \frac{1}{4}A_4 \\ &+ \frac{4m_l}{\sqrt{q^2}}\,(A_5 + A_6) + A_7\Big]\,, \quad (3.2)\end{aligned}$$

where

$$
\begin{aligned}
A_1 &= 2\sin^2\theta_l\big(H^2_{\frac{1}{2},0}+H^2_{-\frac{1}{2},0}\big)+(1-\cos\theta_l)^2H^2_{\frac{1}{2},+}+(1+\cos\theta_l)^2H^2_{-\frac{1}{2},-}\,,\\
A_2 &= 2\cos^2\theta_l\big(H^2_{\frac{1}{2},0}+H^2_{-\frac{1}{2},0}\big)+\sin^2\theta_l\big(H^2_{\frac{1}{2},+}+H^2_{-\frac{1}{2},-}\big)+2\big(H^2_{\frac{1}{2},t}+H^2_{-\frac{1}{2},t}\big)\\
&\quad -4\cos\theta_l\big(H_{\frac{1}{2},0}H_{\frac{1}{2},t}+H_{-\frac{1}{2},0}H_{-\frac{1}{2},t}\big)\ ,\\
A_3 &= H^{SP^2}_{\frac{1}{2},0}+H^{SP^2}_{-\frac{1}{2},0}\,,\\
A_4 &= \frac{m_l^2}{q^2}\Big[2\sin^2\theta_l\big(H^{T^2}_{\frac{1}{2},+,-}+H^{T^2}_{\frac{1}{2},0,t}+H^{T^2}_{-\frac{1}{2},+,-}+H^{T^2}_{-\frac{1}{2},0,t}+2H^T_{\frac{1}{2},+,-}H^T_{\frac{1}{2},0,t}+2H^T_{-\frac{1}{2},+,-}H^T_{-\frac{1}{2},0,t}\big)\\
&\quad +(1+\cos\theta_l)^2\big(H^{T^2}_{-\frac{1}{2},0,-}+H^{T^2}_{-\frac{1}{2},-,t}+2H^T_{-\frac{1}{2},0,-}H^T_{-\frac{1}{2},-,t}\big)\\
&\quad +(1-\cos\theta_l)^2\big(H^{T^2}_{\frac{1}{2},+,0}+H^{T^2}_{\frac{1}{2},+,t}+2H^T_{\frac{1}{2},+,0}H^T_{\frac{1}{2},+,t}\big)\Big]\\
&\quad +2\cos^2\theta_l\big(H^{T^2}_{\frac{1}{2},+,-}+H^{T^2}_{\frac{1}{2},0,t}+H^{T^2}_{-\frac{1}{2},+,-}+H^{T^2}_{-\frac{1}{2},0,t}+2H^T_{\frac{1}{2},+,-}H^T_{\frac{1}{2},0,t}+2H^T_{-\frac{1}{2},+,-}H^T_{-\frac{1}{2},0,t}\big)\\
&\quad +\sin^2\theta_l\big(H^{T2}_{\frac{1}{2},+,0}+H^{T^2}_{\frac{1}{2},+,t}+H^{T2}_{-\frac{1}{2},0,-}+H^{T^2}_{-\frac{1}{2},-,t}+2H^T_{\frac{1}{2},+,0}H^T_{\frac{1}{2},+,t}+2H^T_{-\frac{1}{2},0,-}H^T_{-\frac{1}{2},-,t}\big)\,,\\
A_5 &= -\cos\theta_\ell\big(H_{\frac{1}{2},0}H^{SP}_{\frac{1}{2},0}+H_{-\frac{1}{2},0}H^{SP}_{-\frac{1}{2},0}\big)+\big(H_{\frac{1}{2},t}H^{SP}_{\frac{1}{2},0}+H_{-\frac{1}{2},t}H^{SP}_{-\frac{1}{2},0}\big)\,,\\
A_6 &= \frac{\cos^2\theta_l}{2}\big(H_{\frac{1}{2},0}H^T_{\frac{1}{2},+,-}+H_{\frac{1}{2},0}H^T_{\frac{1}{2},0,t}+H_{-\frac{1}{2},0}H^T_{-\frac{1}{2},+,-}+H_{-\frac{1}{2},0}H^T_{-\frac{1}{2},0,t}\big)\\
&\quad -\frac{\cos\theta_l}{2}\big(H_{\frac{1}{2},t}H^T_{\frac{1}{2},+,-}+H_{\frac{1}{2},t}H^T_{\frac{1}{2},0,t}+H_{-\frac{1}{2},t}H^T_{-\frac{1}{2},+,-}+H_{-\frac{1}{2},t}H^T_{-\frac{1}{2},0,t}\big)\\
&\quad +\frac{(1-\cos\theta_l)^2}{4}\big(H_{\frac{1}{2},+}H^T_{\frac{1}{2},+,0}+H_{\frac{1}{2},+}H^T_{\frac{1}{2},+,t}\big)\\
&\quad +\frac{(1+\cos\theta_l)^2}{4}\big(H_{-\frac{1}{2},-}H^T_{-\frac{1}{2},0,-}+H_{-\frac{1}{2},-}H^T_{-\frac{1}{2},-,t}\big)\\
&\quad +\frac{\sin^2\theta_l}{4}\big(H_{\frac{1}{2},+}H^T_{\frac{1}{2},+,0}+H_{\frac{1}{2},+}H^T_{\frac{1}{2},+,t}+H_{-\frac{1}{2},-}H^T_{-\frac{1}{2},0,-}+H_{-\frac{1}{2},-}H^T_{-\frac{1}{2},-,t}\\
&\quad +2H_{\frac{1}{2},0}H^T_{\frac{1}{2},+,-}+2H_{\frac{1}{2},0}H^T_{\frac{1}{2},0,t}+2H_{-\frac{1}{2},0}H^T_{-\frac{1}{2},+,-}+2H_{-\frac{1}{2},0}H^T_{-\frac{1}{2},0,t}\big)\,,\\
A_7 &= -2\cos\theta_l\Big(H^{SP}_{\frac{1}{2},0}H^T_{\frac{1}{2},+,-}+H^{SP}_{\frac{1}{2},0}H^T_{\frac{1}{2},0,t}+H^{SP}_{-\frac{1}{2},0}H^T_{-\frac{1}{2},+,-}+H^{SP}_{-\frac{1}{2},0}H^T_{-\frac{1}{2},0,t}\Big)\,,
\end{aligned}
\tag{3.3}
$$

with

$$
\begin{aligned}
H^{VA}_{\lambda_{\Lambda_c},\lambda} &= H^V_{\lambda_{\Lambda_c},\lambda}-H^A_{\lambda_{\Lambda_c},\lambda},\quad H^V_{\lambda_{\Lambda_c},\lambda_w}=H^V_{-\lambda_{\Lambda_c},-\lambda_w},\quad H^A_{\lambda_{\Lambda_c},\lambda_w}=-H^A_{-\lambda_{\Lambda_c},-\lambda_w},\\
H^{SP}_{\lambda_{\Lambda_c},\lambda=0} &= H^S_{\lambda_{\Lambda_c},\lambda=0}+H^P_{\lambda_{\Lambda_c},\lambda=0},\quad H^S_{\lambda_{\Lambda_c},\lambda_{NP}}=H^S_{-\lambda_{\Lambda_c},-\lambda_{NP}},\quad H^P_{\lambda_{\Lambda_c},\lambda_{NP}}=-H^P_{-\lambda_{\Lambda_c},-\lambda_{NP}},\\
H^T_{\lambda_{\Lambda_c},\lambda,\lambda'} &= -H^T_{\lambda_{\Lambda_c},\lambda',\lambda},\qquad H^T_{\lambda_{\Lambda_c},\lambda,\lambda}=0.
\end{aligned}
\tag{3.4}
$$

and

$$
N=\frac{G_F^2|V_{qb}|^2q^2\sqrt{\lambda(M_{B_1}^2,M_{B_2}^2,q^2)}}{2^{10}\pi^3M_{B_1}^3}\,,\quad \lambda(a,b,c)=a^2+b^2+c^2-2(ab+bc+ca).
\tag{3.5}
$$

Here $M_{B_{1(2)}}$ and m_l are the masses of $B_{1(2)}$ baryon and charged leptons respectively. The helicity amplitudes in terms of the various form factors and the NP couplings are

given as [58, 66]

$$
\begin{aligned}
H^V_{\frac{1}{2}0} &= (1+V_L+V_R)\,\frac{\sqrt{Q_-}}{\sqrt{q^2}}\Big[(M_{B_1}+M_{B_2})\,f_1(q^2)-q^2\,f_2(q^2)\Big],\\
H^A_{\frac{1}{2}0} &= (1+V_L-V_R)\,\frac{\sqrt{Q_+}}{\sqrt{q^2}}\Big[(M_{B_1}-M_{B_2})\,g_1(q^2)+q^2\,g_2(q^2)\Big],\\
H^V_{\frac{1}{2}+} &= (1+V_L+V_R)\,\sqrt{2\,Q_-}\Big[-f_1(q^2)+(M_{B_1}+M_{B_2})\,f_2(q^2)\Big],\\
H^A_{\frac{1}{2}+} &= (1+V_L-V_R)\,\sqrt{2\,Q_+}\Big[-g_1(q^2)-(M_{B_1}-M_{B_2})\,g_2(q^2)\Big],\\
H^V_{\frac{1}{2}t} &= (1+V_L+V_R)\,\frac{\sqrt{Q_+}}{\sqrt{q^2}}\Big[(M_{B_1}-M_{B_2})\,f_1(q^2)+q^2\,f_3(q^2)\Big],\\
H^A_{\frac{1}{2}t} &= (1+V_L-V_R)\,\frac{\sqrt{Q_-}}{\sqrt{q^2}}\Big[(M_{B_1}+M_{B_2})\,g_1(q^2)-q^2\,g_3(q^2)\Big],\\
H^S_{\frac{1}{2}0} &= (S_L+S_R)\,\frac{\sqrt{Q_+}}{m_b-m_q}\Big[(M_{B_1}-M_{B_2})\,f_1(q^2)+q^2\,f_3(q^2)\Big],\\
H^P_{\frac{1}{2}0} &= (S_L-S_R)\,\frac{\sqrt{Q_-}}{m_b+m_q}\Big[(M_{B_1}+M_{B_2})\,g_1(q^2)-q^2\,g_3(q^2)\Big],\\
H^T_{\frac{1}{2},+,0} &= -T_L\sqrt{\frac{2}{q^2}}\Big(f_T\sqrt{Q_+}(M_{B_1}-M_{B_2})+g_T\sqrt{Q_-}(M_{B_1}+M_{B_2})\Big),\\
H^T_{\frac{1}{2},+,-} &= -T_L\Big(f_T\sqrt{Q_+}+g_T\sqrt{Q_-}\Big),\\
H^T_{\frac{1}{2},+,t} &= T_L\Big[-\sqrt{\frac{2}{q^2}}\Big(f_T\sqrt{Q_-}(M_{B_1}+M_{B_2})+g_T\sqrt{Q_+}(M_{B_1}-M_{B_2})\Big)\\
&\quad+\sqrt{2q^2}\Big(f_T^V\sqrt{Q_-}-g_T^V\sqrt{Q_+}\Big)\Big],\\
H^T_{\frac{1}{2},0,t} &= T_L\Big[-f_T\sqrt{Q_-}-g_T\sqrt{Q_+}+f_T^V\sqrt{Q_-}(M_{B_1}+M_{B_2})-g_T^V\sqrt{Q_+}(M_{B_1}-M_{B_2})\\
&\quad+f_T^S\sqrt{Q_-}Q_+ + g_T^S\sqrt{Q_+}Q_-\Big],\\
H^T_{-\frac{1}{2},+,-} &= T_L\Big[f_T\sqrt{Q_+}-g_T\sqrt{Q_-}\Big],\\
H^T_{-\frac{1}{2},0,-} &= T_L\Big[\sqrt{\frac{2}{q^2}}\Big(f_T\sqrt{Q_+}(M_{B_1}-M_{B_2})--g_T\sqrt{Q_-}(M_{B_1}+M_{B_2})\Big)\Big],\\
H^T_{-\frac{1}{2},-,t} &= T_L\Big[-\sqrt{\frac{2}{q^2}}\Big(f_T\sqrt{Q_-}(M_{B_1}+M_{B_2})-g_T\sqrt{Q_+}(M_{B_1}-M_{B_2})\Big)\\
&\quad+\sqrt{2q^2}\Big(f_T^V\sqrt{Q_-}+g_T^V\sqrt{Q_+}\Big)\Big],\\
H^T_{-\frac{1}{2},0,t} &= T_L\Big[-f_T\sqrt{Q_-}+g_T\sqrt{Q_+}+f_T^V\sqrt{Q_-}(M_{B_1}+M_{B_2})++g_T^V\sqrt{Q_+}(M_{B_1}-M_{B_2})\\
&\quad+f_T^S\sqrt{Q_-}Q_+ - g_T^S\sqrt{Q_+}Q_-\Big]. \qquad (3.6)
\end{aligned}
$$

where $Q_\pm = (M_{B_1}\pm M_{B_2})^2 - q^2$ and $f_i^{(a)}, g_i^{(b)}$, $(i=1,2,3,T\ \&\ a,b=V,S)$ are the various form factors. After integrating out $\cos\theta_l$ in Eqn. (3.2), one can obtain the

q^2 dependent differential decay rate. Besides the branching ratios, other interesting observables in these decay modes are

- Forward-backward asymmetry parameter:

$$A_{FB}(q^2) = \left(\int_{-1}^{0} d\cos\theta_l \frac{d^2\Gamma}{dq^2 d\cos\theta_l} - \int_{0}^{1} d\cos\theta_l \frac{d^2\Gamma}{dq^2 d\cos\theta_l} \right) \Big/ \frac{d\Gamma}{dq^2} \,. \tag{3.7}$$

- Convexity parameter:

$$C_F^l(q^2) = \frac{1}{d\Gamma/dq^2} \frac{d^2}{d(\cos\theta_l)^2} \left(\frac{d^2\Gamma}{dq^2 d\cos\theta_l} \right). \tag{3.8}$$

- Longitudinal hadron polarization asymmetry parameter:

$$P_L^h(q^2) = \frac{\mathrm{d}\Gamma^{\lambda_2=1/2}/\mathrm{d}q^2 - \mathrm{d}\Gamma^{\lambda_2=-1/2}/\mathrm{d}q^2}{\mathrm{d}\Gamma/\mathrm{d}q^2} \,, \tag{3.9}$$

  where $\mathrm{d}\Gamma^{\lambda_2=\pm 1/2}$ are the individual helicity-dependent differential decay rates, whose detailed expressions are given in Appendix A [66].

- Longitudinal lepton polarization asymmetry parameter:

$$P_L^\tau(q^2) = \frac{\mathrm{d}\Gamma^{\lambda_\tau=1/2}/\mathrm{d}q^2 - \mathrm{d}\Gamma^{\lambda_\tau=-1/2}/\mathrm{d}q^2}{\mathrm{d}\Gamma/\mathrm{d}q^2} \,, \tag{3.10}$$

  where $\mathrm{d}\Gamma^{\lambda_2=\pm 1/2}$ are the individual helicity-dependent differential decay rates, whose detailed expressions are given in Appendix A [66].

- Lepton non-universality parameter:

$$R_{B_2} = \frac{\mathrm{BR}(B_1 \to B_2 \tau^- \bar{\nu}_\tau)}{\mathrm{BR}(B_1 \to B_2\, l^- \bar{\nu}_l)} \,, \quad l = e, \mu. \tag{3.11}$$

- The LHCb Collaboration has measured the ratio of the partially integrated decay rates of $\Lambda_b^0 \to p\,\mu\,\bar{\nu}_l$ over the $\Lambda_b^0 \to \Lambda_c^+\,\mu\,\bar{\nu}_l$ process as

$$\begin{aligned} R^\mu_{\Lambda_c p} &= \int_{15\,\mathrm{GeV}^2}^{q^2_{\max}} \frac{d\Gamma(\Lambda_b \to p\,\mu\,\bar{\nu}_l)}{dq^2}\, dq^2 \Bigg/ \int_{7\,\mathrm{GeV}^2}^{q^2_{\max}} \frac{d\Gamma(\Lambda_b \to \Lambda_c\,\mu\,\bar{\nu}_l)}{dq^2}\, dq^2 \\ &= (1.00 \pm 0.04 \pm 0.08) \times 10^{-2} \end{aligned} \tag{3.12}$$

  and put constraint on the ratio $|V_{ub}|/|V_{cb}| = 0.083 \pm 0.004 \pm 0.004$ [53]. Similarly, we define the following parameter, to investigate if there is any possible role of NP

$$R^\tau_{\Lambda_c p} = \int_{15\,\mathrm{GeV}^2}^{q^2_{\max}} \frac{d\Gamma(\Lambda_b \to p\,\tau\,\bar{\nu}_\tau)}{dq^2}\, dq^2 \Bigg/ \int_{7\,\mathrm{GeV}^2}^{q^2_{\max}} \frac{d\Gamma(\Lambda_b \to \Lambda_c\,\tau\,\bar{\nu}_\tau)}{dq^2}\, dq^2 \tag{3.13}$$

3.2 Constraint on new couplings

After assembling the expressions for all the interesting observables in presence of NP, we now proceed to constrain the new coefficients by using the experimental bounds on $\mathrm{BR}(B_{u,c} \to \tau\bar{\nu}_\tau)$, $\mathrm{BR}(B \to \pi\tau\bar{\nu}_\tau)$, R_π^l, $R_{D^{(*)}}$ and $R_{J/\psi}$ parameters. In this analysis, the new Wilson coefficients are considered as complex. We further assume that only one new coefficient to present at a time and accordingly compute the allowed parameter space of these couplings.

The branching ratios of $B_q \to l\bar{\nu}_l$ processes in the presence of NP couplings are given by [26]

$$\begin{aligned}\mathrm{BR}(B_q \to l\bar{\nu}_l) &= \frac{G_F^2\,|V_{qb}|^2}{8\,\pi}\,\tau_{B_q} f_{B_q}^2\, m_l^2\, M_{B_q}\left(1-\frac{m_l^2}{M_{B_q}^2}\right)^2 \\ &\times \left|\,(1+V_L-V_R)-\frac{M_{B_q}^2}{m_l\,(m_b+m_q)}\,(S_L-S_R)\,\right|^2, \end{aligned} \tag{3.14}$$

where M_{B_q} is the mass of B_q meson. By using the masses of all the particles, lifetime of B_q meson, CKM matrix elements from [27] and decay constants $f_{B_u} = 190.5 \pm 4.2$ MeV, $f_{B_c} = 489 \pm 4 \pm 3$ MeV from [28, 70], the branching ratios of $B_{u,c}^+ \to \tau^+\nu_\tau$ processes in the SM are found to be

$$\mathrm{BR}(B_u^+ \to \tau^+\nu_\tau)\big|^{\mathrm{SM}} = (8.48 \pm 0.5) \times 10^{-5}, \tag{3.15}$$

$$\mathrm{BR}(B_c^+ \to \tau^+\nu_\tau)\big|^{\mathrm{SM}} = (3.6 \pm 0.14) \times 10^{-2}\,. \tag{3.16}$$

Using the current world average of the B_c lifetime, the upper limit on the branching ratio of $B_c^+ \to \tau^+\nu_\tau$ process is [71]

$$\mathrm{BR}(B_c^+ \to \tau^+\nu_\tau) \lesssim 30\%. \tag{3.17}$$

The branching ratios of $B_q \to Pl\bar{\nu}_l$ ($P = \pi, D$) are given as [30, 72]

$$\begin{aligned}\frac{d\mathrm{BR}(B_q \to Pl\bar{\nu}_l)}{dq^2} &= \tau_{B_q}\frac{G_F^2|V_{qb}|^2}{192\pi^3 M_{B_q}^3} q^2\sqrt{\lambda_P(q^2)}\left(1-\frac{m_l^2}{q^2}\right)^2 \times \\ &\left\{|1+V_L+V_R|^2\left[\left(1+\frac{m_l^2}{2q^2}\right)H_0^2+\frac{3}{2}\frac{m_l^2}{q^2}H_t^2\right]\right. \\ &+\frac{3}{2}|S_L+S_R|^2\,H_S^2+8|T_L|^2\left(1+\frac{2m_l^2}{q^2}\right)H_T^2 \\ &+3\mathrm{Re}[(1+V_L+V_R)(S_L^*+S_R^*)]\frac{m_l}{\sqrt{q^2}}H_S H_t \\ &\left.-12\mathrm{Re}[(1+V_L+V_R)T_L^*]\frac{m_l}{\sqrt{q^2}}H_T H_0\right\}, \end{aligned} \tag{3.18}$$

where the helicity amplitudes in terms of form factors ($F_{0,+}$) are expressed as

$$H_0 = \sqrt{\frac{\lambda(M_{B_q}^2,\, m_P^2,\, q^2)}{q^2}}\, F_+(q^2), \qquad H_t = \frac{M_{B_q}^2 - M_P^2}{\sqrt{q^2}}\, F_0(q^2)\,,$$
$$H_S = \frac{M_{B_q}^2 - M_P^2}{m_b - m_q}\, F_0(q^2) \qquad\qquad H_T = -\frac{\sqrt{\lambda_P(q^2)}}{M_{B_q} + M_P} F_T(q^2). \tag{3.19}$$

Using the values of the $B \to \pi$ form factors from [35, 36, 73, 74], the obtained branching ratios of $B_q \to \pi l \nu_l$ processes, in the SM are given as

$$\mathrm{BR}(B^0 \to \pi^+ \mu^- \bar{\nu}_\mu)|^{\mathrm{SM}} = (1.35 \pm 0.10) \times 10^{-4}, \tag{3.20}$$
$$\mathrm{BR}(B^0 \to \pi^+ \tau^- \bar{\nu}_\tau)|^{\mathrm{SM}} = (9.40 \pm 0.75) \times 10^{-5}. \tag{3.21}$$

It should be noted that, the branching ratio of the muonic channel agrees reasonably well with the experimental value as given in Eqn. (3), whereas the tau-channel is within its current experimental limit [27]

$$\mathrm{BR}(B^0 \to \pi^+ \tau^- \bar{\nu}_\tau)|^{\mathrm{Expt}} < 2.5 \times 10^{-4}. \tag{3.22}$$

The branching ratios of $B_q \to V l \bar{\nu}_l$, where $V = D^*, J/\psi$, are given as [30, 72]

$$\begin{aligned}
\frac{d\mathrm{BR}(\bar{B} \to V l \bar{\nu}_l)}{dq^2} \;=\; & \tau_{B_q} \frac{G_F^2 |V_{qb}|^2}{192\pi^3 M_{B_q}^3} q^2 \sqrt{\lambda_V(q^2)} \left(1 - \frac{m_l^2}{q^2}\right)^2 \times \\
& \left\{ (|1+V_L|^2 + |V_R|^2) \left[\left(1 + \frac{m_l^2}{2q^2}\right) \left(H_{V,+}^2 + H_{V,-}^2 + H_{V,0}^2\right) + \frac{3}{2} \frac{m_l^2}{q^2} H_{V,t}^2 \right] \right. \\
& -2\mathrm{Re}[(1+V_L)V_R^*] \left[\left(1 + \frac{m_l^2}{2q^2}\right) \left(H_{V,0}^2 + 2H_{V,+}H_{V,-}\right) + \frac{3}{2} \frac{m_l^2}{q^2} H_{V,t}^2 \right] \\
& + \frac{3}{2} |S_L - S_R|^2 H_S^2 + 8|T_L|^2 \left(1 + \frac{2m_l^2}{q^2}\right) \left(H_{T,+}^2 + H_{T,-}^2 + H_{T,0}^2\right) \\
& + 3\mathrm{Re}[(1 + V_L - V_R)(S_L^* - S_R^*)] \frac{m_l}{\sqrt{q^2}} H_S H_{V,t} \\
& - 12\mathrm{Re}[(1+V_L)T_L^*] \frac{m_l}{\sqrt{q^2}} \left(H_{T,0}H_{V,0} + H_{T,+}H_{V,+} - H_{T,-}H_{V,-}\right) \\
& \left. + 12\mathrm{Re}[V_R T_L^*] \frac{m_l}{\sqrt{q^2}} \left(H_{T,0}H_{V,0} + H_{T,+}H_{V,-} - H_{T,-}H_{V,+}\right) \right\},
\end{aligned} \tag{3.23}$$

where $H_{V,\pm}$, $H_{V,0}$, $H_{V,t}$ and H_S are the hadronic amplitudes [30, 72]. In this analysis, we consider the new physics contribution to third generation lepton only and the couplings with light leptons are assumed to be SM like. By allowing only one coefficient at a time, we constrain its real and imaginary parts by comparing the theoretically predicted values of $\mathrm{BR}(B_u^+ \to \tau^+ \nu_\tau)$ and R_π^l with their corresponding 3σ range of observed experimental results for $b \to u \tau \bar{\nu}_\tau$ transitions. We have also used the upper limit of the branching ratio

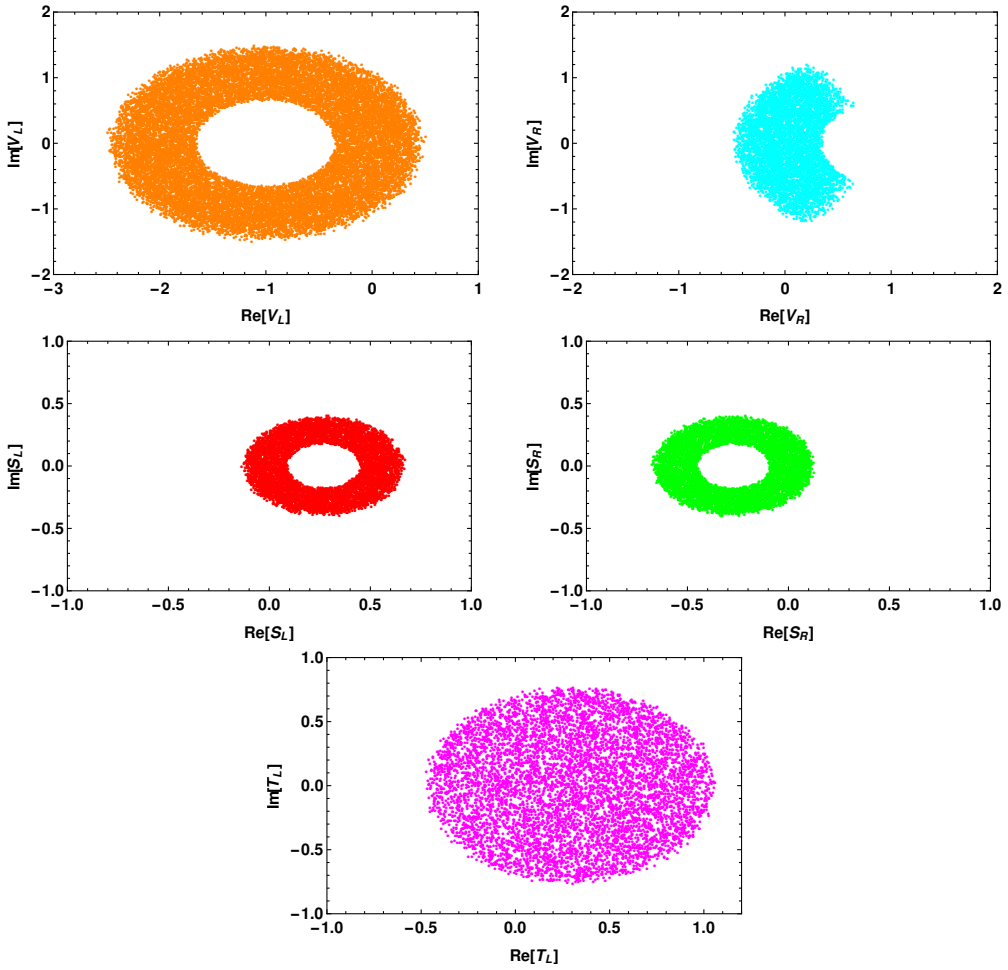

FIGURE 3.1: Allowed parameterspace for NP couplings V_L (top-left panel), V_R (top-right panel), S_L (middle-left panel), S_R (middle-right panel) and T_L (bottom panel) involved with $b \to u\tau\bar{\nu}_\tau$ transition constrained from $\mathrm{Br}(\mathrm{B_u^+} \to \tau^+\nu_\tau)$, $\mathrm{Br}(\mathrm{B} \to \pi\tau\bar{\nu}_\tau)$, R_π^l experimental data. The T_L coupling is constrained from $\mathrm{Br}(\mathrm{B} \to \pi\tau\bar{\nu}_\tau)$ experimental value.

of $B^0 \to \pi^+\tau^-\bar{\nu}_\tau$ process. In Fig. 3.1 , we show the constraints on real and imaginary parts of new coefficients V_L (top-left panel), V_R (top-right panel), S_L (middle-left panel) and S_R (middle-right panel) obtained from the $\mathrm{BR}(B_u^+ \to \tau^+\nu_\tau)$, $\mathrm{BR}(B^0 \to \pi^+\tau^-\bar{\nu}_\tau)$ and R_π^l observables. Since the branching ratio of $B_u^+ \to \tau^+\nu_\tau$ process does not receive any contribution from tensor operator, the allowed region of real and imaginary parts of tensor coupling (T_L) obtained only from the upper limit on $\mathrm{BR}(B^0 \to \pi^+\tau^-\bar{\nu}_\tau)$, and is presented in the bottom panel of this figure. Now imposing the extrema conditions, the allowed range of the new couplings associated with $b \to u\tau\bar{\nu}_\tau$ transition are presented in Table 3.1 . For the case of $b \to c\tau\bar{\nu}_\tau$ decay processes, the constraints on the real and imaginary parts of individual V_L (top-left panel), V_R (top-right panel), S_L (middle-left panel) and S_R (middle-right panel) coefficients obtained from $R_{D^{(*)}}$ and $R_{J/\psi}$ parameters are shown in Fig. 3.2 . Till now, there is no precise determination of the form factors associated with tensorial operators for $B_c \to J/\psi l\bar{\nu}_l$ process both from the theoretical

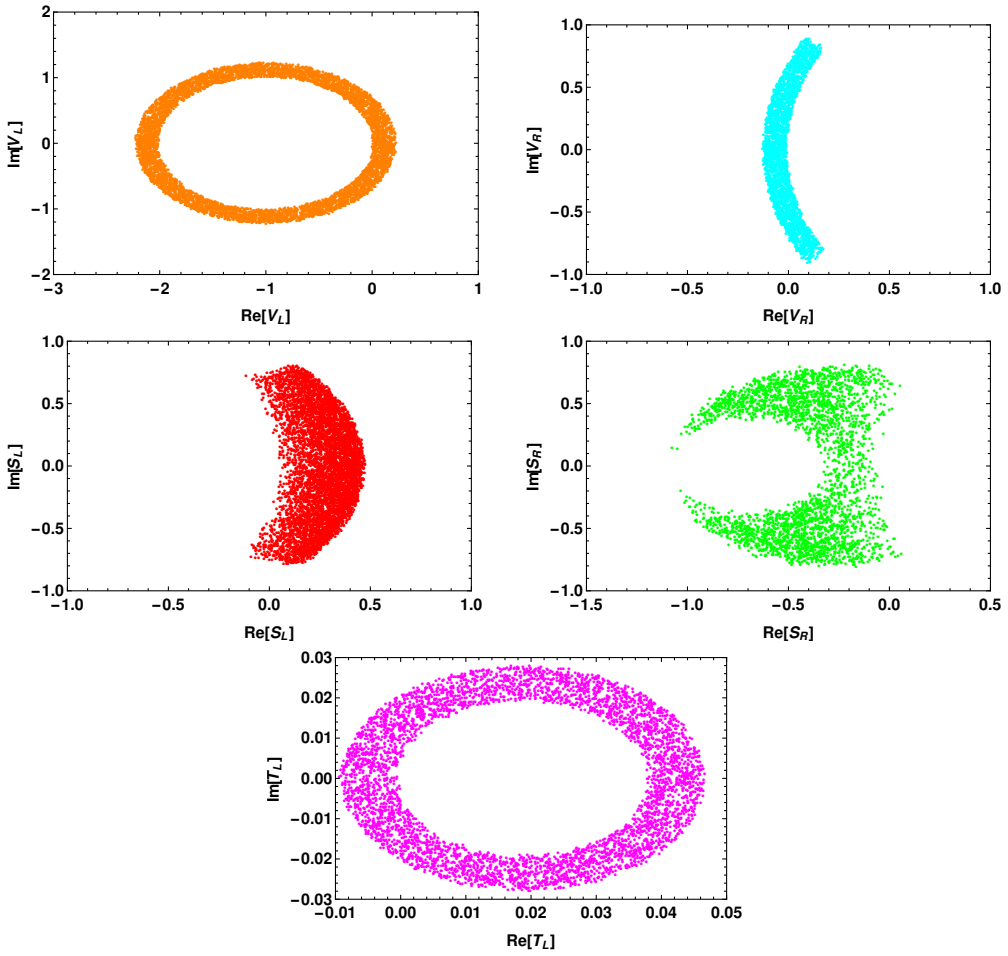

FIGURE 3.2: Allowed parameterspace for NP couplings V_L (top-left panel), V_R (top-right panel), S_L (middle-left panel), S_R (middle-right panel) and T_L (bottom panel) involved with $b \to c\tau\bar{\nu}_\tau$ transition constrained from $\mathrm{Br}(\mathrm{B}_c^+ \to \tau^+\nu_\tau)$, $R_{D^{(*)}}$ and $R_{J/\psi}$ experimental data. The T_L coupling is constrained from $R_{D^{(*)}}$ experimental value.

and experimental sides. In addition, the leptonic B_c meson decays do not receive any contribution from tensor coupling. Therefore, the constraints on T_L coupling is obtained from the experimental data on $R_{D^{(*)}}$, which is shown in the bottom panel of Fig. 3.2. In Table 3.1 , we have presented the allowed values of $(\mathrm{Re}[V_{L(R)}] - \mathrm{Im}[V_{L(R)}])$ and $(\mathrm{Re}[S_{L(R)}] - \mathrm{Im}[S_{L(R)}])$ coefficients, which are compatible with the 3σ range of the experimental data.

The constraints on these parameters are obtained earlier from various B decays in Refs. [22, 26, 58, 62, 72, 75–78]. Our analysis is similar to Refs. [58, 65]. In Ref. [58], the authors have considered the couplings to be complex and constrained the new coefficients associated with $b \to c\tau\bar{\nu}_\tau$ from $R_{D^{(*)}}$ data. However, they have not includeed the tensor couplings in their analysis, and found that the effects produced by the pseudoscalar coefficient are larger than those obtained from the scalar coefficient. In Ref. [62], the author assumed the couplings as real and computed the allowed parameter space by

TABLE 3.1: Constrained parameter space of the new couplings.

Decay processes	New coefficients	Minimum value	Maximum Value
$b \to u\tau\bar{\nu}_\tau$	$(\mathrm{Re}[V_L], \mathrm{Im}[V_L])$	$(-2.489, -1.5)$	$(0.504, 1.48)$
	$(\mathrm{Re}[V_R], \mathrm{Im}[V_R])$	$(-0.478, -1.185)$	$(0.645, 1.198)$
	$(\mathrm{Re}[S_L], \mathrm{Im}[S_L])$	$(-0.136, -0.396)$	$(0.672, 0.398)$
	$(\mathrm{Re}[S_R], \mathrm{Im}[S_R])$	$(-0.6743, -0.398)$	$(0.1265, 0.398)$
	$(\mathrm{Re}[T_L], \mathrm{Im}[T_L])$	$(-0.473, -0.773)$	$(1.07, 0.773)$
$b \to c\tau\bar{\nu}_\tau$	$(\mathrm{Re}[V_L], \mathrm{Im}[V_L])$	$(-2.224, -1.228)$	$(0.225, 1.225)$
	$(\mathrm{Re}[V_R], \mathrm{Im}[V_R])$	$(-0.129, -0.906)$	$(0.173, 0.89)$
	$(\mathrm{Re}[S_L], \mathrm{Im}[S_L])$	$(-0.116, -0.788)$	$(0.474, 0.8)$
	$(\mathrm{Re}[S_R], \mathrm{Im}[S_R])$	$(-1.076, -0.809)$	$(0.06, 0.807)$
	$(\mathrm{Re}[T_L], \mathrm{Im}[T_L])$	$(-0.0094, -0.028)$	$(0.0467, 0.028)$

comparing the $R_{D^{(*)}}$, R^l_π parameters with their corresponding 3σ experimental data. In [78], the authors have considered the covariant confined quark model and studied the effect of new physics in the $\bar{B}^0 \to D^*\tau^-\bar{\nu_\tau}$. They took the new coefficients as complex and constrained them using the experimental values of R_D and R_{D^*} within their 2σ range. Recently, the decay process $B_c \to (J/\psi)\tau\nu_\tau$ has been studied, in the covariant confined quark model [77], where the parameter space is constrained by using the experimental values of $R_D, R_{D^*}, R_{J/\psi}$ within 2σ range. The new coefficients are considered to be complex and their best fit values are $V_L = -1.05 + i1.15, V_R = 0.04 + i0.60, T_L = 0.38 - i0.06$. Though our analysis is similar to these approaches, but we get more severe bounds on the phases and strengths of the couplings due to additional constraints from $\mathrm{BR}(B_c \to \tau\nu_\tau)$ and $R_{J/\psi}$ parameters for $b \to c\tau\bar{\nu}_\tau$ case and from $\mathrm{BR}(B_u \to \tau\nu_\tau)$ and $\mathrm{BR}(B \to \pi\tau\nu_\tau)$ observables for $b \to u\tau\bar{\nu}_\tau$ process.

3.3 Numerical analysis and discussion

In this section, we present the numerical results for semileptonic Λ_b decay modes with third generation leptons in the final state. The masses of all the particles and the lifetime of Λ_b are taken from [27]. The q^2 dependence of the helicity form factors $(f_{+,\perp,0},\ g_{+,\perp,0}, h_{+,\perp}, \widetilde{h}_{+,\perp})$ in the lattice QCD calculation can be parametrized as [61, 65]

$$f_i(q^2) = \frac{1}{1 - q^2/(m^f_{\mathrm{pole}})^2}\Big[a^f_0 + a^f_1 z(q^2)\Big], \quad (i = +, \perp, 0) \tag{3.24}$$

where m^f_{pole} is the pole mass and

$$z(q^2) = \frac{\sqrt{t_+ - q^2} - \sqrt{t_+ - t_0}}{\sqrt{t_+ - q^2} + \sqrt{t_+ - t_0}}\,, \tag{3.25}$$

with $t_\pm = (M_{B_1} \pm M_{B_2})^2$. The values of the parameters $m^f_{\rm pole}$, $a^f_{0,1}$ associated with (axial)vector and (pseudo)scalar form factors ($f_{+,\perp,0}$, $g_{+,\perp,0}$) are taken from [61]. In the lattice QCD approach, the $m^f_{\rm pole}$, $a^f_{0,1}$ parameters linked to tensor form factors ($h_{+,\perp}, \widetilde{h}_{+,\perp}$) of $\Lambda_b \to \Lambda_c l \bar{\nu}_l$ process are computed in [65]. However, currently no lattice results are available on the tensor form factors associated with $\Lambda_b \to p l \bar{\nu}_l$ process. Hence, we relate the tensor form factors of $\Lambda_b \to p l \bar{\nu}_l$ decay mode with its (axial)vector form factors by using the HQET relations as [66, 79, 80],

$$f_T = g_T = f_1 = \frac{(M_{B_1} + M_{B_2})^2 f_+ - q^2 f_\perp}{(M_{B_1} + M_{B_2})^2 - q^2}\,, \quad f_T^V = g_T^V = f_T^S = g_T^S = 0\,. \tag{3.26}$$

The detailed relation between the helicity form factors ($f_{+,\perp,0}$, $g_{+,\perp,0}, h_{+,\perp}, \widetilde{h}_{+,\perp}$) with other various hadronic form factors ($f_{1,2,3}$, $g_{1,2,3}$, f_T, g_T, $f_T^{V(S)}$, $g_T^{V(S)}$) are listed in Appendix A.1 [79]. Using all these input parameters, the predicted branching ratios of $\Lambda_b \to (\Lambda_c, p)\mu\bar{\nu}_\mu$ processes in the SM are given by

$$\begin{aligned} &{\rm BR}(\Lambda_b \to p\mu^-\bar{\nu}_\mu)|^{\rm SM} = (4.31 \pm 0.345) \times 10^{-4}, \\ &{\rm BR}(\Lambda_b \to \Lambda_c\mu^-\bar{\nu}_\mu)|^{\rm SM} = (4.994 \pm 0.4) \times 10^{-2}, \end{aligned} \tag{3.27}$$

which are in reasonable agreement with the corresponding experimental data [27]

$$\begin{aligned} &{\rm BR}(\Lambda_b \to p\mu^-\bar{\nu}_\mu) = (4.1 \pm 1.0) \times 10^{-4}, \\ &{\rm BR}(\Lambda_b \to \Lambda_c l^-\bar{\nu}_l) = \left(6.2^{+1.4}_{-1.3}\right) \times 10^{-2}. \end{aligned} \tag{3.28}$$

The values of the forward-backward asymmetries in these channels are found to be

$$\langle A^\mu_{FB}\rangle|^{\rm SM}_{\Lambda_b\to p} = 0.316 \pm 0.025, \qquad \langle A^\mu_{FB}\rangle|^{\rm SM}_{\Lambda_b\to \Lambda_c} = 0.19 \pm 0.0152. \tag{3.29}$$

In Eqn. (3.27 , 3.29), the theoretical uncertainties are mainly due to the uncertainties associated with the CKM matrix elements and the form factor parameters. After having idea on all the required input parameters and the allowed parameter space of new couplings, we now proceed to discuss various new physics scenarios and their impact on $\Lambda_b \to (\Lambda_c, p)\tau\bar{\nu}_\tau$ decay modes in a model independent way.

3.3.1 Scenario A: Only V_L coefficient

In this scenario, we assume that the additional new physics contribution to the SM result is coming only from the coupling associated with the left-handed vector like quark currents i.e., $V_L \neq 0$ and $V_R, S_{L,R}, T_L = 0$. Since in this case, the NP operator has the same Lorentz structure as the SM operator, the SM decay rate gets modified by the

factor $|1+V_L|^2$. Imposing 3σ constraint on $\mathrm{Br}(B^+_{u,c} \to \tau^+\nu_\tau)$, $\mathrm{Br}(B^0 \to \pi^+\tau^-\bar{\nu}_\tau)$, R^l_π, $R_{D^{(*)}}$ and $R_{J/\psi}$ observables, the allowed parameter space of V_L couplings associated with $b \to (u,c)\tau\nu_\tau$ are shown in Figs. 3.1 and 3.2 respectively. Using the minimum

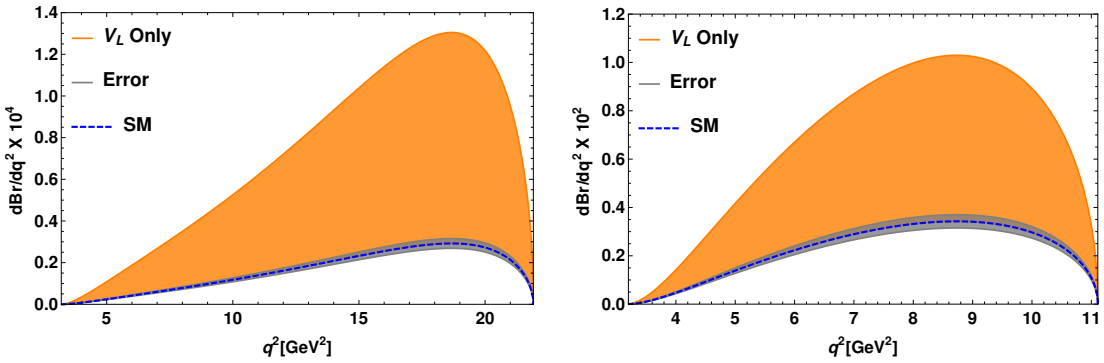

FIGURE 3.3: The q^2 variation of branching ratio of $\Lambda_b \to p\tau^-\bar{\nu}_\tau$ (left panel) and $\Lambda_b \to \Lambda_c^+\tau^-\bar{\nu}_\tau$ (right panel) processes in the presence of only V_L new coefficient. Here the orange bands represent the new physics contribution. Blue dashed lines stand for the SM and the theoretical uncertainties arising due to the input parameters are presented in grey color.

and maximum values on real and imaginary parts of V_L coefficient from Table 3.1 , we present the differential branching ratios of $\Lambda_b \to p\tau^-\bar{\nu}_\tau$ (left panel) and $\Lambda_b \to \Lambda_c\tau^-\bar{\nu}_\tau$ (right panel) processes with respect to q^2 in Fig. 3.3 . In these figures, the blue dashed lines represent the SM contribution, the orange bands are due to the presence of new V_L coefficient and the grey bands stand for the theoretical uncertainties associated with the input parameters like form factors, CKM matrix elements etc. The branching ratios of $\Lambda_b \to (\Lambda_c, p)\tau^-\bar{\nu}_\tau$ deviate significantly from their corresponding SM values due to the NP contribution. In addition to the decay rate, other interesting observables, which can be used to probe new physics, are the zero crossing of the forward-backward asymmetry and the convexity parameters. From Eqn. (3.8), one can notice that the convexity parameter depends only on the $V_{L,R}$ and T_L couplings. The values for forward-backward asymmetries of $\Lambda_b \to (\Lambda_c, p)\tau\bar{\nu}_\tau$ processes in the SM are

$$\langle A^\tau_{FB}\rangle|^{\rm SM}_{\Lambda_b\to p} = 0.115 \pm 0.0092\ , \quad \langle A^\tau_{FB}\rangle|^{\rm SM}_{\Lambda_b\to\Lambda_c} = -0.09 \pm 0.007\ , \tag{3.30}$$

and the corresponding values for the convexity parameters are

$$\langle C^\tau_F\rangle|^{\rm SM}_{\Lambda_b\to p} = -0.157 \pm 0.013\ , \quad \langle C^\tau_F\rangle|^{\rm SM}_{\Lambda_b\to\Lambda_c} = -0.098 \pm 0.008\ . \tag{3.31}$$

We found no deviation from SM results for the forward-backward asymmetry and convexity parameters due to the presence of V_L coefficient. In Fig. 3.4 , left (right) panel depicts the q^2 variation of lepton universality violating parameters R_p (R_{Λ_c}). We observe that the NP contribution coming from the V_L coupling has significant impact on

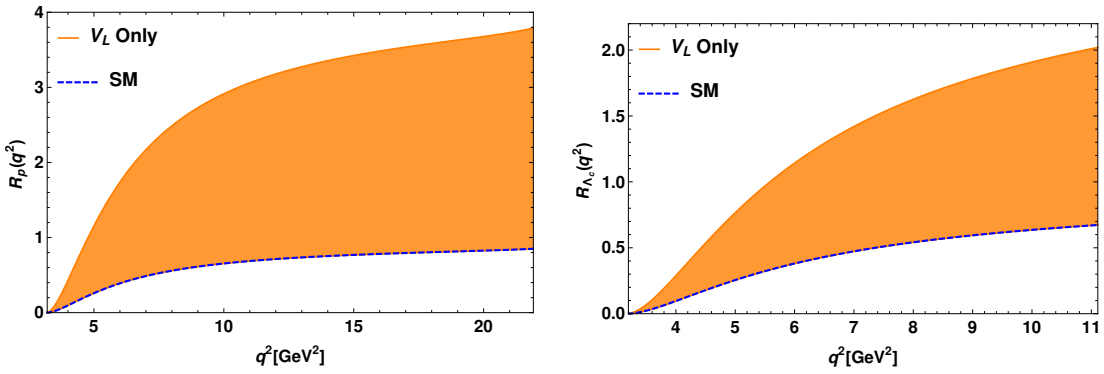

FIGURE 3.4: The variation of R_p (left panel) and R_{Λ_c} (right panel) LNU parameters with respect to q^2 in the presence of only V_L new coefficient.

R_p and R_{Λ_c} parameters. The variation of $R^{\tau}_{\Lambda_c p}$ parameter with q^2 for this case, is presented in the left panel of Fig. 3.7. The numerical values of the branching ratios and the LNU parameters for both the SM and the V_L-type NP scenario are given in Table 3.2. Besides the branching ratios, forward-backward asymmetry and LNU parameters of $\Lambda_b \to (\Lambda_c, p)\tau\bar{\nu}_\tau$ processes, the NP effects can also be observed in the hadron and lepton polarization asymmetries. However, no deviation has been found in the presence of V_L coupling from their corresponding SM results.

3.3.2 Scenario B: Only V_R coefficient

Here, we assume that only the new V_R coefficient is present in addition to the SM contribution, in the effective Lagrangian (3.1). To investigate the effect of NP coming from V_R coefficient, we first constrain the new coefficient by imposing 3σ experimental bound on the $b \to (u, c)\tau\bar{\nu}_\tau$ anomalies. Using the values from Table 3.1, we show the plots for the branching ratios of $\Lambda_b \to p\ (\Lambda_c)\tau\bar{\nu}_\tau$ process in the top-left panel (top-right panel) of Fig. 3.5. In these figures, the cyan bands are due to the additional contribution from V_R coefficient. We notice significant deviation in the branching ratios from their corresponding SM results. The predicted values of the branching ratios for V_R coefficient are presented in Table 3.2. Apart from branching ratios, we are also interested to see the effect of this new coefficient on various q^2 dependent observables. The q^2 variation of the forward backward asymmetry and the convexity parameters for $\Lambda_b \to p\tau^-\bar{\nu}_\tau$ (left) and $\Lambda_b \to \Lambda_c\tau^-\bar{\nu}_\tau$ (right) decay processes are depicted in the middle and bottom panels of Fig. 3.5, respectively. The deviation of convexity parameters from their SM prediction are quite noticeable in these plots. In the presence of V_R coefficient, the numerical values of the C^{τ}_F parameters are

$$\langle C^{\tau}_F\rangle|^{V_R}_{\Lambda_b\to p} = -0.169 \to -0.147\,, \qquad \langle C^{\tau}_F\rangle|^{V_R}_{\Lambda_b\to\Lambda_c} = -0.105 \to -0.094\,. \tag{3.32}$$

The effect of V_R coefficient is found to be rather significant on the forward-backward

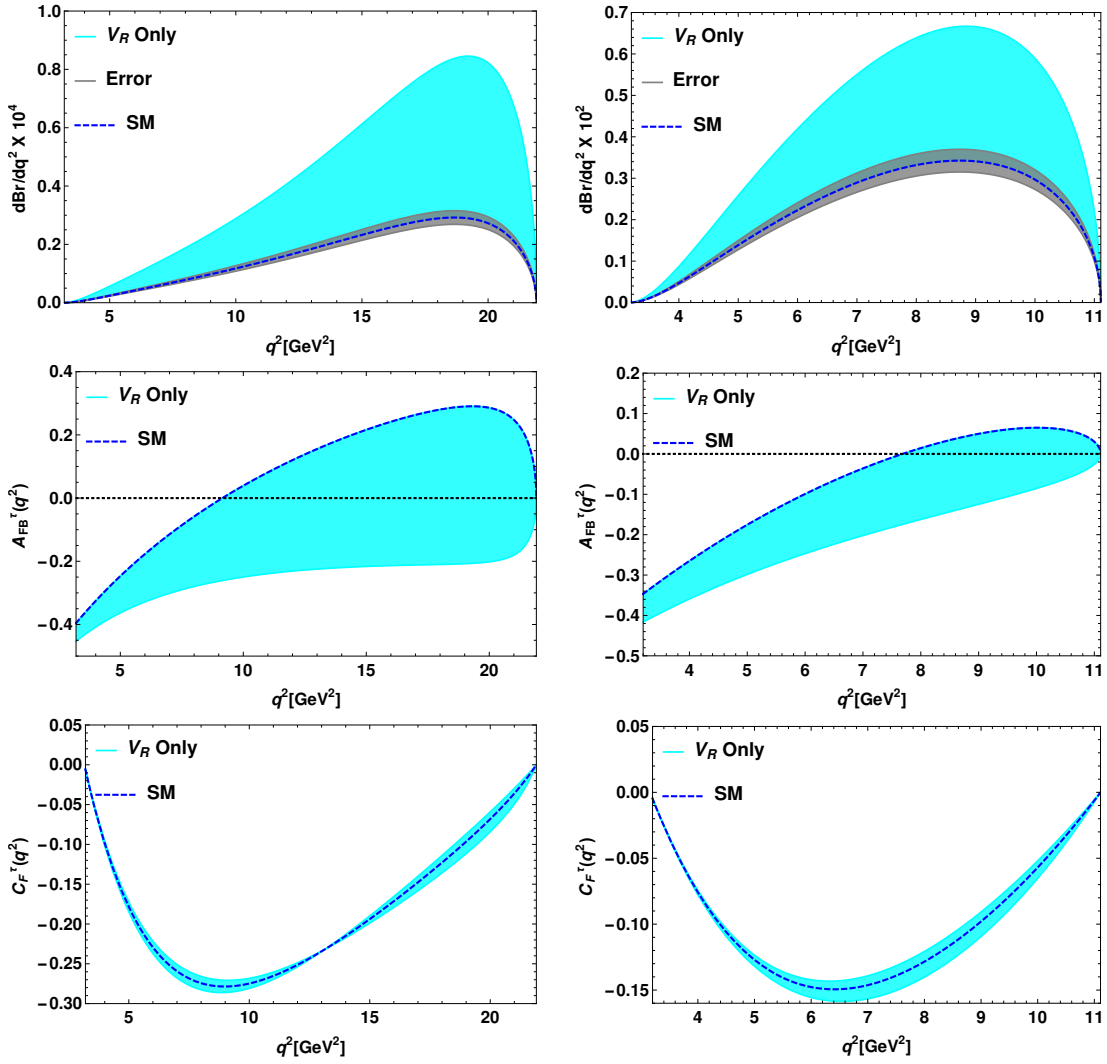

FIGURE 3.5: Top panel represents the q^2 variation of branching ratio of $\Lambda_b \to p\tau^-\bar{\nu}_\tau$ (left panel) and $\Lambda_b \to \Lambda_c^+\tau^-\bar{\nu}_\tau$ (right panel) for only V_R new coefficient. The corresponding plots of forward backward asymmetry and the convexity parameters are shown in the middle and bottom panels respectively. Here cyan bands are due to the additional new physics contribution coming from only V_R coefficient.

asymmetry observables of both $\Lambda_b \to p(\Lambda_c)\tau^-\bar{\nu}_\tau$ decay modes and the corresponding numerical values are

$$\langle A_{FB}^{\tau}\rangle|^{V_R}_{\Lambda_b\to p} = -0.248 \to 0.115\ , \quad \langle A_{FB}^{\tau}\rangle|^{V_R}_{\Lambda_b\to\Lambda_c} = -0.23 \to -0.09\ . \quad (3.33)$$

Left and right panels of Fig. 3.6, depict the variation of R_p and R_{Λ_c} parameters with respect to q^2. Though there are no experimental limits on these parameters, significant deviation from their SM values are noticed in the scenario with only V_R coupling. The right panel of Fig. 3.7 represents the q^2 variation of $R^{\tau}_{\Lambda_c p}$ parameter. The corresponding numerical values are listed in Table 3.2 .

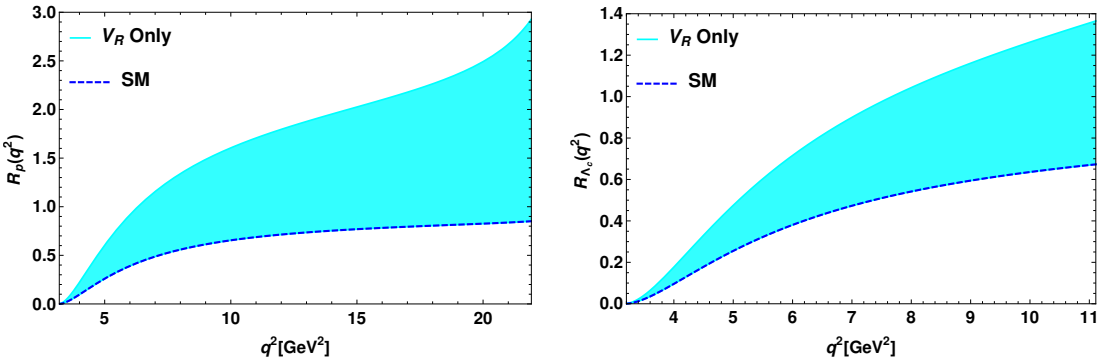

FIGURE 3.6: The variation of R_p (left panel) and R_{Λ_c} (right panel) LNU parameters with respect to q^2 in the presence of only V_R new coefficient.

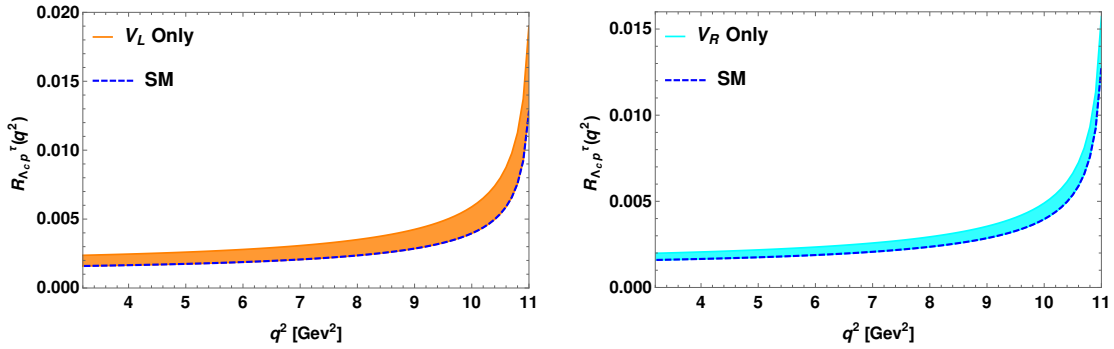

FIGURE 3.7: The variation of $R^{\tau}_{\Lambda_c p}$ parameter with respect to q^2 in the presence of only V_L (left panel) and V_R (right panel) new coefficients.

TABLE 3.2: The predicted values of branching ratios and lepton non-universality parameters of $\Lambda_b \to (\Lambda_c, p)\tau\bar{\nu}_\tau$ processes in the SM and in the presence of only $V_{L,R}$ coefficients.

Observables	SM prediction	Values for V_L coupling	Values for V_R coupling
$\text{BR}(\Lambda_b \to p\tau^-\bar{\nu}_\tau)$	$(2.98 \pm 0.238) \times 10^{-4}$	$(0.298 - 1.34) \times 10^{-3}$	$(2.98 - 8.17) \times 10^{-4}$
R_p	0.692	$0.692 - 3.09$	$0.692 - 1.895$
$\text{BR}(\Lambda_b \to \Lambda_c^+\tau^-\bar{\nu}_\tau)$	$(1.76 \pm 0.14) \times 10^{-2}$	$(1.76 - 5.29) \times 10^{-2}$	$(1.76 - 3.4) \times 10^{-2}$
R_{Λ_c}	0.353	$0.353 - 1.06$	$0.353 - 0.68$
$R_{\Lambda_c p}$	$(1.693 \pm 0.19) \times 10^{-2}$	$(1.693 - 2.533) \times 10^{-2}$	$(1.693 - 2.4) \times 10^{-2}$

Though the presence of V_L coefficient has no effect on the lepton and hadron polarization asymmetries of $b \to (u, c)\tau\bar{\nu}_\tau$ decay modes, the V_R coefficient has significant impact on these parameters. In the top panel of Fig. 3.8, the distribution of the longitudinal polarization components of the daughter baryon p (left panel) and Λ_c (right panel) are shown both in the SM and in the presence of only V_R coefficient, and the corresponding plots for the charged τ lepton are presented in the bottom panel. The integrated values of the hadron longitudinal polarization asymmetry parameters in the full physical phase

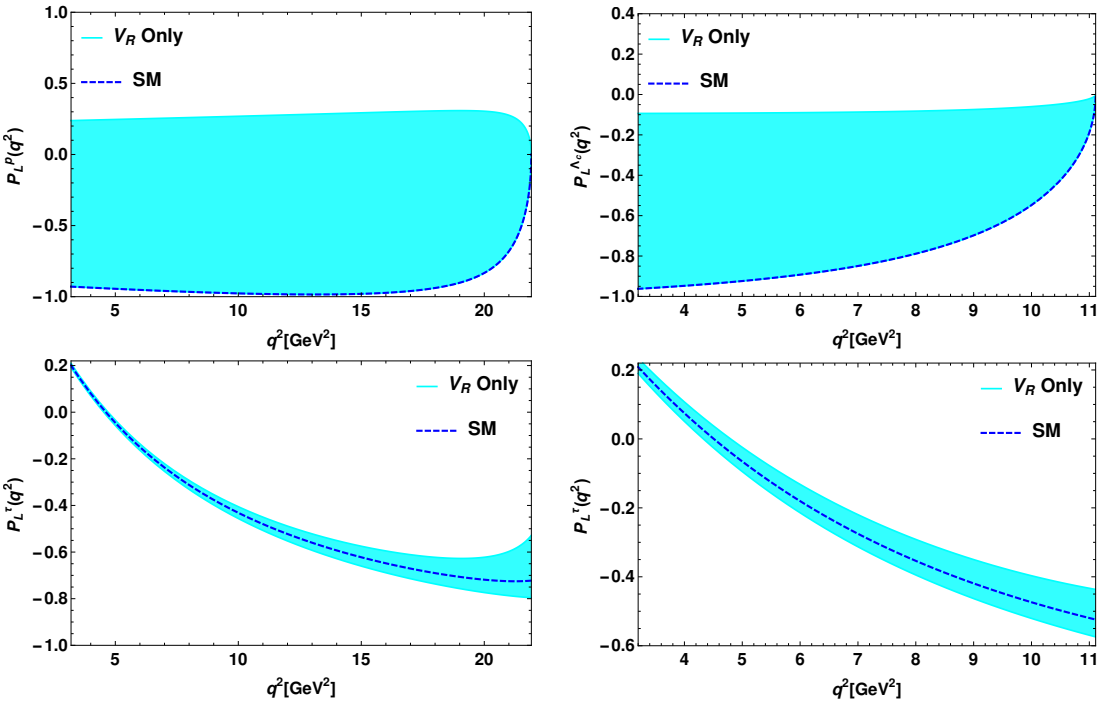

FIGURE 3.8: The plots in the left panel represent the longitudinal polarizations of daughter light baryon p (left-top panel) and the charged τ lepton (left-bottom) with respect to q^2 for only V_R coefficient. The corresponding plots for $\Lambda_b \to \Lambda_c \tau^- \bar{\nu}_\tau$ mode are shown in the right panel.

space are

$$\langle P_L^p \rangle|^{\rm SM}_{\Lambda_b \to p} = -0.897 \,, \qquad \langle P_L^{\Lambda_c} \rangle|^{\rm SM}_{\Lambda_b \to \Lambda_c} = -0.797 \,, \tag{3.34}$$

$$\langle P_L^p \rangle|^{V_R \text{ Only}}_{\Lambda_b \to p} = -0.897 \to 0.276 \,, \qquad \langle P_L^{\Lambda_c} \rangle|^{\rm V_R \text{ Only}}_{\Lambda_b \to \Lambda_c} = -0.797 \to -0.068 \tag{3.35}$$

and the corresponding numerical values for the charged lepton τ, are

$$\langle P_L^\tau \rangle|^{\rm SM}_{\Lambda_b \to p} = -0.514 \,, \qquad \langle P_L^\tau \rangle|^{\rm SM}_{\Lambda_b \to \Lambda_c} = -0.207 \,, \tag{3.36}$$

$$\langle P_L^\tau \rangle|^{V_R}_{\Lambda_b \to p} = -0.577 \to -0.433 \,, \qquad \langle P_L^\tau \rangle|^{V_R}_{\Lambda_b \to \Lambda_c} = -0.25 \to -0.146 \,. \tag{3.37}$$

3.3.3 Scenario C: Only S_L coefficient

Here, we explore the impact of only S_L coefficient on the angular observables of heavy-heavy and heavy-light semileptonic decays of Λ_b baryon. In section III, we discussed the constraints on the S_L coupling. In the top panel Fig. 3.9 , we present the plots for the differential branching ratios of $\Lambda_b \to p\tau\bar{\nu}_\tau$ (left) and $\Lambda_b \to \Lambda_c \tau \bar{\nu}_\tau$ (right) decay processes with respect to q^2 in the presence of S_L coefficient. The corresponding plots for the forward-backward asymmetry are shown in the bottom panel. In these figures, the red bands stand for the NP contribution from S_L coefficient. The additional contributions

provide deviation in the branching ratios and forward-backward asymmetries from their SM values. The q^2 variation of the R_p (left panel) and R_{Λ_c} (right panel) LNU parameters in the presence of S_L coupling are given in Fig. 3.10 . In the presence of only S_L coupling, the longitudinal polarization components of the p (top-left panel) and Λ_c (top-right panel) daughter baryons with respect to q^2 are presented in the top panel of Fig. 3.11 and the bottom panel depicts the longitudinal lepton polarization asymmetry parameters for $\Lambda_b \to p(\Lambda_c)\tau\bar{\nu}_\tau$ processes. The lepton polarization asymmetry parameters provide profound deviation from the SM in comparison to their longitudinal hadron polarization parameters. The top-left panel of Fig. 3.18 shows the variation of $R^{\tau}_{\Lambda_c p}$ parameter with q^2. In Table 3.3 , we report the numerical values of all these parameters.

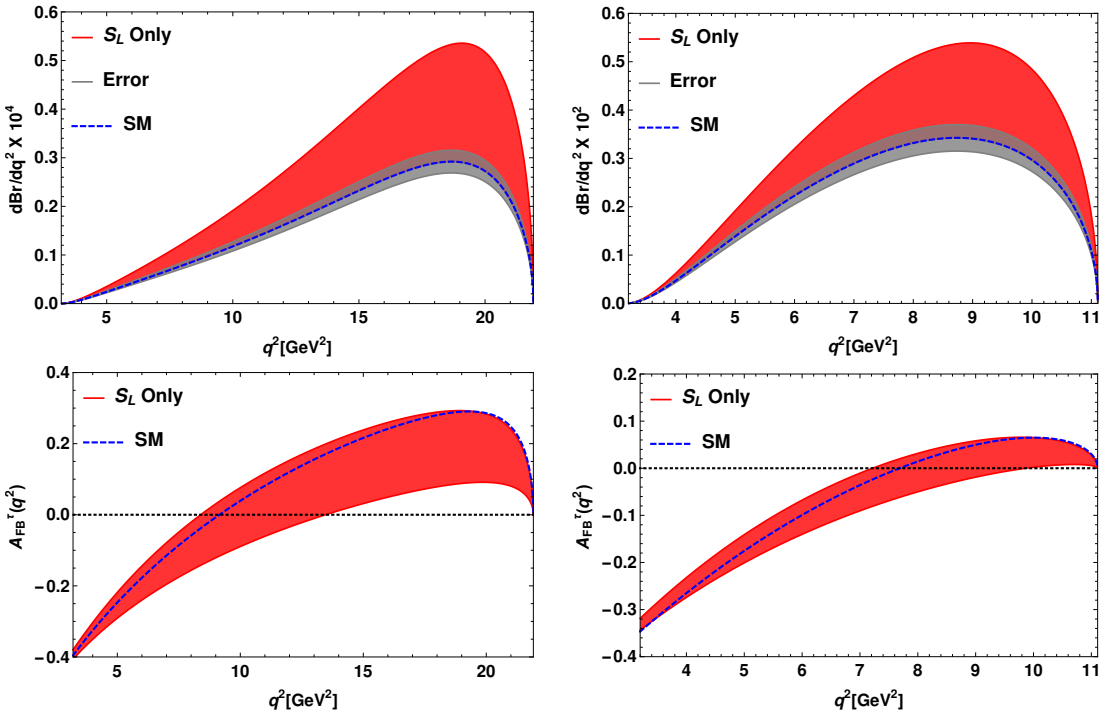

FIGURE 3.9: Top panel represents the q^2 variation of branching ratios of $\Lambda_b \to p\tau^-\bar{\nu}_\tau$ (left panel) and $\Lambda_b \to \Lambda_c^+\tau^-\bar{\nu}_\tau$ (right panel) decay modes in the presence of only S_L new coefficient. The corresponding plots for forward-backward asymmetries are shown in the bottom panel. Here red bands are due to the additional new physics contribution coming from only S_L coefficient.

3.3.4 Scenario D: Only S_R coefficient

In this subsection, we perform an analysis for semileptonic decay modes of Λ_b baryon with the additional S_R coupling. Using the allowed ranges of the real and imaginary part of S_R coupling from Table 3.1 , the branching ratios of $\Lambda_b \to p\tau\bar{\nu}_\tau$ (left) and $\Lambda_b \to \Lambda_c\tau\bar{\nu}_\tau$ (right) decay processes with respect to q^2 are presented in Fig. 3.12 . The bottom panel of this figure represents the q^2 variation of the forward-backward asymmetry for

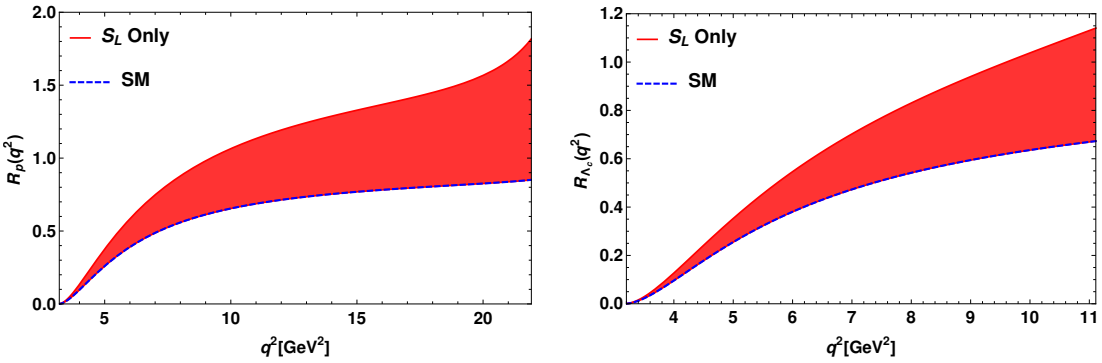

FIGURE 3.10: The variation of R_p (left panel) and R_{Λ_c} (right panel) with respect to q^2 in the presence of only S_L coefficient.

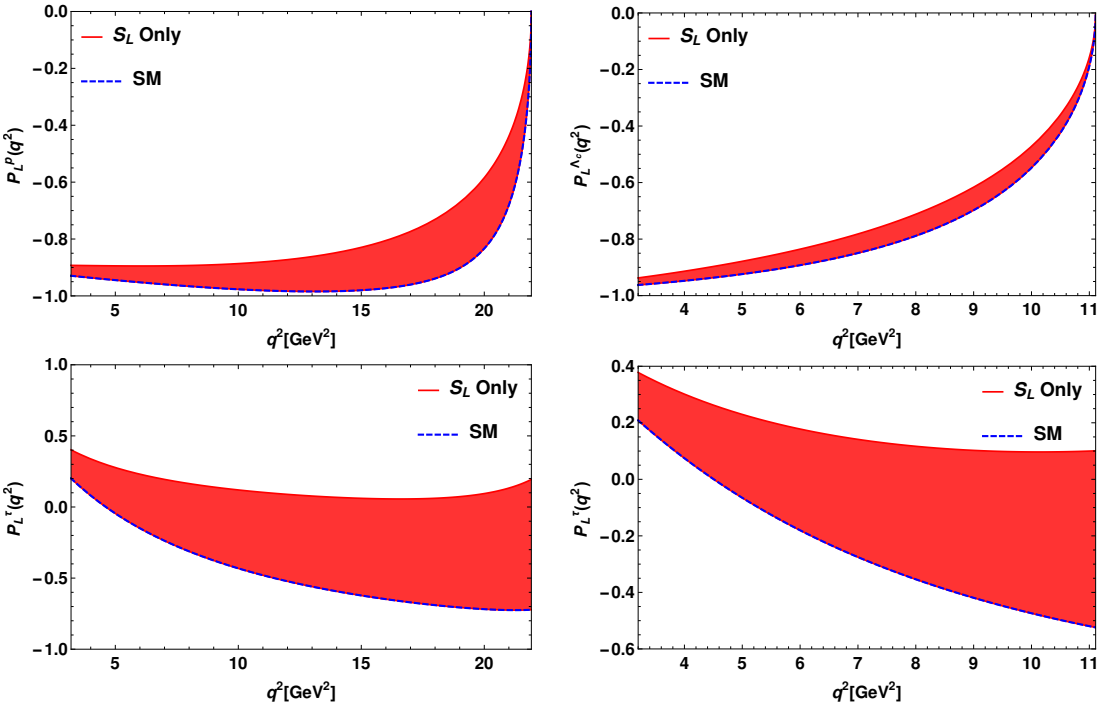

FIGURE 3.11: The plots in the left panel represent the longitudinal polarizations of daughter light baryon p (left-top panel) and the charged τ lepton (left-bottom) with respect to q^2 for only S_L coefficient. The corresponding plots for $\Lambda_b \to \Lambda_c \tau^- \bar{\nu}_\tau$ mode are shown in the right panel.

$\Lambda_b \to p\tau\bar{\nu}_\tau$ (left) and $\Lambda_b \to \Lambda_c\tau\bar{\nu}_\tau$ (right). In these figures, the green bands are due to the additional new contribution of S_R coefficient to the SM. We observe profound deviation in the branching ratios and forward-backward asymmetries of these decay modes from their SM values. Left (right) panel of Fig. 3.13, show the effect of S_R coupling on the q^2 variation of R_p (R_{Λ_c}) parameter. The longitudinal polarization components of the p (top-left panel) and Λ_c (top-right panel) daughter baryons with respect to q^2 in the presence of contribution from only S_R coefficient, are presented in the top panel of Fig. 3.14 and the bottom panel depict the longitudinal lepton polarization asymmetry parameters for $\Lambda_b \to p(\Lambda_c)\tau\bar{\nu}_\tau$ processes. We notice significant deviation of hadron and

lepton polarization asymmetries from their corresponding SM values due to additional contribution from S_R coupling. The plot for the $R^{\tau}_{\Lambda_c p}$ parameter with q^2 in the presence of only S_R coefficient is presented in the right panel of Fig. 3.18 . The numerical values of all these parameters are presented in Table 3.3 . Since the convexity parameters are independent of scalar type couplings, the $S_{L,R}$ coefficients play no role for this parameter.

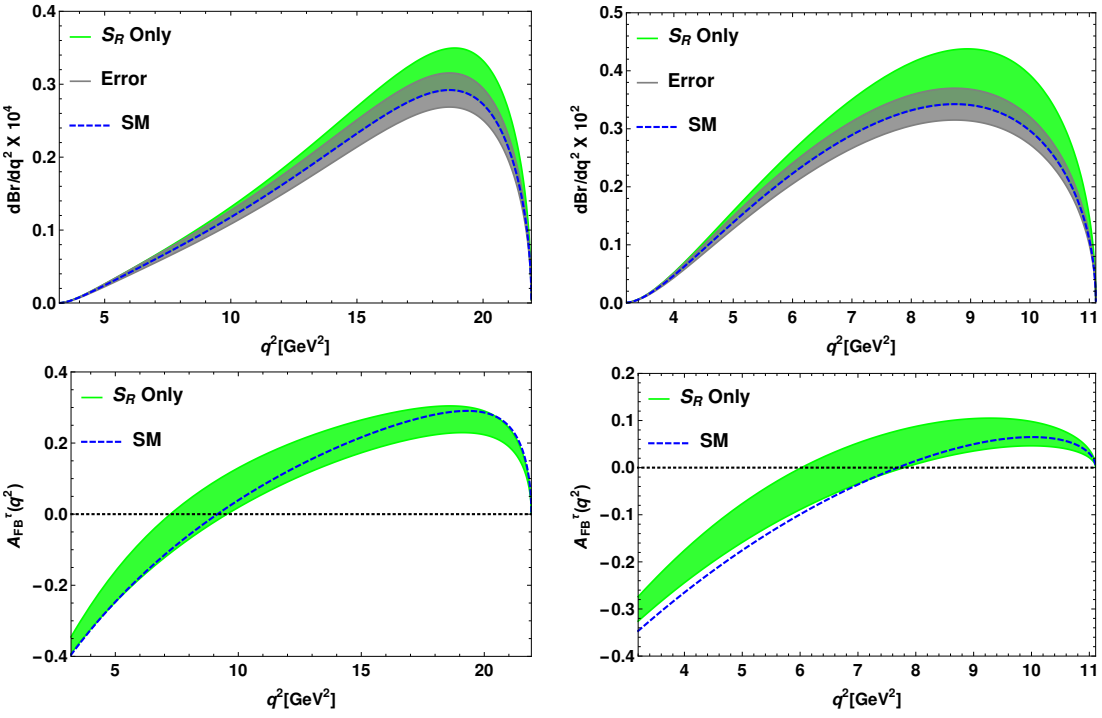

FIGURE 3.12: Top panel represents the q^2 variation of branching ratios of $\Lambda_b \to p\tau^-\bar{\nu}_\tau$ (left panel) and $\Lambda_b \to \Lambda_c^+\tau^-\bar{\nu}_\tau$ (right panel) decay processes in the presence of only S_R coefficient. The corresponding plots for the forward-backward asymmetries are shown in the bottom panel. Here green bands stand for the additional new physics contribution coming from only S_R coefficient.

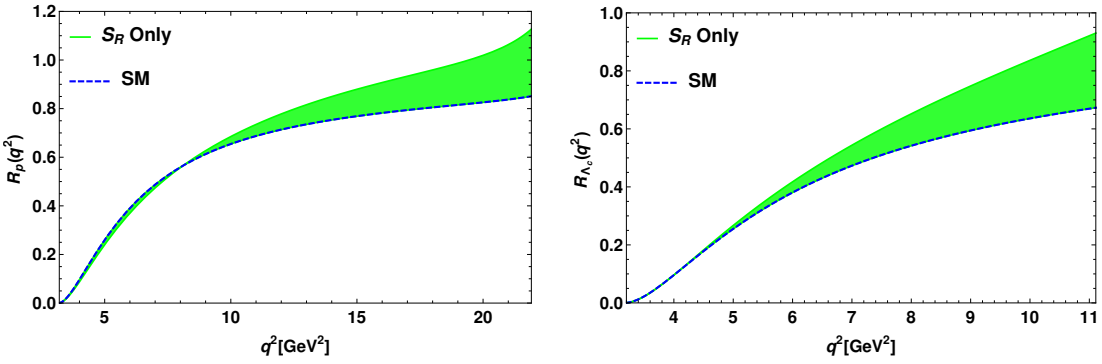

FIGURE 3.13: The variation of R_p (left panel) and R_{Λ_c} (right panel) with respect to q^2 in the presence of only S_R coefficient.

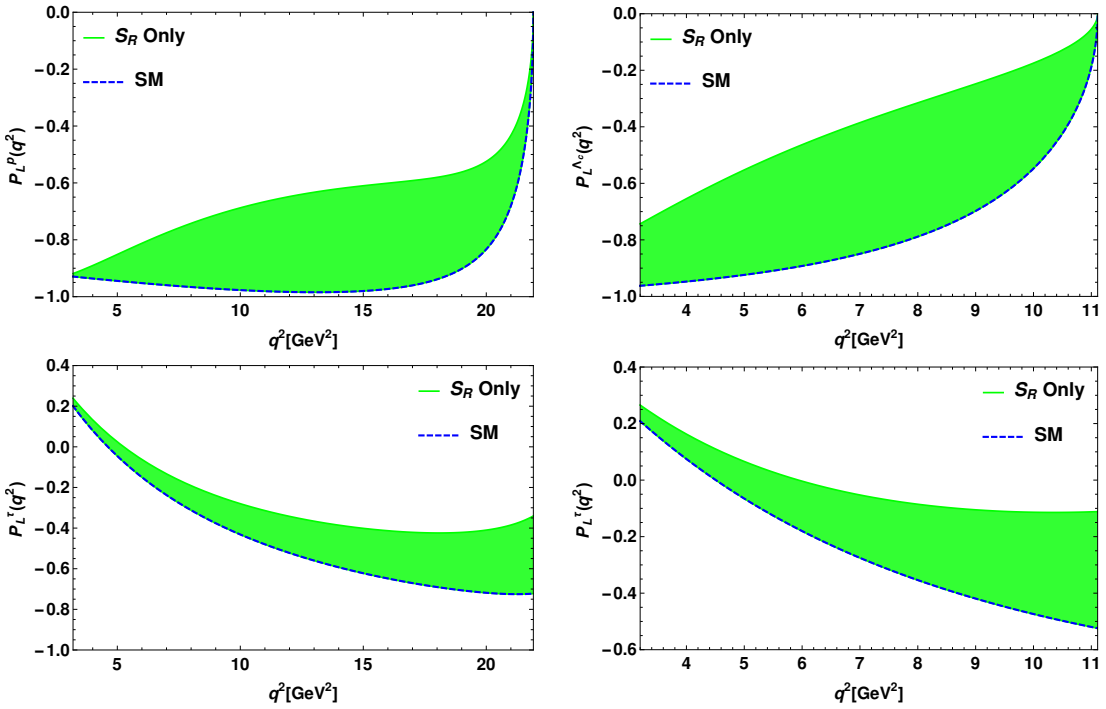

FIGURE 3.14: The plots in the left panel represent the longitudinal polarizations of daughter light baryon p (left-top panel) and the charged τ lepton (left-bottom) with respect to q^2 for only S_R coefficient. The corresponding plots for $\Lambda_b \to \Lambda_c \tau^- \bar{\nu}_\tau$ mode are shown in the right panel.

3.3.5 Scenario E: Only T_L coefficient

The sensitivity of tensor coupling on various physical observables associated with semileptonic baryonic $b \to (c, u)\tau\bar{\nu}_\tau$ decay processes will be investigated in this subsection. The allowed region of real and imaginary parts of the tensor coupling are presented in section III. Using all the input parameters and the constrained new tensor coefficient, we show the q^2 variation of branching ratio (left-top panel), forward-backward asymmetry (left-middle panel) and convexity parameter (left-bottom panel) of $\Lambda_b \to p\tau\bar{\nu}_\tau$ decay mode in the left panel of Fig. 3.15 . The right panel of this figure represents the corresponding plots for $\Lambda_b \to \Lambda_c\tau\bar{\nu}_\tau$ process. Here the magenta bands represent the additional contribution coming from the new T_L coefficient. For $\Lambda_b \to p\tau\bar{\nu}_\tau$ process, as the bound on T_L is weak, the branching ratio, forward-backward asymmetry and the convexity parameter deviate significantly from their SM predications compared to the observables for $\Lambda_b \to \Lambda_c\tau\bar{\nu}_\tau$ process. For $\Lambda_b \to \Lambda_c\tau\bar{\nu}_\tau$ process, the deviations are quite minimal as the coefficient T_L is severely constrained. In the presence of T_L coefficient, the numerical values of the convexity parameters are

$$\langle C_F^\tau \rangle|^{T_L}_{\Lambda_b \to p} = -0.017 \to -0.027 \,, \qquad \langle C_F^\tau \rangle|^{T_L}_{\Lambda_b \to \Lambda_c} = -0.121 \to -0.098 \,. \tag{3.38}$$

The plots for the lepton nonuniversality parameter R_p (left panel) and R_{Λ_c} (right panel) are shown in Fig. 3.16 . The top panel of Fig. 3.17 represents the hadron polarization asymmetry parameters of $\Lambda_b \to p\tau\bar{\nu}_\tau$ (left panel) and $\Lambda_b \to \Lambda_c\tau\bar{\nu}_\tau$ (right panel) process and the corresponding plots for lepton polarization asymmetries are given in the bottom panel of this figure. We observe that, the LNU parameter, longitudinal hadron and lepton polarization asymmetries of $\Lambda_b \to p\tau\bar{\nu}_\tau$ process have large deviation from their SM values due to the presence of tensor coupling, whereas negligible deviations (R_{Λ_c} has some deviation from its SM result) are noticed for the observables of $\Lambda_b \to \Lambda_c\tau\bar{\nu}_\tau$ decay mode. The q^2 variation of $R^{\tau}_{\Lambda_c p}$ parameter is depicted in the bottom panel of Fig. 3.18 . Table 3.3 shows the integrated values of all these angular observables.

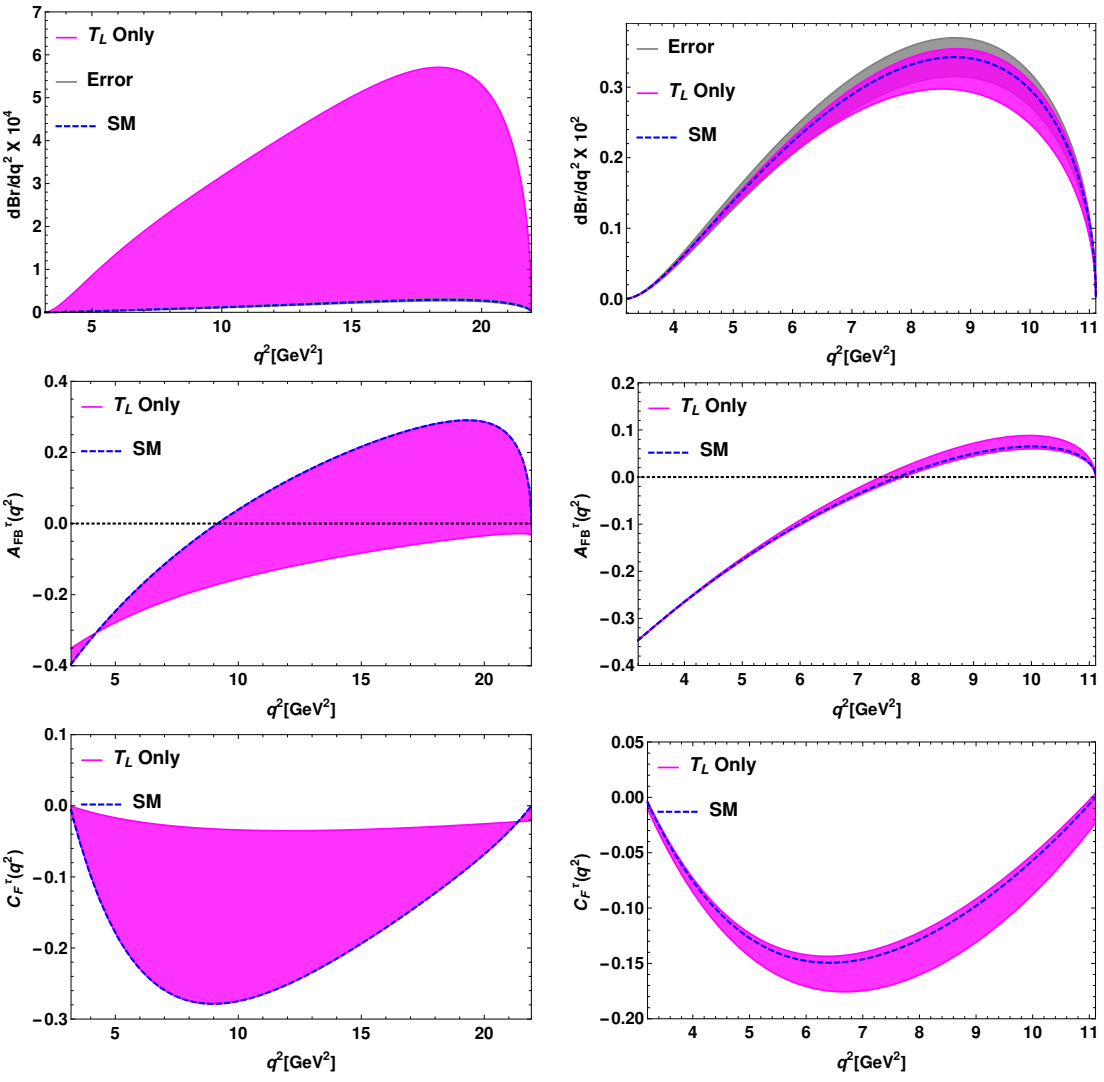

FIGURE 3.15: Top panel represents the q^2 variation of branching ratio of $\Lambda_b \to p\tau^-\bar{\nu}_\tau$ (left panel) and $\Lambda_b \to \Lambda_c^+\tau^-\bar{\nu}_\tau$ (right panel) for only T_L new coefficient. The corresponding plots of forward backward asymmetry and the convexity parameters are shown in the middle and bottom panels respectively. Here magenta bands are due to the additional new physics contribution coming from only T_L coefficient.

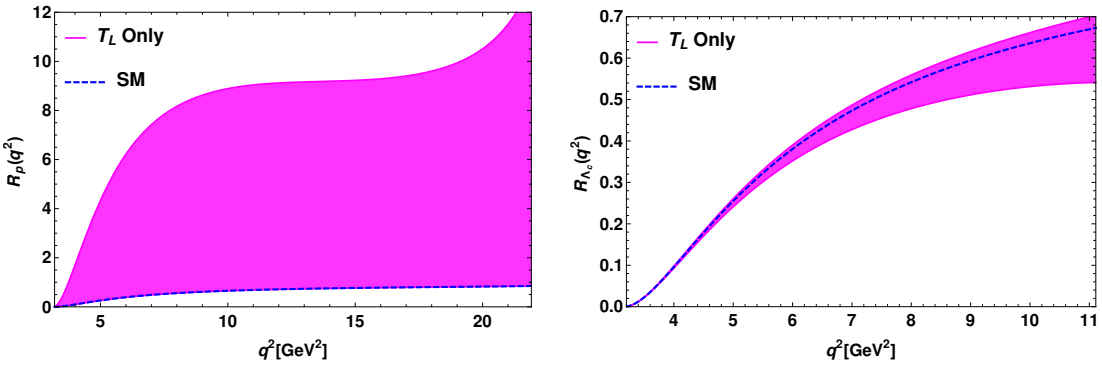

FIGURE 3.16: The variation of R_p (left panel) and R_{Λ_c} (right panel) with respect to q^2 in the presence of only T_L coefficient.

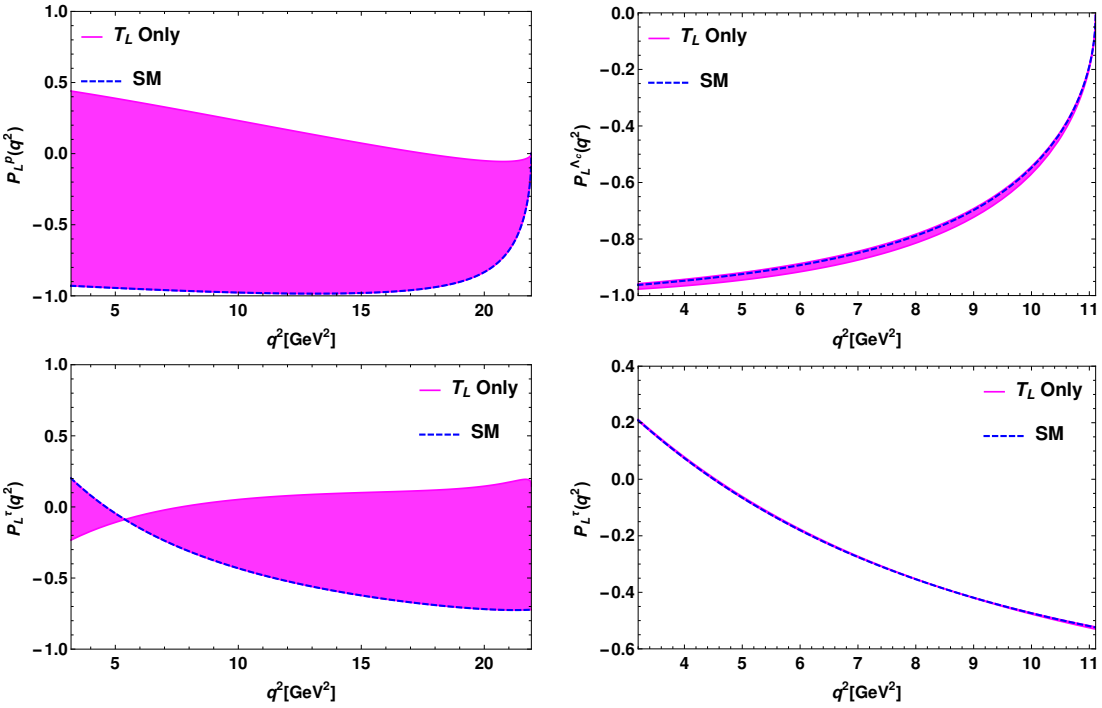

FIGURE 3.17: The plots in the left panel represent the longitudinal polarizations of daughter light baryon p (left-top panel) and the charged τ lepton (left-bottom) with respect to q^2 for only T_L coefficient. The corresponding plots for $\Lambda_b \to \Lambda_c \tau^- \bar{\nu}_\tau$ mode are shown in the right panel.

3.4 Chapter summary

In this work, we have performed a model independent analysis of baryonic $\Lambda_b \to (\Lambda_c, p) l \bar{\nu}_l$ decay processes by considering the generalized effective Lagrangian in the presence of new physics. We considered the new couplings to be complex in our analysis. In order to constrain the new couplings, we have assumed that only one coefficient to be present at a time and constrained the new coefficients by comparing the theoretical predictions of BR$(B^+_{u,c} \to \tau^+ \nu_\tau)$, BR$(B \to \pi \tau \bar{\nu}_\tau)$, R^l_π, $R_{D^{(*)}}$ and $R_{J/\psi}$ observables

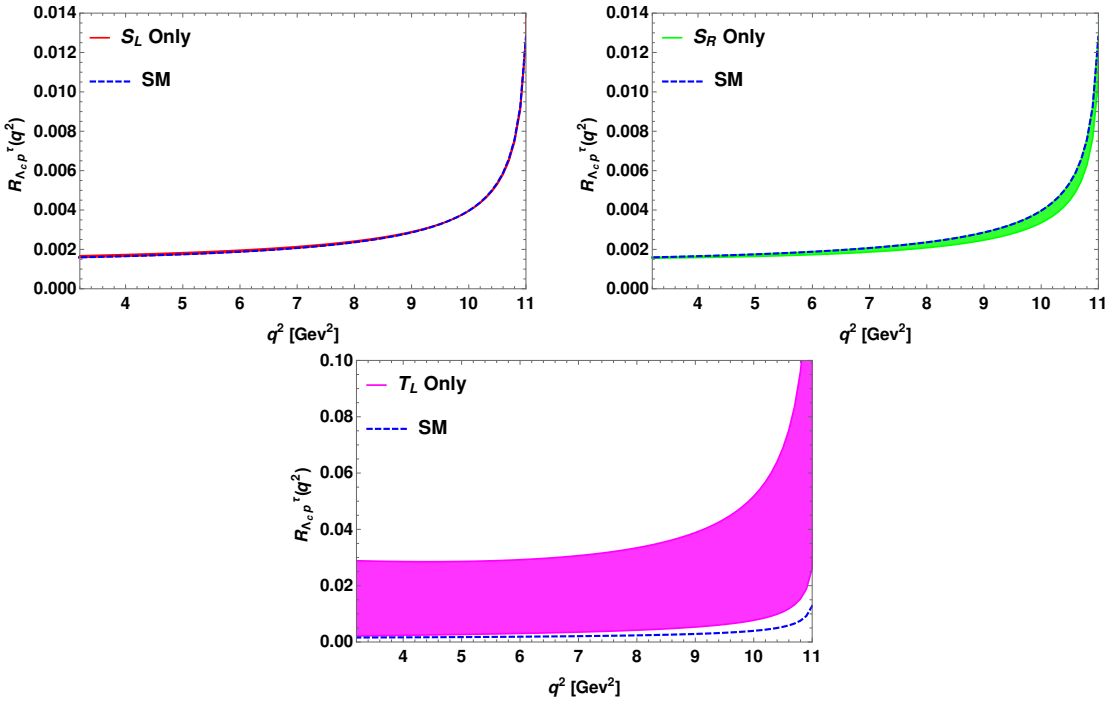

FIGURE 3.18: The variation of $R^{\tau}_{\Lambda_c p}$ parameter with respect to q^2 in the presence of only S_L (top-left panel), S_R (top-right panel) and T_L (bottom panel) coefficients.

TABLE 3.3: The predicted values of branching ratios, forward-backward asymmetries, longitudinal hadron ad lepton polarization asymmetries and lepton non-universality parameters of $\Lambda_b \to (\Lambda_c, p)\tau\bar{\nu}_\tau$ processes in the SM and in the presence of only $S_{L,R}$ and T_L new coefficients.

Observables	Values for S_L coupling	Values for S_R coupling	Values for T_L coupling
$\mathrm{BR}(\Lambda_b \to p\tau^-\bar{\nu}_\tau)$	$(2.98 - 5.25).10^{-4}$	$(2.98 - 3.48).10^{-4}$	$(0.298 - 6.68).10^{-3}$
A^{τ}_{FB}	$-0.019 \to 0.139$	$0.086 \to 0.177$	$-0.172 \to -0.125$
P^{p}_{L}	$-0.896 \to -0.73$	$-0.896 \to -0.6$	$-0.896 \to 0.337$
P^{τ}_{L}	$-0.515 \to 0.123$	$-0.515 \to -0.31$	$-0.515 \to 0.037$
R_p	$0.692 - 1.266$	$0.692 - 0.81$	$0.692 - 8.8$
$\mathrm{BR}(\Lambda_b \to \Lambda_c^+\tau^-\bar{\nu}_\tau)$	$(1.76 - 2.7).10^{-2}$	$(1.76 - 2.2).10^{-2}$	$(1.553 - 1.82).10^{-2}$
A^{τ}_{FB}	$-0.121 \to -0.06$	$-0.786 \to -0.005$	$-0.034 \to -0.09$
$P^{\Lambda_c}_{L}$	$-0.796 \to -0.725$	$-0.796 \to -0.4$	$-0.79 \to -0.812$
P^{τ}_{L}	$-0.207 \to 0.178$	$-0.207 \to -0.0021$	-0.207
R_{Λ_c}	$0.353 - 0.539$	$0.353 - 0.44$	$0.31 \to 0.364$
$R_{\Lambda_c p}$	$(1.693 - 1.95).10^{-2}$	$(1.582 - 1.693).10^{-2}$	$0.0192 - 0.367$

with their measured experimental data. Using the allowed parameter space, we estimated the branching ratios, forward-backward asymmetries, convexity parameters of $\Lambda_b \to (\Lambda_c, p)l\bar{\nu}_\tau$ decay processes. We also investigated the longitudinal polarization components of the daughter baryon (p, Λ_c) and the final state charged lepton, τ. The convexity parameter only depend on the (axial)vector and tensor type couplings and

are independent of the $S_{L,R}, T_L$ coefficients. Inspired by the observation of lepton non-universality parameters in various B meson decays, we have also scrutinized the lepton universality violating parameters ($R_p, R_{\Lambda_c}, R^{\tau}_{\Lambda_c p}$) in the baryonic decay modes.

Chapter 4

Exploring the role of New Physics in $B^* \to Pl\bar{\nu}_l$ decay processes

In this chapter, we study the semileptonic decays of vector mesons $B^*_{d,(s)}$ to pseudoscalar mesons $(D(D_s), \pi(K))$ in a model independent framework. The weak decay channels of $B*$ meson are quite suppressed. Primarily they decay through electromagnetic processes $B^*_{d,s} \to B_{d,s}\gamma$, but due to the high luminosity of Belle II experiment the rare decay modes of B^* mesons are expected to be observed. The production crosssection of $\Upsilon(5S)$ in e^+, e^- colision ($\sigma(e^+e \to \Upsilon(5S)) = 0.301$ nb and $\text{Br}(\Upsilon(5S) \to B^*\bar{B}^*) = (38.1 \pm 3.4)\%$ implies the yearly production of around 4×10^9 B^* meson pairs $(B^*_{u,d} + \bar{B}^*_{u,d})$. As the production cross section of $\Upsilon(5S)$ in $p\bar{p}$ collision is larger in comparision to e^+e^- collision, LHCb is also going to play an important role to observe B^* decay channels. The leptonic decay mode of $B^*_{d,s}$ are studied in [81–84], where as in ref. [85–87] various semileptonic decays of B^* meson to a pseudoscalar meson are studied.

4.1 Analysis of $B^* \to Pl\nu_l$ processes

In effective field theory approach the most general effective Lagrangian associated with $B^* \to Pl\bar{\nu}_l$ processes which is mediated by $b \to ql^-\bar{\nu}_l$ $(q = u, c)$ can be expressed as [72],

$$\begin{aligned}\mathcal{L}_{eff} &= -2\sqrt{2}G_F V_{qb}\Big[(1+V_L)\ \bar{q}_L\gamma^\mu b_L\ \bar{l}_L\gamma_\mu\nu_L + V_R\ \bar{q}_R\gamma^\mu b_R\ \bar{l}_L\gamma_\mu\nu_L + S_L\ \bar{q}_R b_L\ \bar{l}_R\nu_L \\ &\quad + S_R\ \bar{q}_L b_R\ \bar{l}_R\nu_L + T_L\ \bar{q}_R\sigma^{\mu\nu}b_L\ \bar{l}_R\sigma_{\mu\nu}\nu_L + \text{h.c.}\Big], \end{aligned} \tag{4.1}$$

where P is any pseudoscalr meson, G_F is the Fermi constant, V_{qb} is the CKM matrix element, $V_{L,R},\ S_{L,R}, T_L$ are the new vector, scalar, and tensor type new physics couplings, which are zero in the standard model. All these new physics couplings are considered

to be complex. Furthermore, we consider the neutrinos as left handed. We assume the NP effect is mainly through the third generation leptons and do not consider the effect of tensor operators in our analysis for simplicity. Here $(q,l)_{L,R} = P_{L,R}(q,l)$, where $P_{L,R} = (1 \mp \gamma_5)/2$ are the chiral projection operators.

We consider the kinematics of the decay process $B^* \to Pl\bar{\nu}_l$ using helicity amplitudes. In this formalism, the decay process $B^* \to Pl\bar{\nu}_l$ is considered to proceed through $\bar{B}^* \to PW^{*-}$, where the off-shell W^{*-} decays to $l^-\bar{\nu}_l$. One can write the amplitude from Eq. (4.1) as

$$\mathcal{M}(B^* \to Pl\bar{\nu}_l) = \frac{G_F}{\sqrt{2}} V_{qb} \sum_k \langle P|\bar{q}\Gamma^k b|B^*\rangle \ \bar{u}_l \Gamma_k v_\nu \ , \tag{4.2}$$

where Γ^k denotes the product of gamma matrices, which gives rise to different Lorentz structure of hadronic and leptonic currents of Eq. (4.1) i.e., $\Gamma^k = \gamma^\mu(1\pm\gamma_5)$, and $(1\pm\gamma_5)$. Hence, the square of the matrix element can be expressed as the product of leptonic $(L_{\mu\nu})$ and hadronic $(H^{\mu\nu})$ tensors (related to the corresponding helicity amplitudes)

$$\left|\mathcal{M}(B^* \to Pl\bar{\nu}_l\right|^2 = \frac{G_F^2}{2}|V_{qb}|^2 \sum_{i,j} L^{ij}_{\mu\nu} H^{\mu\nu,ij} \ , \tag{4.3}$$

where the superscripts i, j represent the combination of four operators $(V \mp A), (S \mp P)$ in the effective Lagrangian (4.1). We omit these superscripts in the following discussion for convenience. It should be noted that, the polarization vector of the off-shell particle W^* $(\bar{\epsilon}^\mu(m))$, satisfies the following orthonormality and completeness relations:

$$\begin{aligned} &\bar{\epsilon}^{*\mu}(m)\bar{\epsilon}_\mu(m') = g_{mm'} \ , \\ &\sum_{mm'} \bar{\epsilon}^{*\mu}(m)\bar{\epsilon}^\nu(m') g_{mm'} = g^{\mu\nu} \ , \end{aligned} \tag{4.4}$$

where $g_{mm'} = \text{diag}(+,-,-,-)$ and $m, m' = \pm, 0, t$ represent the transverse, longitudinal and time-like polarization components. Now inserting the completeness relation from Eq. (4.4) into (4.3), the product of $L_{\mu\nu}$ and $H^{\mu\nu}$ can be expressed as

$$L_{\mu\nu}H^{\mu\nu} = \sum_{m,m',n,n'} L(m,n)H(m',n')g_{mm'}g_{nn'} \ , \tag{4.5}$$

where $L(m,n) = L^{\mu\nu}\bar{\epsilon}_\mu(m)\bar{\epsilon}^*_\nu(n)$ and $H(m,n) = H^{\mu\nu}\bar{\epsilon}^*_\mu(m)\bar{\epsilon}_\nu(n)$ are the Lorentz invariant parameters, and hence their values are independent of any specific reference frame. So for calculational convenience, we will evaluate $H(m,n)$ in the B^* rest frame and $L(m,n)$ in $l - \bar{\nu}_l$ center of mass frame as discussed in [85, 86].

4.1.1 Hadronic helicity amplitudes

In the rest frame of B^* meson, we consider the pseudoscalar meson P to be moving along the positive z-direction. The polarization vector of the virtual W^* boson are chosen to be

$$\bar{\epsilon}^\mu(t) = \frac{1}{q^2}(q_0, 0, 0, -|\vec{p}|), \quad \bar{\epsilon}^\mu(0) = \frac{1}{q^2}(|\vec{p}|, 0, 0, -q_0), \quad \bar{\epsilon}^\mu(\pm) = \frac{1}{\sqrt{2}}(0, \pm 1, -i, 0), \quad (4.6)$$

where $q_0 = (m_{B^*}^2 - m_P^2 + q^2)/2m_{B^*}$, $|\vec{p}| = \lambda^{1/2}(m_{B^*}^2, m_P^2, q^2)/2m_B^*$, $q^2 = (p_{B^*} - p_P)^2$, is the momentum transferred square and $\lambda(a, b, c) = a^2 + b^2 + c^2 - 2(ab + bc + ca)$. The polarization vector of the on-shell B^* meson $\varepsilon^\mu(m = 0, \pm)$, takes the form

$$\varepsilon^\mu(0) = (0, 0, 0, 1), \quad \varepsilon^\mu(\pm) = \frac{1}{\sqrt{2}}(0, \mp 1, -i, 0) \ . \quad (4.7)$$

In order to calculate the hadronic helicity amplitudes, we use the following matrix elements of $B^* \to P$ transition

$$\begin{aligned}
\langle P(p_P)|\bar{q}\gamma_\mu b|\bar{B}^*(\varepsilon, p_{B^*})\rangle &= -\frac{2iV(q^2)}{m_{B^*} + m_P}\epsilon_{\mu\nu\rho\sigma}\varepsilon^\nu p_P^\rho p_{B^*}^\sigma, \\
\langle P(p_P)|\bar{q}\gamma_\mu\gamma_5 b|\bar{B}^*(\varepsilon, p_{B^*})\rangle &= 2m_{B^*}A_0(q^2)\frac{\varepsilon\cdot q}{q^2}q_\mu + (m_P + m_{B^*})A_1(q^2)(\varepsilon_\mu - \frac{\varepsilon\cdot q}{q^2}q_\mu) \\
&+ A_2(q^2)\frac{\varepsilon\cdot q}{m_P + m_{B^*}}\big[(p_{B^*} + p_P)_\mu - \frac{m_{B^*}^2 - m_P^2}{q^2}q_\mu\big] \ , \quad (4.8)
\end{aligned}$$

where $V(q^2)$, $A_{0,1,2}(q^2)$ are the various form factors. The matrix elements for the scalar and pseudoscalar currents can be obtained by using the equation of motion

$$i\partial_\mu(\bar{q}\gamma^\mu b) = (m_b - m_q)\bar{q}b \ , \qquad i\partial_\mu(\bar{q}\gamma^\mu\gamma_5 b) = -(m_b + m_q)\bar{q}\gamma_5 b \ , \quad (4.9)$$

as

$$\begin{aligned}
\langle P(p_P)|\bar{q}b|\bar{B}^*(\varepsilon, p_{B^*})\rangle &= 0 \ , \\
\langle P(p_P)|\bar{q}\gamma_5 b|\bar{B}^*(\varepsilon, p_{B^*})\rangle &= -(\varepsilon.q)\frac{2m_{B^*}}{m_b + m_q}A_0(q^2), \quad (4.10)
\end{aligned}$$

where the $m_{b,q}$ represent the current quark masses evaluated at the $b-$quark mass scale. The helicity amplitudes are defined as

$$\begin{aligned}
H^{V_L}_{\lambda_{B^*}\lambda_{W^*}}(q^2) &= \bar{\epsilon}^{*\mu}(\lambda_{W^*})\langle P(p_P)|\bar{q}\gamma_\mu(1 - \gamma_5)b|\bar{B}^*(\varepsilon(\lambda_{B^*}), p_{B^*})\rangle, \\
H^{V_R}_{\lambda_{B^*}\lambda_{W^*}}(q^2) &= \bar{\epsilon}^{*\mu}(\lambda_{W^*})\langle P(p_P)|\bar{q}\gamma_\mu(1 + \gamma_5)b|\bar{B}^*(\varepsilon(\lambda_{B^*}), p_{B^*})\rangle, \\
H^{S_L}_{\lambda_{B^*}\lambda_{W^*}}(q^2) &= (\lambda_{W^*})\langle P(p_P)|\bar{q}(1 - \gamma_5)b|\bar{B}^*(\varepsilon(\lambda_{B^*}), p_{B^*})\rangle, \\
H^{S_R}_{\lambda_{B^*}\lambda_{W^*}}(q^2) &= (\lambda_{W^*})\langle P(p_P)|\bar{q}\ (1 + \gamma_5)b|\bar{B}^*(\varepsilon(\lambda_{B^*}), p_{B^*})\rangle, \quad (4.11)
\end{aligned}$$

where for convenience, we use the notations $\lambda_{B^*} = 0, \pm$ and $\lambda_{W^*} = 0, \pm, t$ to represent the helicity states of the B^* and W^* boson. Thus, with Eqs. (4.8), (4.10) and (4.11), one obtains the following non-vanishing helicity amplitudes

$$\begin{aligned}
H_{0t}(q^2) &= H_{0t}^{V_L}(q^2) = -H_{0t}^{V_R}(q^2) = \frac{2m_{B^*}|\vec{p}|}{\sqrt{q^2}} A_0(q^2) \,, \\
H_{00}(q^2) &= H_{00}^{V_L}(q^2) = -H_{00}^{V_R}(q^2) \\
&= \frac{1}{2m_{B^*}\sqrt{q^2}} \Big[(m_{B^*} + m_P)(m_{B^*}^2 - m_P^2 + q^2) A_1(q^2) + \frac{4m_{B^*}^2 |\vec{p}|^2}{m_{B^*} + m_P} A_2(q^2) \Big] \,, \\
H_{\pm\mp}(q^2) &= H_{\pm\mp}^{V_L}(q^2) = -H_{\mp\pm}^{V_R}(q^2) = -(m_{B^*} + m_P) A_1(q^2) \mp \frac{2m_{B^*}|\vec{p}|}{m_{B^*} + m_P} V(q^2) \,, \\
H'_{0t} &= H_{0t}^{S_L}(q^2) = -H_{0t}^{S_R}(q^2) = -\frac{2m_{B^*}|\vec{p}|}{m_b + m_q} A_0(q^2) \,.
\end{aligned} \tag{4.12}$$

4.1.2 Leptonic helicty amplitudes

The leptonic helicity amplitudes are defined as

$$h_{\lambda_l, \lambda_{\nu_l}} = \frac{1}{2} \bar{\epsilon}_\mu(\lambda_{W^*}) \; \bar{u}_l(\lambda_l) \; \Gamma^i \; v_{\bar{\nu}_l}(\lambda_{\bar{\nu}_l}) \,, \tag{4.13}$$

where $\lambda_{W^*} = \lambda_l - \lambda_{\bar{\nu}_l}$. In the center of mass frame of $l - \bar{\nu}_l$, the four momenta of l and $\bar{\nu}_l$ pair are expressed as

$$p_l^\mu = \big(E_l, |\vec{p}_l| \sin\theta, 0, |\vec{p}_l| \cos\theta\big), \quad p_{\nu_l}^\mu = \big(|\vec{p}_l|, -|\vec{p}_l| \sin\theta, 0, -|\vec{p}_l| \cos\theta\big) \,, \tag{4.14}$$

where $E_l = (q^2 + m_l^2)/2\sqrt{q^2}$, $|\vec{p}_l| = (q^2 - m_l^2)/2\sqrt{q^2}$ and θ is the angle between the three momenta of of P and l. The polarization vector of the virtual W^* boson in this frame is

$$\bar{\epsilon}^\mu(t) = (1,0,0,0), \quad \bar{\epsilon}^\mu(0) = (0,0,0,1), \quad \bar{\epsilon}^\mu(\pm) = \frac{1}{\sqrt{2}}(0, \mp 1, -i, 0) \,. \tag{4.15}$$

Thus, with Eqs. (4.13) and (4.15), one obtains the following non-vanishing contributions

$$\begin{aligned}
&|h_{-\frac{1}{2},\frac{1}{2}}^{V_{L,R}}|^2 = 8(q^2 - m_l^2), \qquad |h_{\frac{1}{2},\frac{1}{2}}^{V_{L,R}}|^2 = 8\frac{m_l^2}{2q^2}(q^2 - m_l^2), \\
&|h_{\frac{1}{2},\frac{1}{2}}^{S_{L,R}}|^2 = 4(q^2 - m_l^2), \qquad |h_{\frac{1}{2},\frac{1}{2}}^{V_{L,R}}| \times |h_{\frac{1}{2},\frac{1}{2}}^{S_{L,R}}| = 8\frac{m_l}{2\sqrt{q^2}}(q^2 - m_l^2) \,.
\end{aligned} \tag{4.16}$$

4.1.3 Decay distribution and other observables

The double differential decay rate of $B^* \to Pl\bar{\nu}_l$ decay process can be expressed as

$$\frac{d^2\Gamma}{dq^2 d\cos\theta} = \frac{G_F^2}{192\pi^3} \frac{|\vec{p}|}{m_{B^*}^2} |V_{qb}|^2 \left(1 - \frac{m_l^2}{q^2}\right) \big|\mathcal{M}(\bar{B}^* \to Pl\bar{\nu}_l)\big|^2 \,. \tag{4.17}$$

Now, with Eqs. (4.12) and (4.16), one can obtain $L_{\mu\nu}H^{\mu\nu}$ in terms of Wigner d^J-functions as [86]

$$L_{\mu\nu}H^{\mu\nu} = \frac{1}{8}\sum_{\lambda_l,\lambda_\nu,\lambda_{W^*},\lambda'_{W^*},J,J'}(-1)^{J+J'}h^i_{\lambda_l,\lambda_\nu}h^{j*}_{\lambda_l,\lambda_\nu}\delta_{\lambda_{B^*},-\lambda_{W^*}}\delta_{\lambda_{B^*},-\lambda'_{W^*}} \quad (4.18)$$

$$\times d^J_{\lambda_{W^*},\lambda_{l-1/2}}d^{J'}_{\lambda'_{W^*},\lambda_{l-1/2}}H^i_{\lambda_{B^*}\lambda_{W^*}}H^{j*}_{\lambda_{B^*}\lambda'_{W^*}}\ , \quad (4.19)$$

where J and J' take the values 0 and 1 and the various helicity components run over their allowed values. Thus, one can obtain the the differential decay rate to particular leptonic helicity state ($\lambda = \pm\frac{1}{2}$) as

$$\begin{aligned}\frac{d^2\Gamma(\lambda_l=-\frac{1}{2})}{dq^2 d\cos\theta} &= \frac{G_F^2}{768\pi^3}\frac{|\vec{p}|}{m^2_{B^*}}|V_{qb}|^2\ q^2\left(1-\frac{m_l^2}{q^2}\right)^2\Big\{|1+V_L|^2\big[(1-\cos\theta)^2H^2_{-+}+(1+\cos\theta)^2H^2_{+-}\\ &+ 2\sin^2\theta H^2_{00}\big]+|V_R|^2\big[(1-\cos\theta)^2H^2_{+-}+(1+\cos\theta)^2H^2_{-+}+2\sin^2\theta H^2_{00}\big]\\ &- 4\mathcal{R}e\big[(1+V_L)V_R^*\big]\big[(1+\cos\theta)^2H_{+-}H_{-+}+\sin^2\theta H^2_{00}\big]\Big\}\ , \end{aligned} \quad (4.20)$$

$$\begin{aligned}\frac{d^2\Gamma(\lambda_l=\frac{1}{2})}{dq^2 d\cos\theta} &= \frac{G_F^2}{768\pi^3}\frac{|\vec{p}|}{m^2_{B^*}}|V_{qb}|^2\ \left(1-\frac{m_l^2}{q^2}\right)^2 m_l^2\Big\{\big(|1+V_L|^2+|V_R|^2\big)\big[\sin^2\theta(H^2_{-+}+H^2_{+-})\\ &+ 2(H_{0t}-\cos\theta H_{00})^2\big]-4\mathcal{R}e\big[(1+V_L)V_R^*\big]\big[\sin^2\theta H_{-+}H_{+-}+(H_{0t}-\cos\theta H_{00})^2\big]\\ &+ 4\mathcal{R}e[(1+V_L-V_R)(S_L^*-S_R^*)]\frac{\sqrt{q^2}}{m_l}\big[H'_{0t}(H_{0t}-\cos\theta H_{00})\big]\\ &+ 2|S_L-S_R|^2\frac{q^2}{m_l^2}{H'_{0t}}^2\Big\}. \end{aligned} \quad (4.21)$$

From Eqs. (4.20) and (4.21), one can obtain the differential decay rate as

$$\begin{aligned}\frac{d\Gamma}{dq^2} &= \frac{G_F^2}{288\pi^3}\frac{|\vec{p}|}{m^2_{B^*}}|V_{qb}|^2\ q^2\left(1-\frac{m_l^2}{q^2}\right)^2\Big[(|1+V_L|^2+|V_R|^2)\\ &\times\ \big[\ \big(H^2_{-+}+H^2_{+-}+H^2_{00}\big)\left(1+\frac{m_l^2}{2q^2}\right)+\frac{3m_l^2}{2q^2}H^2_{0t}\big]\\ &- 2\mathcal{R}e[(1+V_L)V_R^*]\Big[(2H_{-+}H_{+-}+H^2_{00})\left(1+\frac{m_l^2}{2q^2}\right)+\frac{3m_l^2}{2q^2}H^2_{0t}\Big]\\ &+ 3\frac{m_l}{\sqrt{q^2}}\mathcal{R}e\Big[(1+V_L-V_R)(S_L^*-S_R^*)\Big]H'_{0t}H_{0t}+\frac{3}{2}|S_L-S_R|^2H'_{0t}\Big], \end{aligned} \quad (4.22)$$

where the values of the helicity amplitudes are given in Eq. (4.12).

Apart from the differential decay rate, the other NP sensitive observables, considered here are

- Lepton nonuniversality parameter:

$$R_P^*(q^2) = \frac{d\Gamma(B^* \to P\tau^-\bar{\nu}_\tau)/dq^2}{d\Gamma(B^* \to Pl^-\bar{\nu}_l)/dq^2} \ . \tag{4.23}$$

- Forward-backward asymmetry:

$$A_{\rm FB}^P(q^2) = \frac{\int_{-1}^0 d\cos\theta(d^2\Gamma/dq^2 d\cos\theta) - \int_0^1 d\cos\theta(d^2\Gamma/dq^2 d\cos\theta)}{\int_{-1}^0 d\cos\theta(d^2\Gamma/dq^2 d\cos\theta) + \int_0^1 d\cos\theta(d^2\Gamma/dq^2 d\cos\theta)} \ , \tag{4.24}$$

which can be expressed in terms of the helicity amplitudes as

$$A_{\rm FB}^P(q^2) = \frac{3}{4}\frac{X}{Y} \ , \tag{4.25}$$

where the parameters X and Y are given as

$$\begin{aligned}
X &= \left(|1+V_L|^2 - |V_R|^2\right)\left(H_{-+}^2 - H_{+-}^2\right) + 2\left(\frac{m_l^2}{q^2}\right)\left(|1+V_L|^2 + |V_R|^2\right)H_{0t}H_{00} \\
&+ 4\mathcal{R}e[(1+V_L)V_R^*]\left(H_{+-}H_{-+} - \frac{m_l^2}{q^2}H_{0t}H_{00}\right) \\
&+ 2\mathcal{R}e[(1+V_L-V_R)(S_L^* - S_R^*)]\frac{m_l}{\sqrt{q^2}}H'_{0t}H_{00} \ , \\
Y &= \left(|1+V_L|^2 + |V_R|^2\right)\left[\left(H_{-+}^2 + H_{+-}^2 + H_{00}^2\right)\left(1+\frac{m_l^2}{2q^2}\right) + \frac{3m_l^2}{2q^2}H_{0t}^2\right] \\
&- 2\mathcal{R}e[(1+V_L)V_R^*]\Big[(2H_{-+}H_{+-} + H_{00}^2)\left(1+\frac{m_l^2}{2q^2}\right) + \frac{3m_l^2}{2q^2}H_{0t}^2\Big] \\
&+ 3\frac{m_l}{\sqrt{q^2}}\mathcal{R}e\Big[(1+V_L-V_R)(S_L^* - S_R^*)\Big]H'_{0t}H_{0t} + \frac{3}{2}|S_L - S_R|^2 H'_{0t} \ .
\end{aligned} \tag{4.26}$$

- Lepton-spin asymmetry:

$$A_\lambda^P(q^2) = \frac{d\Gamma(\lambda_l = -1/2)/dq^2 - d\Gamma(\lambda_l = 1/2)/dq^2}{d\Gamma(\lambda_l = -1/2)/dq^2 + d\Gamma(\lambda_l = 1/2)/dq^2}. \tag{4.27}$$

4.1.4 Form factors and their q^2 dependence

The main inputs required for the numerical analysis are the values of the form factors. As the first principle lattice calculation results of the form factors for $B_{d,s}^* \to D, D_s(\pi, K)$ transitions are not yet available, we use their values evaluated in the BSW model [88, 89].

Their values at zero-momentum transfer are listed below

$$\begin{aligned}
&A_0^{\bar{B}^*\to D}(0) = 0.71, \quad A_1^{\bar{B}^*\to D}(0) = 0.75, \quad A_2^{\bar{B}^*\to D}(0) = 0.62, \quad V^{\bar{B}^*\to D}(0) = 0.76,\\
&A_0^{\bar{B}_s^*\to D_s}(0) = 0.66, \quad A_1^{\bar{B}_s^*\to D_s}(0) = 0.69, \quad A_2^{\bar{B}_s^*\to D_s}(0) = 0.59, \quad V^{\bar{B}_s^*\to D_s}(0) = 0.72,\\
&A_0^{\bar{B}^*\to \pi}(0) = 0.34, \quad A_1^{\bar{B}^*\to \pi}(0) = 0.38, \quad A_2^{\bar{B}^*\to \pi}(0) = 0.30, \quad V^{\bar{B}^*\to \pi}(0) = 0.35,\\
&A_0^{\bar{B}_s^*\to K}(0) = 0.28, \; A_1^{\bar{B}_s^*\to K}(0) = 0.29, \; A_2^{\bar{B}_s^*\to K}(0) = 0.26, \; V^{\bar{B}_s^*\to K}(0) = 0.30. \qquad (4.28)
\end{aligned}$$

The q^2 dependence of the form factors can be written as,

$$\begin{aligned}
A_0(q^2) &\simeq \frac{A_0(0)}{1 - q^2/m^2_{B_q}(0^-)}, \quad A_1(q^2) \simeq \frac{A_1(0)}{1 - q^2/m^2_{B_q}(1^+)},\\
A_2(q^2) &\simeq \frac{A_2(0)}{1 - q^2/m^2_{B_q}(1^+)}, \quad V(q^2) \simeq \frac{V(0)}{1 - q^2/m^2_{B_q}(1^-)}\,, \qquad (4.29)
\end{aligned}$$

where $m_{B_q}(0^\pm)$ and $m_{B_q}(1^\pm)$ are the pole masses whose values are presented in 4.1.

TABLE 4.1: Pole masses in GeV.

current	$m(0^-)$	$m(0^+)$	$m(1^-)$	$m(1^+)$
$\bar{u}b$	5.27	5.99	5.32	5.71
$\bar{c}b$	6.30	6.80	6.34	6.73

4.2 Constraints on new couplings

In this study we consider the new couplings as complex quantities. The allowed parameter space of individual couplings are obtained by performing chi-square fitting where we take in to account the effect of one coupling at a time while Considering the contribution of all other coefficients as zero. The χ^2 is defined as

$$\chi^2 = \sum_i \frac{(\mathcal{O}_i^{\rm th} - \mathcal{O}_i^{\rm exp})^2}{(\Delta\mathcal{O}_i^{\rm exp})^2}, \qquad (4.30)$$

where $\mathcal{O}_i^{\rm th}$ stands for the theoretically predicted values of the observables, $\mathcal{O}_i^{\rm exp}$ symbolizes the measured central value of the observables and $\Delta\mathcal{O}_i^{\rm exp}$ denotes the corresponding 1σ uncertainty. The real and imaginary parts of the new Wilson coefficients associated with $b \to cl\bar{\nu}_l$ transitions are constrained from the χ^2 fit of $R_{D^{(*)}}$, $R_{J/\psi}$ and $\mathrm{Br}(B_c^+ \to \tau^+\nu_\tau)$ observables. and the coefficients related to $b \to u\tau\bar{\nu}_\tau$ processes are constrained from the fit of R_π^l, $\mathrm{Br}(B_u^+ \to \tau^+\nu)$ and $\mathrm{Br}(B^0 \to \pi^+\tau^-\bar{\nu})$ data. For the fitting we use the mesured values of considered parameters from [15]. The upper limit on the branching ratio of $B_c^+ \to \tau^+\nu_\tau$ decay process with the current world average of

the B_c lifetime is [71]

$$\mathrm{Br}(B_c^+ \to \tau^+ \nu_\tau) \lesssim 30\%. \tag{4.31}$$

The theoretical expressions of these parameters and their corresponding SM predicted values are used from [90].

In Fig. 4.1 , we present the constraints on V_L (top-left panel), V_R (top-right panel), S_L (bottom-left panel) and S_R (bottom-right panel) coefficients of $b \to c$ decay modes and the corresponding plots for the coefficients of $b \to u$ are shown in Fig. 4.2 . The best-fit values and the corresponding 1σ ranges of all the new coefficients are presented in Table 4.2 . Since there are infinite solutions for the 1σ range of the parameters, the above listed values are obtained by fixing one parameter at its best-fit value, while varying the other, which gives $\Delta\chi^2 \equiv \chi^2 - \chi^2_{\rm min} = 1$ (i.e., for one degree of freedom). The χ^2/d.o.f for all the coefficients are also listed in this Table. One can notice that, the Wilson coefficient corresponding to $b \to c$ scalar operators have χ^2/d.o.f > 1, which implies that the fit is not robust.

TABLE 4.2: Allowed parameter space for new couplings.

New coefficients	Best-fit	1σ range	χ^2/d.o.f
$b \to c\tau\bar{\nu}_\tau$ decay modes			
$(\mathrm{Re}[V_L], \mathrm{Im}[V_L])$	$(-1.1474, 1.1171)$	$([-1.3, -0.7],\ [1.088, 1.148])$	0.988
$(\mathrm{Re}[V_R], \mathrm{Im}[V_R])$	$(6.57 \times 10^{-3}, -0.5368)$	$([-0.015, 0.025],\ [-0.6, -0.48])$	0.966
$(\mathrm{Re}[S_L], \mathrm{Im}[S_L])$	$(0.2052, 0)$	$([0.12, 0.28],\ [-0.35, 0.35])$	6.097
$(\mathrm{Re}[S_R], \mathrm{Im}[S_R])$	$(-1.003, -0.78906)$	$([-1.17, -0.77],\ [-0.89, -0.71])$	3.6
$b \to u\tau\bar{\nu}_\tau$ decay modes			
$(\mathrm{Re}[V_L], \mathrm{Im}[V_L])$	$(-0.8318, 1.098)$	$([-1.43, -0.43], [1.0, 1.2])$	0.265
$(\mathrm{Re}[V_R], \mathrm{Im}[V_R])$	$(-0.115, 0)$	$([-0.2, -0.025], [-0.45, 0.45])$	0.1363
$(\mathrm{Re}[S_L], \mathrm{Im}[S_L])$	$(-0.0236, 0)$	$([-0.042, -0.006],\ [-0.09, 0.09])$	0.1906
$(\mathrm{Re}[S_R],\ \mathrm{Im}[S_R])$	$(-0.439, 0)$	$([-0.46, -0.42],\ [-0.09, 0.09])$	0.1906

4.3 Effect of new coefficients on $B^*_{d,s} \to (D, D_s, \pi, K)\tau\bar{\nu}_\tau$ decay modes

TABLE 4.3: SM predicted value of branching ratio of $B^*_{d,s} \to P\mu\nu_\mu$ processes.

Decay processes	SM Branching fraction
$\mathrm{Br(B^{*0} \to D^+\mu^-\bar{\nu}_\mu)}$	9.318×10^{-8}
$\mathrm{Br(B_s^* \to D_s^+\mu^-\bar{\nu}_\mu)}$	1.709×10^{-7}
$\mathrm{Br(B^{*0} \to \pi^+\mu^-\bar{\nu}_\mu)}$	1.487×10^{-9}
$\mathrm{Br(B_s^* \to K^+\mu^-\bar{\nu}_\mu)}$	1.618×10^{-9}

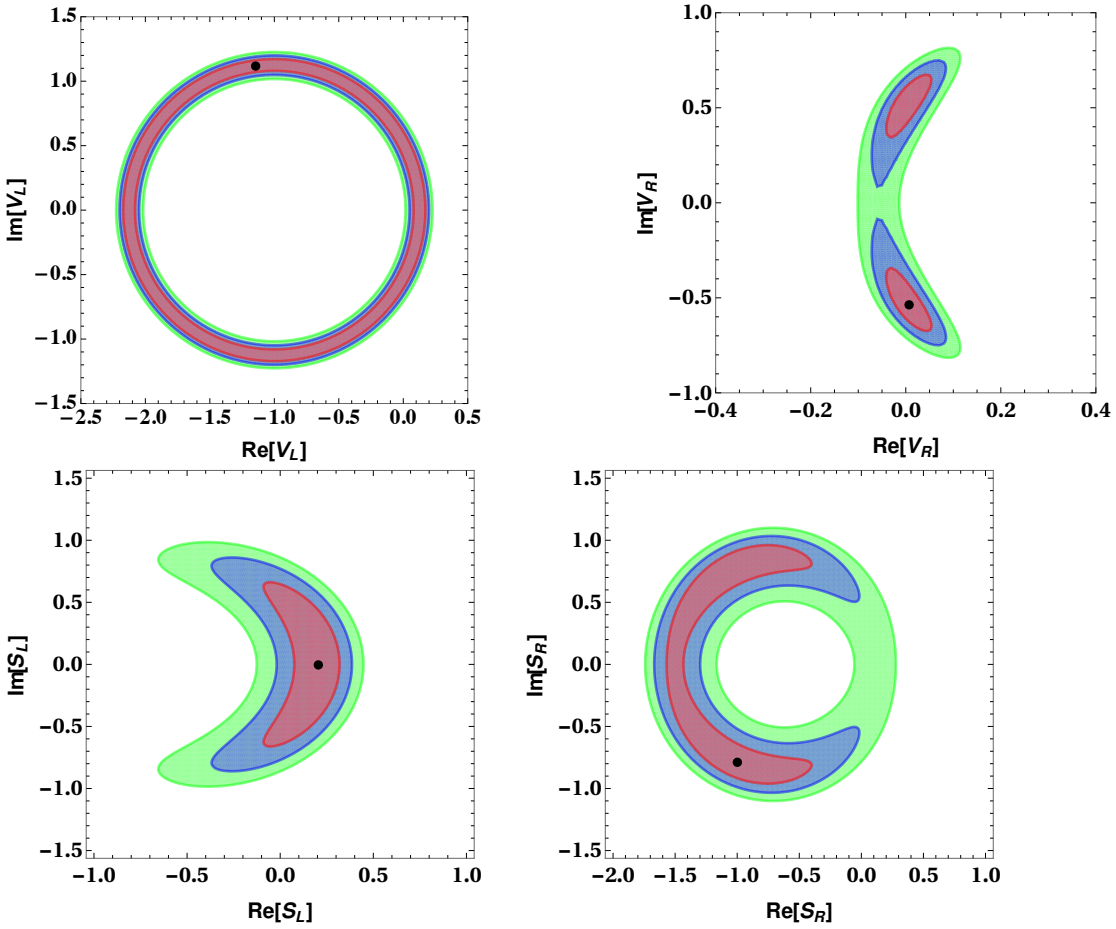

FIGURE 4.1: Constrained parameter space for individual new complex couplings related to $b \to c\tau\bar{\nu}_\tau$ transition obtained from the χ^2 fit of $R_{D^{(*)}}, R_{J/\psi}$ and upper limit on $\mathrm{Br}(B_c^+ \to \tau^+\nu_\tau)$. Here the red, blue and green bands represent the 1σ, 2σ and 3σ contours respectively where as the black dots stand for the corresponding best-fit values.

4.3.1 Effect of V_L only

Here we consider the case, where the additional contribution to the SM Lagrangian arising only from V_L coefficient and all other new coefficients are set to zero i.e., ($S_L = S_R = V_R = 0$). Using the 1σ allowed parameter space of V_L, obtained from the χ^2 fit of $R_{D^{(*)}}, R_{J/\psi}$, $\mathrm{Br}(B_c^+ \to \tau^+\nu)$ for $b \to c\tau\nu$ transitions (R_π^l, $\mathrm{Br}(B^0 \to \pi^+ l^- \bar{\nu})$, $\mathrm{Br}(B_u^+ \to \tau^+\nu$ for $b \to u\tau\nu$ transitions), we then calculate the differential decay rate, LNU parameter, lepton spin asymmetry and forward-backward asymmetry of $B^{*0} \to D^+\tau\nu$ and $B_s^* \to D_s^+\tau\nu$ ($B^{*0} \to \pi^+\tau\nu$ and $B_s^* \to K^+\tau\nu$) decay processes. In the left panel of Fig. 4.3, we show the q^2 variation of decay rate (top) and R_D^* parameter (bottom) of $B^{*0} \to D^+\tau\nu$ process and the corresponding plots for $B^{*0} \to \pi^+\tau\nu$ channel are presented in the right panel of this figure. Here the blue dashed lines correspond to the SM prediction. The solid black lines are obtained by using the best-fit values of the left handed vectorial new V_L coupling and the orange bands represent the 1σ allowed ranges. From the plots, one can notice profound deviation in the branching ratios and

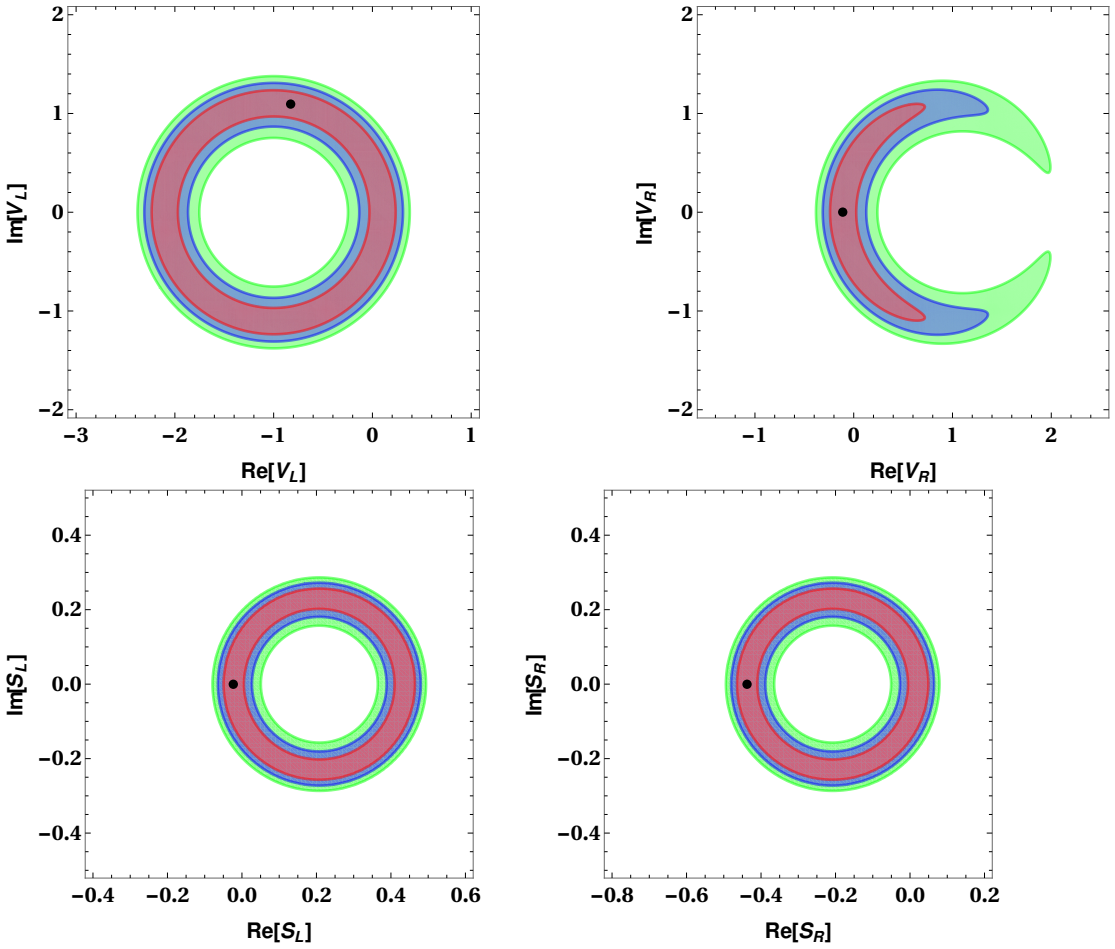

FIGURE 4.2: Allowed parameter space for individual new complex coefficients related to $b \to u\tau\bar{\nu}_\tau$ transition obtained from the χ^2 fit of R_π^l, $\mathrm{Br}(B_u^+ \to \tau^+\nu_l)$ and upper limit on $\mathrm{Br}(B^0 \to \pi^+ l^- \bar{\nu}_l)$.

LNU parameters from their corresponding SM predictions due to presence of additional V_L coefficient. The plots for $B_s^* \to D_s^+\tau\nu$ ($B_s^* \to K^+\tau\nu$) process follow the same form as $B^{*0} \to D^+\tau\nu$ ($B^{*0} \to \pi^+\tau\nu$), and hence, are not included in this article. The numerical values of these observables are presented in Table 4.4. Furthermore, no deviations have been observed in the forward-backward asymmetry and lepton-spin asymmetry parameters from their SM results, so we don't provide the corresponding plots. The values of q^2 at which the forward-backward asymmetry vanishes are provided in Table 4.6.

4.3.2 Effect of V_R only

In this scenario, we explore the effect of only V_R coefficient on the decay rate and angular observables of $B^* \to (D^0, \pi^0)\tau\nu_\tau$ processes. Using the best-fit values and corresponding 1σ allowed ranges of V_R coefficients associated with $b \to (c, u)\tau\bar{\nu}_\tau$ transitions, we present

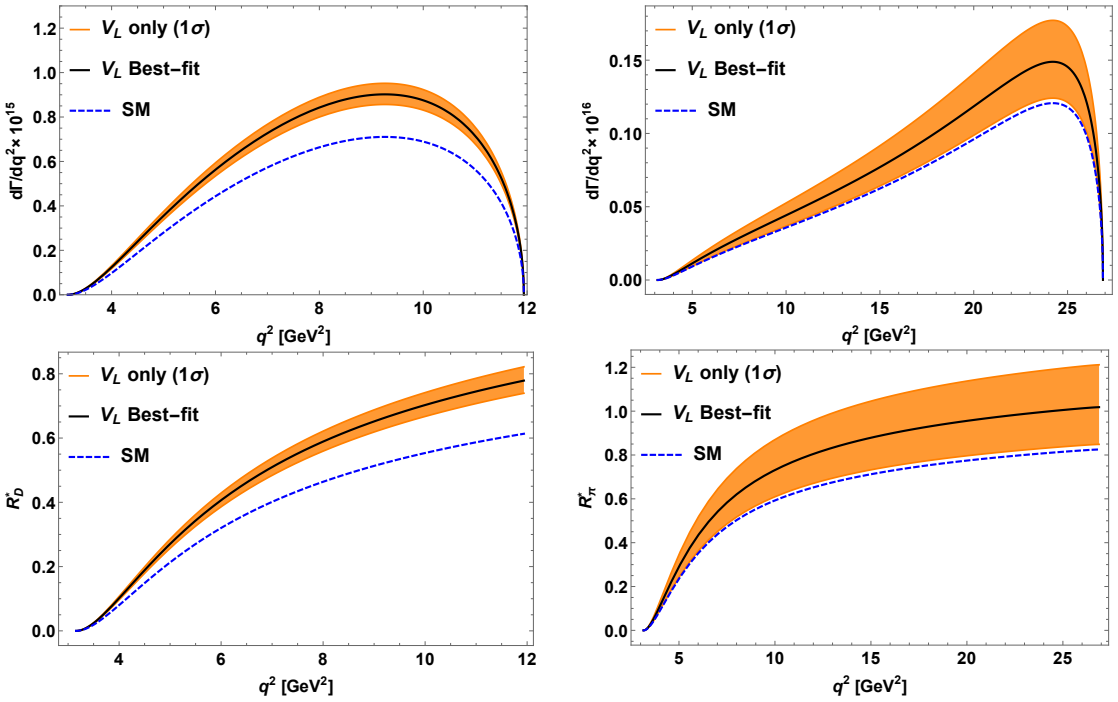

FIGURE 4.3: The q^2 variation of differential decay rates and LNU parameters of $\bar{B}_d^* \to D^+\tau^-\bar{\nu_\tau}$ (left panel) and $\bar{B}_d^* \to \pi^+\tau\bar{\nu}_\tau$ (right panel) in presence of only V_L new coefficient. Here the blue dashed lines represent the standard model predictions. The black solid lines and the orange bands are obtained by using the best-fit values and corresponding 1σ range of V_L coefficient.

the plots for the decay rate (left-top panel), R_D^* parameter (left-middle) and forward-backward asymmetry (left-bottom panel) of $B^* \to D^+\tau\nu$ decay modes in Fig. 4.4. The corresponding plots for $B^* \to \pi^+\tau\nu$ process are depicted in the right panel of Fig. 4.4. Here the solid black lines are obtained by using the best-fit values of new V_R couplings and the green bands from their corresponding 1σ range. Reasonable deviation in all the observables (except the lepton-spin asymmetry parameters) from their SM results are found due to the presence of additional V_R coefficient. In Table 4.4, we present the numerical values of decay rates and all these parameters. Due to the additional contribution from V_R coefficient, we notice deviation in the zero crossing of the forward-backward asymmetry towards high q^2 and the q^2 values of the zero crossing point are given in Table 4.6.

4.3.3 Effect of S_L only

In this subsection, we consider the contribution of S_L new coefficient by assuming that all other new Wilson coefficients have vanishing values. As seen from Figs. 4.1 and 4.2, the S_L parameters are severely constrained by the current data. Within the allowed parameter space for S_L coefficient presented in Table 4.2, we show the q^2 variation of lepton-spin asymmetry (top) and forward-backward asymmetry (bottom) of $B^* \to$

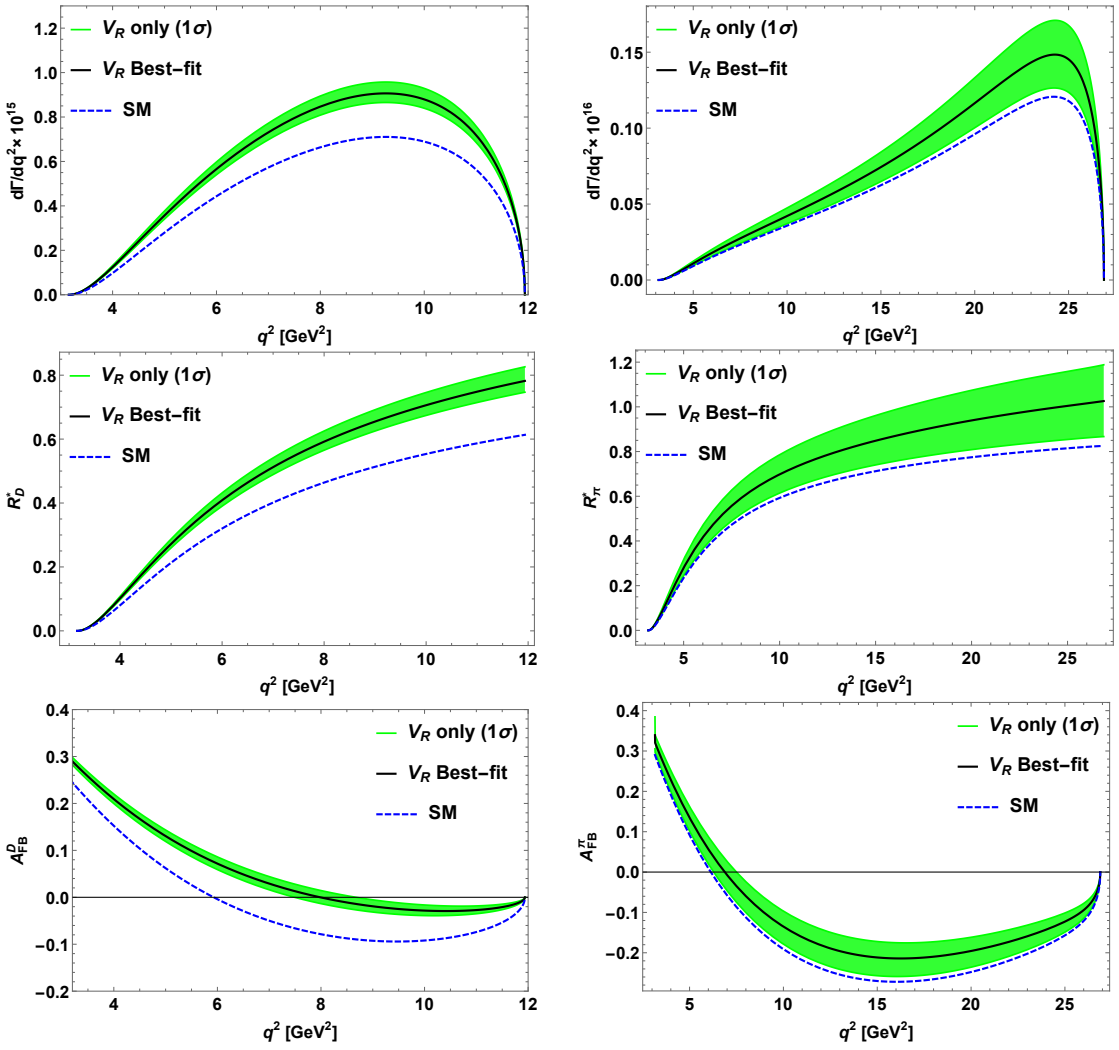

FIGURE 4.4: The q^2 variation of differential decay rate, lepton nonuniversaity parameter and forward-backward asymmetry of $\bar{B}_d^* \to D^+\tau^-\bar{\nu}$ (left panel) and $\bar{B}_d^* \to \pi^+\tau\bar{\nu}$ (right panel) in presence of new V_R coefficient. The black solid lines and the green bands are obtained by using the best-fit values and corresponding 1σ range of V_R coefficient.

.

$D^+\tau\bar{\nu}$ ($B^* \to \pi^+\tau\bar{\nu}$) process on the left panel (right panel) of Fig. 4.5. Here the plots obtained from the best-fit values (1σ range) of S_L coupling are represented by dashed black lines (red bands). The numerical values of these observables are given in Table 4.5. With the additional S_L contribution, the deviation in the branching ratios and LNU parameters from their SM predictions are found to be minimal. Though the lepton spin asymmetry and forward-backward asymmetry parameters of $B^* \to D^+\tau\bar{\nu}$ channel provide slight deviation from their SM results, the deviation is negligible in the $B^* \to \pi^+\tau\bar{\nu}$ modes. The zero crossing point of the forward-backward asymmetry of $B^* \to D^+\tau\bar{\nu}$ process shifted towards the low q^2 region. The $A^P_{\rm FB}$ vanishing values of q^2 predicted from the best-fit values and 1σ range of new S_L coefficient are presented in Table 4.6.

TABLE 4.4: Predicted numerical values of differential decay rate, LNU parameters, lepton spin asymmetry and forward-backward asymmetry of $\bar{B}^*_{d,(s)} \to D^+(D_s^+)\tau^-\bar{\nu}_\tau$ and $\bar{B}^*_{d(s)} \to \pi^+(K^+)\tau\bar{\nu}_\tau$ decay processes in the SM and in the presence of $V_{L,R}$ coefficients.

Observables	SM Predictions	Values with V_L	Values with V_R
$\mathrm{Br(B^{*0} \to D^+\tau^-\bar{\nu}_\tau)}$	2.786×10^{-8}	$(3.358 \to 3.732) \times 10^{-8}$	$(3.394 \to 3.755) \times 10^{-8}$
R^*_D	0.299	$0.360 \to 0.40$	$0.364 \to 0.403$
A^D_λ	0.576	0.576	0.576
A^D_{FB}	-0.054	-0.054	$(0.002 \to 0.026)$
$\mathrm{Br(B_s^{*0} \to D_s^+\tau^-\bar{\nu}_\tau)}$	5.074×10^{-8}	$(6.116 \to 6.797) \times 10^{-8}$	$(6.181 \to 6.838) \times 10^{-8}$
$R^*_{D_s}$	0.297	$0.358 \to 0.398$	$0.362 \to 0.400$
$A^{D_s}_\lambda$	0.573	0.573	0.573
A^D_{FB}	-0.053	-0.053	$0.003 \to 0.027$
$\mathrm{Br(B^{*0} \to \pi^+\tau^-\bar{\nu}_\tau)}$	1.008×10^{-9}	$(1.036 \to 1.479) \times 10^{-9}$	$(1.051 \to 1.392) \times 10^{-9}$
R^*_π	0.678	$0.697 \to 0.995$	$0.707 \to 0.936$
A^π_λ	0.781	0.781	$0.780 \to 0.781$
A^π_{FB}	-0.209	-0.209	$(-0.198 \to -0.129)$
$\mathrm{Br(B_s^{*0} \to K^+\tau^-\bar{\nu}_\tau)}$	1.034×10^{-9}	$(1.063 \to 1.518) \times 10^{-9}$	$(1.078 \to 1.421) \times 10^{-9}$
R^*_K	0.639	$0.657 \to 0.939$	$0.666 \to 0.878$
A^K_λ	0.747	0.747	$0.745 \to 0.746$
A^K_{FB}	-0.207	-0.207	$(-0.196 \to -0.124)$

4.3.4 Effect of S_R only

Here we investigate the observables of $B^* \to (D^+, \pi^+)\tau\bar{\nu}$ decay modes by considering the presence of only additional S_R coefficient. Using the available experimental data on $b \to (u, c)\tau\bar{\nu}$ transitions, we fit the corresponding S_R coefficients, which is already discussed in section II. In the left panel of Fig. 4.6 , we present the q^2 variation of decay rate (top), R^*_D (second from top), lepton spin asymmetry (third from top) and forward-backward asymmetry (bottom) of $B^* \to D^+\tau\bar{\nu}$ and the corresponding plots for $B^* \to \pi^+\tau\bar{\nu}$ are shown in the right panel. In this case also, the deviation in the lepton spin asymmetry and forward-backward asymmetry parameters are comparatively large, whereas the deviations in the branching ratios and LNU parameters are nominal. The numerical values are presented in Table 4.5 . From Fig. 4.6 , one can notice that the zero crossing point of the forward-backward asymmetry deviates significantly towards left (low q^2 region) and the corresponding q^2 values of the crossings are shown in Table 4.6 .

4.4 Chapter summary

As the vector meson B^* decay dominantly through electromagnetic channel $B^* \to B\gamma$, it's week decay process are not experimentally probed. Due to recent development of

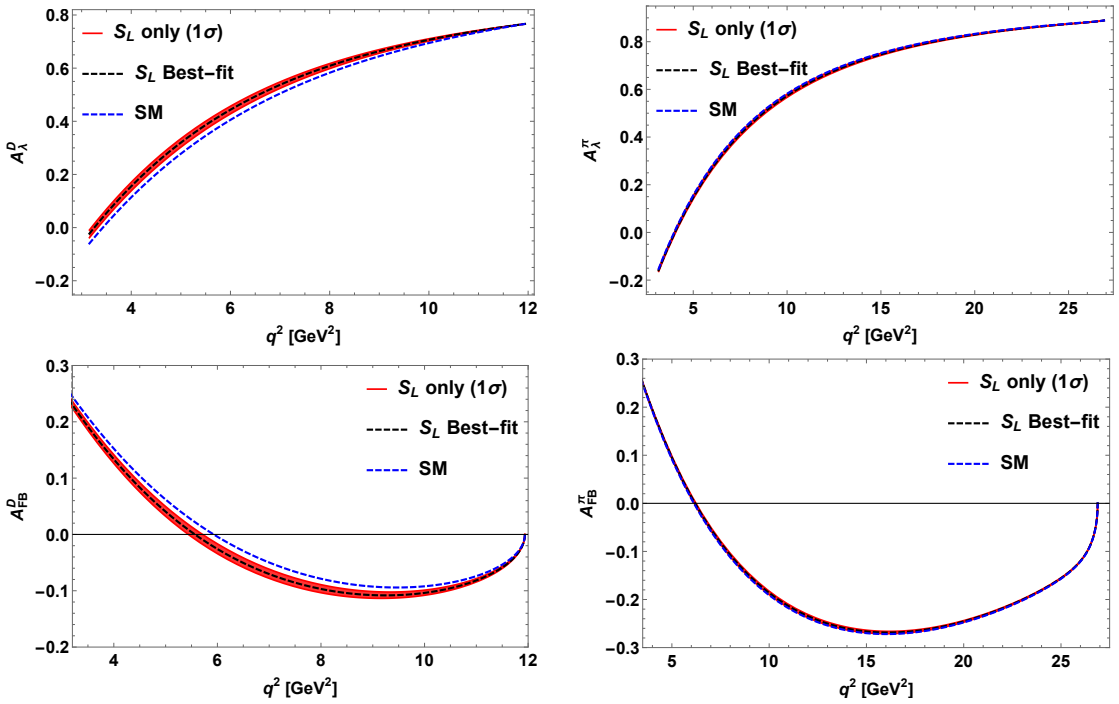

FIGURE 4.5: The q^2 variation of lepton spin asymmetry and forward-backward asymmetry of $\bar{B}_d^* \to D^+\tau^-\bar{\nu_\tau}$ (left panel) and $\bar{B}_d^* \to \pi^+\tau\bar{\nu}_\tau$ (right panel) in presence of S_L coefficient only. The black dashed lines and the red bands are obtained by using the best-fit values and corresponding 1σ range of S_L coefficient.

LHCb experiment resulting into high luminosity, several weak decay process of branching ratio $\sim \mathcal{O}(10^{-9})$ are expected to be observed in near future. So LHCb is going to play a very important role to explore rare decay channels of B^* mesons. In this regard we study the semileptonic decay of vector meson B^* to a pseudo scalar meson. In this analysis we considered the general effective Lagrangian associated with this decay process and constrained the parameter space of the new couplings using χ^2 fitting. The allowed parameter space associated with $b \to u\tau\bar{\nu}_\tau$ transition are obtained from R_π^l, branching ratio of $B_u \to \tau\bar{\nu}_\tau$ and upper limit on branching ratio of $B^0 \to \pi^+\tau^-\bar{\nu}_\tau$ data where as the constrained parameter space associated with $btoc\tau\bar{\nu}_\tau$ transition is obtained from the upper limit on the branching ratio of $B_c^+ \to tau^+\nu_\tau$, R_{D^*} and $R_{J/\psi}$ experimental values. With presence of individual new couplings we calculated the values of various parameters sensitive to NP such as branching ratio, LNU parameter, forward-backward asymmetry and lepton spin asymmetry parameters. we got significant deviation of these parameters in presence of these new couplings which will play an important role to probe new physics in B^* vector meson decay.

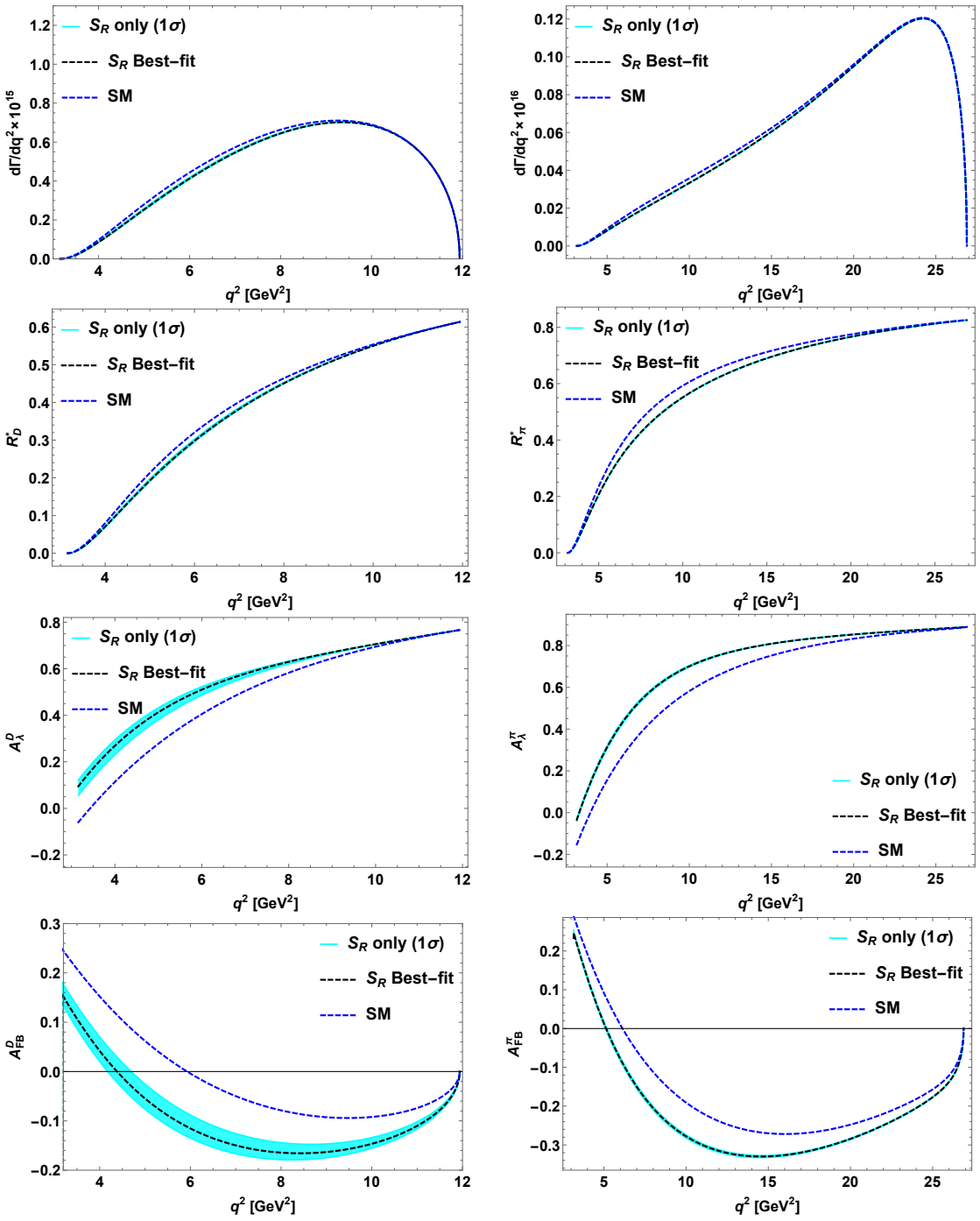

FIGURE 4.6: The q^2 variation of differential decay rate, LNU parameter, lepton spin asymmetry and forward-backward asymmetry of $\bar{B}_d^* \to D^+\tau^-\bar{\nu}_\tau$ (left panel) and $\bar{B}_d^* \to \pi^+\tau\bar{\nu}_\tau$ (right panel) in presence of S_R coefficient only. The black dashed lines and the cyan bands are obtained by using the best-fit values and corresponding 1σ range of S_R coefficient.

.

TABLE 4.5: Predicted numerical values of differential decay rate, LNU parameters, lepton spin asymmetry and forward-backward asymmetry of $\bar{B}^*_{d(s)} \to D^+(D_s^+)\tau^-\bar{\nu}_\tau$ and $\bar{B}^*_{d,(s)} \to \pi^+(K^+)\tau\bar{\nu}_\tau$ decay processes in presence of $S_{L,R}$ coefficients.

Observables	Values with S_L	Values with S_R
$\mathrm{Br}(\mathrm{B}^{*0} \to \mathrm{D}^+\tau^-\bar{\nu}_\tau)$	$(2.731 \to 2.761) \times 10^{-8}$	$(2.670 \to 2.715) \times 10^{-8}$
R^*_D	$0.293 \to 0.296$	$0.289 \to 0.291$
A^D_λ	$0.591 \to 0.608$	$0.617 \to 0.633$
A^D_{FB}	$-0.076 \to -0.064$	$-0.145 \to -0.114$
$\mathrm{Br}(\mathrm{B}^*_\mathrm{s} \to \mathrm{D}^+_\mathrm{s}\tau^-\bar{\nu}_\tau)$	$(4.971 \to 5.027) \times 10^{-8}$	$(4.894 \to 4.941) \times 10^{-8}$
$R^*_{D_s}$	$0.291 \to 0.294$	$0.286 \to 0.289$
$A^{D_s}_\lambda$	$0.588 \to 0.606$	$0.615 \to 0.631$
$A^{D_s}_{\mathrm{FB}}$	$-0.075 \to -0.062$	$-0.144 \to -0.113$
$\mathrm{Br}(\mathrm{B}^{*0} \to \pi^+\tau^-\bar{\nu}_\tau)$	$(1.008 \to 1.011) \times 10^{-9}$	$(9.845 \to 9.850) \times 10^{-10}$
R^*_π	$0.678 \to 0.680$	$0.662 \to 0.663$
A^π_λ	$0.774 \to 0.780$	$0.822 \to 0.823$
A^π_{FB}	$-0.208 \to -0.204$	$(-0.254 \to -0.251)$
$\mathrm{Br}(\mathrm{B}^*_\mathrm{s} \to \mathrm{K}^+\tau^-\bar{\nu}_\tau)$	$(1.034 \to 1.039) \times 10^{-9}$	$(1.002 \to 1.003) \times 10^{-9}$
R^*_K	$0.640 \to 0.642$	$0.619 \to 0.620$
A^K_λ	$0.738 \to 0.745$	$0.800 \to 0.802$
A^K_{FB}	$-0.206 \to -0.202$	$-0.261 \to -0.256$

TABLE 4.6: The q^2 values (in GeV^2) of the zero crossing of forward-backward asymmetries of $B^*_{d,s} \to P\tau\bar{\nu}_\tau$ decay modes in the SM and in the presence of individual V_R, $S_{L,R}$ coefficients. The presence of additional V_L coefficient don't change the q^2 crossing values of the A^P_{FB}.

Model	$B^*_d \to D\tau\bar{\nu}_\tau$	$B^*_d \to \pi\tau\bar{\nu}_\tau$	$B^*_s \to D_s\tau\bar{\nu}_\tau$	$B^*_s \to K\tau\bar{\nu}_\tau$
SM	5.93	6.13	5.96	6.26
V_R Only (Best-fit)	7.98	6.87	8.02	7.02
(1σ)	$7.49 - 8.68$	$6.28 - 7.50$	$7.53 - 8.71$	$6.42 - 7.66$
S_L Only (Best-fit)	5.56	6.19	5.59	6.33
(1σ)	$5.44 - 5.71$	$6.14 - 6.23$	$5.47 - 5.74$	$6.28 - 6.37$
S_R Only (Best-fit)	4.38	5.13	4.4	5.22
(1σ)	$4.17 - 4.69$	$5.09 - 5.17$	$4.19 - 4.71$	$5.18 - 5.26$

Chapter 5

Summary and Conclusion

This chapter summarizes our research work presented in this thesis, which is mainly focused on the phenomenological study of the rare semileptonic B meson decays and baryonic Λ_b decays which are mainly mediated by $b \to (c, u)$ transitions. Chapter 1, starts with a brief introduction to the SM, its particle content, the SM effective Lagrangian, the CKM paradigm and CP violation. Then we shed light on the drawbacks of the SM. Explaining the importance of study of B decays, we present the theoretical tools to study the rare semileptonic B meson decays. We conclude this chapter with introducing the recent anomalies observed in beauty sector. Being inspired from the observed anomalies in the LNU parameters $R_D, R_{D^*}, R_{J/\psi}$ associated with the charged current transition $b \to cl\bar{\nu}_l$ and R_K, R_{K^*}, associated with flavour changing neutral current transitions ($b \to s\ell\ell$) we test the possibility of observing lepton non universality associated with semileptonic $b \to u\ell\bar{\nu}_\ell$ transition in chapter-2. In this analysis we consider the most general effective Lagrangian in a model independent way containing new Wilson coefficients. The allowed parameter space of these new couplings are obtained from the experimental values of $B_u^+ \to \ell^+\bar{\nu}_\ell$ decay process where $\ell = e, \mu, \tau$. The allowed parameter space for $b \to u\mu\bar{\nu}_\mu$ process is also obtained from the experimental value of branching fraction of $B^- \to \pi^0\mu^-\bar{\nu}_\mu$ decay process. Then we computed the branching ratio, forward backward asymmetry and LNU parameter within the SM and in presence of NP couplings as well. We also present plots showing the q^2 variation of these parameters in presence of individual new couplings. In this study we considered the processes $\bar{B}_s \to K^+\ell^-\bar{\nu}_\ell$, $\bar{B} \to \pi^+\ell^-\bar{\nu}_\ell$, $\bar{B}^- \to \eta\ell^-\bar{\nu}_\ell$ and $\bar{B}^- \to \eta'\ell^-\bar{\nu}_\ell$, where $\ell = \mu, \tau$. In case of $\bar{B}_s \to V^+\ell^-\bar{\nu}_\ell$, we consider V as K^{*+}, ρ^+.

Chapter-3 comprises of studying the sensitivity of various parameters to NP associated with $\Lambda_b \to (\Lambda_c, p)\ell\bar{\nu}_\ell$ decay process. In this analysis, we calculated the branching ratio, forward backward asymmetry, LNU parameter, lepton and hadron polarization

asymmetry and convexity parameter in presence of new physics. Starting from the most general effective Lagrangian containing new scalar, vector and tensor type of NP couplings we expressed all the relevant parameters in terms of the new Wilson coefficients. We constrain the parameter space of the new couplings V_L, V_R, S_L and S_R associated with $b \to c$ quark level transition from the measured values of R_{D^*}, $R_{J/\psi}$ and $\text{BR}(B_c^+ \to \tau^+\nu_\tau)$ observables, whereas the allowed parameter space for T_L coefficient is obtained from the measured value of R_{D^*}. Similarly we got the allowed values for these new couplings associated with $b \to u$ transition from the measured values of $\text{BR}(B_u \to \tau^+\nu_\tau)$, $\text{BR}(B \to \pi\tau\bar{\nu}_\tau)$ and R_π^ℓ observables. The values for T_L is obtained from $\text{BR}(B \to \pi\tau\bar{\nu}_\tau)$ experimental data. We calculated the parameters sensitive to NP in presence of the individual couplings. We also showed the q^2 variation of these considered parameters in the SM and also in the presence of NP.

In chapter-4, we performed a model independent analysis of vector meson B^* decaying to a pseudo scalar meson ($\bar{B}^*_{d,(s)} \to P\ell\bar{\nu}_\ell$), where $P = D, \pi$ (D_s, K). We considered the most general effective Lagrangian containing additional NP couplings to the SM, assuming them to be complex in nature. We constrained the parameter space of the new couplings by performing the χ^2 fitting of $R_{D^*}, R_{J/\psi}$ and upper limit of $\text{BR}(B_c^+ \to \tau^+\nu_\tau)$ for $b \to c\tau\bar{\nu}_\tau$ transition. For $b \to u\tau\bar{\nu}_\tau$ the allowed parameter space is obtained from the χ^2 fitting of $R_\pi^\ell, \text{BR}(B_u \to \tau\nu_\tau)$ and upper limit on $\text{BR}(B \to \pi\tau\bar{\nu}_\tau)$ experimental data. We calculated the branching ratio, forward backward asymmetry, LNU parameter, lepton spin asymmetry for the best-fit values and one sigma allowed ranges of the new couplings. We also presented the plots showing the q^2 variation of all the parameters sensitive for the SM, as well as in the presence of individual new couplings for their best fit value and 1σ allowed regions. Thus, we can see how different couplings affect the parameters and in presence of which parameter we are getting maximum deviation from the SM. This will help us to probe NP in case of B^* semileptonic decays.

To conclude, in this thesis we have studied in detail some of the semiletonic decay modes of pesudoscalar B and vector B^*mesons as well as Λ baryon, mediated by $b \to (c, u)\ell\nu_\ell$ transitions. Adopting the model independent approach, we considered the effect of new physics physics as additional contributions to the SM effective Hamiltonian and constrained the new physics couplings from the existing data. We found that several observables show significant deviations from their SM predictions, the observation of which definitely shed light in our understanding of the nature of New Physics beyond the Standard Model.

Appendix A

Helicity-dependent differential decay rates

The expressions for the helicity-dependent differential decay rates required to analyze the longitudinal hadron and lepton polarization asymmetries for Λ_b decays are given by

[66]

$$
\begin{aligned}
\frac{\mathrm{d}\Gamma^{\lambda_2=1/2}}{\mathrm{d}q^2} &= \frac{m_l^2}{q^2}\Big[\frac{4}{3}\big(H^2_{\frac{1}{2},+}+H^2_{\frac{1}{2},0}+3H^2_{\frac{1}{2},t}\big)+\frac{2}{3}\big(H^{T^2}_{\frac{1}{2},+,-}+H^{T^2}_{\frac{1}{2},0,t}+H^{T^2}_{\frac{1}{2},+,0}+H^{T^2}_{\frac{1}{2},+,t}\\
&\quad +2H^T_{\frac{1}{2},+,-}H^T_{\frac{1}{2},0,t}+2H^T_{\frac{1}{2},+,0}H^T_{\frac{1}{2},+,t}\big)\Big]+\frac{8}{3}\big(H^2_{\frac{1}{2},0}+H^2_{\frac{1}{2},+}\big)+4H^{SP^2}_{\frac{1}{2},0}\\
&\quad +\frac{1}{3}\big(H^{T^2}_{\frac{1}{2},+,-}+H^{T^2}_{\frac{1}{2},0,t}+H^{T^2}_{\frac{1}{2},+,0}+H^{T^2}_{\frac{1}{2},+,t}+2H^T_{\frac{1}{2},+,-}H^T_{\frac{1}{2},0,t}+2H^T_{\frac{1}{2},+,0}H^T_{\frac{1}{2},+,t}\big)\\
&\quad +\frac{4m_l}{\sqrt{q^2}}\Big[\big(H_{\frac{1}{2},0}H^T_{\frac{1}{2},+,-}+H_{\frac{1}{2},0}H^T_{\frac{1}{2},0,t}+H_{\frac{1}{2},+}H^T_{\frac{1}{2},+,0}+H_{\frac{1}{2},+}H^T_{\frac{1}{2},+,t}\big)\\
&\quad +2\big(H_{\frac{1}{2},t}H^{SP}_{\frac{1}{2},0}\big)\Big],\\
\frac{\mathrm{d}\Gamma^{\lambda_2=-1/2}}{\mathrm{d}q^2} &= \frac{m_l^2}{q^2}\Big[\frac{4}{3}\big(H^2_{-\frac{1}{2},-}+H^2_{-\frac{1}{2},0}+3H^2_{-\frac{1}{2},t}\big)+\frac{2}{3}\big(H^{T^2}_{-\frac{1}{2},+,-}+H^{T^2}_{-\frac{1}{2},0,t}+H^{T^2}_{-\frac{1}{2},0,-}+H^{T^2}_{-\frac{1}{2},-,t}\\
&\quad +2H^T_{-\frac{1}{2},+,-}H^T_{-\frac{1}{2},0,t}+2H^T_{-\frac{1}{2},0,-}H^T_{-\frac{1}{2},-,t}\big)\Big]+\frac{8}{3}\big(H^2_{-\frac{1}{2},-}+H^2_{-\frac{1}{2},0}\big)+4H^{SP^2}_{-\frac{1}{2},0}\\
&\quad +\frac{1}{3}\big(H^{T^2}_{-\frac{1}{2},+,-}+H^{T^2}_{-\frac{1}{2},0,t}+H^{T^2}_{-\frac{1}{2},0,-}+H^{T^2}_{-\frac{1}{2},-,t}+2H^T_{-\frac{1}{2},+,-}H^T_{-\frac{1}{2},0,t}+2H^T_{-\frac{1}{2},0,-}H^T_{-\frac{1}{2},-,t}\big)\\
&\quad +\frac{4m_l}{\sqrt{q^2}}\Big[\big(H_{-\frac{1}{2},0}H^T_{-\frac{1}{2},+,-}+H_{-\frac{1}{2},0}H^T_{-\frac{1}{2},0,t}+H_{-\frac{1}{2},-}H^T_{-\frac{1}{2},0,-}+H_{-\frac{1}{2},-}H^T_{-\frac{1}{2},-,t}\big)\\
&\quad +2\big(H_{-\frac{1}{2},t}H^{SP}_{-\frac{1}{2},0}\big)\Big],\\
\frac{\mathrm{d}\Gamma^{\lambda_\tau=1/2}}{\mathrm{d}q^2} &= \frac{m_l^2}{q^2}\Big[\frac{4}{3}\big(H^2_{\frac{1}{2},+}+H^2_{\frac{1}{2},0}+H^2_{-\frac{1}{2},-}+H^2_{-\frac{1}{2},0}\big)+4\big(H^2_{\frac{1}{2},t}+H^2_{-\frac{1}{2},t}\big)\Big]+4\big(H^{SP^2}_{\frac{1}{2},0}+H^{SP^2}_{-\frac{1}{2},0}\big)\\
&\quad +\frac{1}{3}\Big[H^{T^2}_{\frac{1}{2},+,-}+H^{T^2}_{\frac{1}{2},0,t}+H^{T^2}_{\frac{1}{2},+,0}+H^{T^2}_{\frac{1}{2},+,t}+H^{T^2}_{-\frac{1}{2},+,-}+H^{T^2}_{-\frac{1}{2},0,t}+H^{T^2}_{-\frac{1}{2},0,-}+H^{T^2}_{-\frac{1}{2},-,t}\\
&\quad +2\big(H^T_{\frac{1}{2},+,-}H^T_{\frac{1}{2},0,t}+H^T_{\frac{1}{2},+,0}H^T_{\frac{1}{2},+,t}+H^T_{-\frac{1}{2},+,-}H^T_{-\frac{1}{2},0,t}+H^T_{-\frac{1}{2},0,-}H^T_{-\frac{1}{2},-,t}\big)\Big]\\
&\quad +\frac{4m_l}{3\sqrt{q^2}}\Big[6\big(H_{\frac{1}{2},t}H^{SP}_{\frac{1}{2},0}+H_{-\frac{1}{2},t}H^{SP}_{-\frac{1}{2},0}\big)+\big(H_{\frac{1}{2},0}H^T_{\frac{1}{2},+,-}+H_{\frac{1}{2},0}H^T_{\frac{1}{2},0,t}\\
&\quad +H_{\frac{1}{2},+}H^T_{\frac{1}{2},+,0}+H_{\frac{1}{2},+}H^T_{\frac{1}{2},+,t}+H_{-\frac{1}{2},0}H^T_{-\frac{1}{2},+,-}+H_{-\frac{1}{2},0}H^T_{-\frac{1}{2},0,t}+H_{-\frac{1}{2},-}H^T_{-\frac{1}{2},0,-}\\
&\quad +H_{-\frac{1}{2},-}H^T_{-\frac{1}{2},-,t}\big)\Big],
\end{aligned}
$$

$$
\begin{aligned}
\frac{\mathrm{d}\Gamma^{\lambda_\tau=-1/2}}{\mathrm{d}q^2} &= \frac{8}{3}\big(H^2_{\frac{1}{2},+}+H^2_{\frac{1}{2},0}+H^2_{-\frac{1}{2},-}+H^2_{-\frac{1}{2},0}\big)+\frac{2m_l^2}{3q^2}\Big[H^{T^2}_{\frac{1}{2},+,-}+H^{T^2}_{\frac{1}{2},0,t}+H^{T^2}_{\frac{1}{2},+,0}+H^{T^2}_{\frac{1}{2},+,t}\\
&\quad +H^{T^2}_{-\frac{1}{2},+,-}+H^{T^2}_{-\frac{1}{2},0,t}+H^{T^2}_{-\frac{1}{2},0,-}+H^{T^2}_{-\frac{1}{2},-,t}+2\big(H^T_{\frac{1}{2},+,-}H^T_{\frac{1}{2},0,t}+H^T_{\frac{1}{2},+,0}H^T_{\frac{1}{2},+,t}\\
&\quad +H^T_{-\frac{1}{2},+,-}H^T_{-\frac{1}{2},0,t}+H^T_{-\frac{1}{2},0,-}H^T_{-\frac{1}{2},-,t}\big)\Big]\\
&\quad +\frac{8m_l}{3\sqrt{q^2}}\big(H_{\frac{1}{2},0}H^T_{\frac{1}{2},+,-}+H_{\frac{1}{2},0}H^T_{\frac{1}{2},0,t}+H_{\frac{1}{2},+}H^T_{\frac{1}{2},+,0}+H_{\frac{1}{2},+}H^T_{\frac{1}{2},+,t}\\
&\quad +H_{-\frac{1}{2},0}H^T_{-\frac{1}{2},+,-}+H_{-\frac{1}{2},0}H^T_{-\frac{1}{2},0,t}+H_{-\frac{1}{2},-}H^T_{-\frac{1}{2},0,-}+H_{-\frac{1}{2},-}H^T_{-\frac{1}{2},-,t}\big). \qquad \text{(A.1)}
\end{aligned}
$$

A.1 Form factors relations

The relation betwen various form factors are given as [79, 80]

$$
\begin{aligned}
f_0 &= f_1 + \frac{q^2}{M_{\Lambda_b} - m_\Lambda} f_3 \,, \qquad f_+ = f_1 - \frac{q^2}{M_{\Lambda_b} + m_\Lambda} f_2 \,, \qquad f_\perp = f_1 - (M_{\Lambda_b} + m_\Lambda) f_2 \,, \\
g_0 &= g_1 - \frac{q^2}{M_{\Lambda_b} + m_\Lambda} g_3 \,, \qquad g_+ = g_1 + \frac{q^2}{M_{\Lambda_b} - m_\Lambda} g_2 \,, \qquad g_\perp = g_1 + (M_{\Lambda_b} - m_\Lambda) g_2 \,, \\
h_+ &= f_2^T - \frac{M_{\Lambda_b} + m_\Lambda}{q^2} f_1^T \,, \qquad h_\perp = f_2^T - \frac{1}{M_{\Lambda_b} + m_\Lambda} f_1^T \,, \\
\tilde{h}_+ &= g_2^T + \frac{M_{\Lambda_b} - m_\Lambda}{q^2} g_1^T \,, \qquad \tilde{h}_\perp = g_2^T + \frac{1}{M_{\Lambda_b} - m_\Lambda} g_1^T \,,
\end{aligned}
\tag{A.2}
$$

with

$$
\begin{aligned}
f_2^T &= f_T - f_T^S q^2, \qquad f_1^T = \left(f_T^V + f_T^S (M_{B_1} - M_{B_2})\right) q^2, \qquad f_1^T = -\frac{q^2}{M_{B_1} - M_{B_2}} f_3^T, \\
g_2^T &= g_T - g_T^S q^2, \qquad g_1^T = \left(g_T^V + g_T^S (M_{B_1} + M_{B_2})\right) q^2, \qquad g_1^T = \frac{q^2}{M_{B_1} + M_{B_2}} g_3^T
\end{aligned}
\tag{A.3}
$$

Bibliography

[1] S. L. Glashow, "*Partial Symmetries of Weak Interactions*," Nucl. Phys. **22** (1961) 579–588.

[2] S. Weinberg, "*A Model of Leptons*," Phys. Rev. Lett. **19** (1967) 1264–1266.

[3] A. Salam, "*Weak and Electromagnetic Interactions*," Conf. Proc. **C680519** (1968) 367–377.

[4] F. Englert and R. Brout, "*Broken Symmetry and the Mass of Gauge Vector Mesons*," Phys. Rev. Lett. **13** (1964) 321–323.

[5] P. W. Higgs, "*Broken Symmetries and the Masses of Gauge Bosons*," Phys. Rev. Lett. **13** (1964) 508–509.

[6] G. S. Guralnik, C. R. Hagen, and T. W. B. Kibble, "*Global Conservation Laws and Massless Particles*," Phys. Rev. Lett. **13** (1964) 585–587.

[7] Y. Grossman, "*Introduction to flavor physics*," in *Flavianet School on Flavour Physics Karlsruhe, Germany, September 7-18, 2009*, pp. 111–144. 2014. arXiv:1006.3534.

[8] N. Cabibbo, "*Unitary Symmetry and Leptonic Decays*," Phys. Rev. Lett. **10** (1963) 531–533.

[9] M. Kobayashi and T. Maskawa, "*CP Violation in the Renormalizable Theory of Weak Interaction*," Prog. Theor. Phys. **49** (1973) 652–657.

[10] L.-L. Chau and W.-Y. Keung, "*Comments on the Parametrization of the Kobayashi-Maskawa Matrix*," Phys. Rev. Lett. **53** (1984) 1802.

[11] L. Wolfenstein, "*Parametrization of the Kobayashi-Maskawa Matrix*," Phys. Rev. Lett. **51** (1983) 1945.

[12] C. Jarlskog, "*Commutator of the Quark Mass Matrices in the Standard Electroweak Model and a Measure of Maximal CP Violation*," Phys. Rev. Lett. **55** (1985) 1039.

[13] A. D. Sakharov, "*Violation of CP Invariance, C asymmetry, and baryon asymmetry of the universe*," Pisma Zh. Eksp. Teor. Fiz. **5** (1967) 32–35. [JETP Lett.5,24(1967); Sov. Phys. Usp.34,no.5,392(1991); Usp. Fiz. Nauk161,no.5,61(1991)].

[14] J. H. Christenson, J. W. Cronin, V. L. Fitch, and R. Turlay, "*Evidence for the* 2π *Decay of the* K_2^0 *Meson*," Phys. Rev. Lett. **13** (1964) 138–140.

[15] **Particle Data Group**, M. Tanabashi *et al.*, "*Review of Particle Physics*," Phys. Rev. **D98** (2018) no. 3, 030001.

[16] **LHCb**, R. Aaij *et al.*, "*Search for lepton-universality violation in* $B^+ \to K^+\ell^+\ell^-$ *decays*," Phys. Rev. Lett. **122** (2019) no. 19, 191801, arXiv:1903.09252.

[17] **LHCb**, R. Aaij *et al.*, "*Test of lepton universality with* $B^0 \to K^{*0}\ell^+\ell^-$ *decays*," JHEP **08** (2017) 055, arXiv:1705.05802.

[18] **HFLAV**, Y. S. Amhis *et al.*, "*Averages of b-hadron, c-hadron, and* τ*-lepton properties as of 2018*," arXiv:1909.12524.

[19] **LHCb**, R. Aaij *et al.*, "*Measurement of the ratio of branching fractions* $\mathcal{B}(B_c^+ \to J/\psi\tau^+\nu_\tau)/\mathcal{B}(B_c^+ \to J/\psi\mu^+\nu_\mu)$," Phys. Rev. Lett. **120** (2018) no. 12, 121801, arXiv:1711.05623.

[20] C. Bobeth, G. Hiller, and G. Piranishvili, "*Angular distributions of* $\bar{B} \to \bar{K}\ell^+\ell^-$ *decays*," JHEP **12** (2007) 040, arXiv:0709.4174.

[21] B. Capdevila, A. Crivellin, S. Descotes-Genon, J. Matias, and J. Virto, "*Patterns of New Physics in* $b \to s\ell^+\ell^-$ *transitions in the light of recent data*," JHEP **01** (2018) 093, arXiv:1704.05340.

[22] S. Fajfer, J. F. Kamenik, and I. Nisandzic, "*On the* $B \to D^*\tau\bar{\nu}_\tau$ *Sensitivity to New Physics*," Phys. Rev. **D85** (2012) 094025, arXiv:1203.2654.

[23] D. Bigi, P. Gambino, and S. Schacht, "$R(D^*)$, $|V_{cb}|$, *and the Heavy Quark Symmetry relations between form factors*," JHEP **11** (2017) 061, arXiv:1707.09509.

[24] R. Dutta and A. Bhol, "$B_c \to (J/\psi, \eta_c)\tau\nu$ *semileptonic decays within the standard model and beyond*," Phys. Rev. **D96** (2017) no. 7, 076001, arXiv:1701.08598.

[25] T. Bhattacharya, V. Cirigliano, S. D. Cohen, A. Filipuzzi, M. Gonzalez-Alonso, M. L. Graesser, R. Gupta, and H.-W. Lin, "*Probing Novel Scalar and Tensor Interactions from (Ultra)Cold Neutrons to the LHC*," Phys. Rev. D **85** (2012) 054512, arXiv:1110.6448.

[26] P. Biancofiore, P. Colangelo, and F. De Fazio, "*On the anomalous enhancement observed in $B \to D^{(*)}\tau\bar{\nu}_\tau$ decays*," Phys. Rev. D **87** (2013) no. 7, 074010, arXiv:1302.1042.

[27] **Particle Data Group**, C. Patrignani *et al.*, "*Review of Particle Physics*," Chin. Phys. C **40** (2016) no. 10, 100001.

[28] S. Aoki *et al.*, "*Review of Lattice Results Concerning Low-Energy Particle Physics*," Eur. Phys. J. C **74** (2014) 2890, arXiv:1310.8555.

[29] M. Beneke and T. Feldmann, "*Symmetry breaking corrections to heavy to light B meson form-factors at large recoil*," Nucl. Phys. B **592** (2001) 3–34, arXiv:hep-ph/0008255.

[30] Y. Sakaki, M. Tanaka, A. Tayduganov, and R. Watanabe, "*Testing leptoquark models in $\bar{B} \to D^{(*)}\tau\bar{\nu}$*," Phys. Rev. D **88** (2013) no. 9, 094012, arXiv:1309.0301.

[31] W.-F. Wang and Z.-J. Xiao, "*The semileptonic decays $B/B_s \to (\pi, K)(\ell^+\ell^-, \ell\nu, \nu\bar{\nu})$ in the perturbative QCD approach beyond the leading-order*," Phys. Rev. D **86** (2012) 114025, arXiv:1207.0265.

[32] U.-G. Meißner and W. Wang, "$\mathbf{B_s \to K^{(*)}\ell\bar{\nu}}$*, Angular Analysis, S-wave Contributions and* $|\mathbf{V_{ub}}|$," JHEP **01** (2014) 107, arXiv:1311.5420.

[33] Y.-Y. Keum, H.-n. Li, and A. Sanda, "*Fat penguins and imaginary penguins in perturbative QCD*," Phys. Lett. B **504** (2001) 6–14, arXiv:hep-ph/0004004.

[34] H.-n. Li, Y.-L. Shen, and Y.-M. Wang, "*Next-to-leading-order corrections to $B \to \pi$ form factors in k_T factorization*," Phys. Rev. D **85** (2012) 074004, arXiv:1201.5066.

[35] A. Khodjamirian, T. Mannel, N. Offen, and Y.-M. Wang, "*$B \to \pi\ell\nu_l$ Width and $|V_{ub}|$ from QCD Light-Cone Sum Rules*," Phys. Rev. D **83** (2011) 094031, arXiv:1103.2655.

[36] C. Boyd, B. Grinstein, and R. F. Lebed, "*Model independent extraction of $|V_{cb}|$ using dispersion relations*," Phys. Lett. B **353** (1995) 306–312, arXiv:hep-ph/9504235.

[37] J. L. Rosner, "*Quark Content of Neutral Mesons*," Phys. Rev. D **27** (1983) 1101.

[38] A. Bramon, R. Escribano, and M. Scadron, "*The eta - eta-prime mixing angle revisited*," Eur. Phys. J. C **7** (1999) 271–278, arXiv:hep-ph/9711229.

[39] T. Feldmann, P. Kroll, and B. Stech, "*Mixing and decay constants of pseudoscalar mesons*," Phys. Rev. D **58** (1998) 114006, arXiv:hep-ph/9802409.

[40] T. Feldmann, "*Quark structure of pseudoscalar mesons*," Int. J. Mod. Phys. A **15** (2000) 159–207, arXiv:hep-ph/9907491.

[41] T. Feldmann, P. Kroll, and B. Stech, "*Mixing and decay constants of pseudoscalar mesons: The Sequel*," Phys. Lett. B **449** (1999) 339–346, arXiv:hep-ph/9812269.

[42] J. Flynn, T. Izubuchi, T. Kawanai, C. Lehner, A. Soni, R. Van de Water, and O. Witzel, "$B \to \pi \ell \nu$ *and* $B_s \to K \ell \nu$ *form factors and* $|V_{ub}|$ *from 2+1-flavor lattice QCD with domain-wall light quarks and relativistic heavy quarks*," Phys. Rev. D **91** (2015) no. 7, 074510, arXiv:1501.05373.

[43] F. U. Bernlochner, "$B \to \pi \tau \overline{\nu}_\tau$ *decay in the context of type II 2HDM*," Phys. Rev. D **92** (2015) no. 11, 115019, arXiv:1509.06938.

[44] C. Kim, S. Oh, and C. Yu, "$B \to \eta' l \nu$ *decays and the flavor-singlet form factors*," Phys. Lett. B **590** (2004) 223–232, arXiv:hep-ph/0305032.

[45] T. Aliev, I. Kanik, and A. Ozpineci, "*Semileptonic* $B \to \eta l \nu$ *decay in light cone QCD*," Phys. Rev. D **67** (2003) 094009, arXiv:hep-ph/0210403.

[46] C. Kim and Y.-D. Yang, "*Study of semileptonic decays* $B^+ \to \eta^{(\prime)} l^+ \nu$," Phys. Rev. D **65** (2002) 017501, arXiv:hep-ph/0107226.

[47] R. Dutta and A. Bhol, "$b \to (c, , u), \tau \nu$ *leptonic and semileptonic decays within an effective field theory approach*," Phys. Rev. D **96** (2017) no. 3, 036012, arXiv:1611.00231.

[48] P. Ball and R. Zwicky, "$B_{d,s} \to \rho, \omega, K^*, \phi$ *decay form-factors from light-cone sum rules revisited*," Phys. Rev. **D71** (2005) 014029, arXiv:hep-ph/0412079.

[49] R. Dutta, A. Bhol, and A. K. Giri, "*Effective theory approach to new physics in* $b \to u$ *and* $b \to c$ *leptonic and semileptonic decays*," Phys. Rev. **D88** (2013) no. 11, 114023, arXiv:1307.6653.

[50] T. Feldmann, B. Mller, and D. van Dyk, "*Analyzing* $b \to u$ *transitions in semileptonic* $\bar{B}_s \to K^{*+}(\to K\pi)\ell^- \bar{\nu}_\ell$ *decays*," Phys. Rev. **D92** (2015) no. 3, 034013, arXiv:1503.09063.

[51] **LHCb**, R. Aaij *et al.*, "*Measurement of b-hadron production fractions in* 7 TeV *pp collisions*," Phys. Rev. **D85** (2012) 032008, arXiv:1111.2357.

[52] **LHCb**, R. Aaij *et al.*, "*Study of the kinematic dependences of* Λ_b^0 *production in pp collisions and a measurement of the* $\Lambda_b^0 \to \Lambda_c^+ \pi^-$ *branching fraction*," JHEP **08** (2014) 143, arXiv:1405.6842.

[53] **LHCb**, R. Aaij *et al.*, "*Determination of the quark coupling strength $|V_{ub}|$ using baryonic decays*," Nature Phys. **11** (2015) 743–747, arXiv:1504.01568.

[54] M. Fiore, "*New results on semileptonic b decays from LHCb*," in *Proceedings, Meeting of the APS Division of Particles and Fields (DPF 2015): Ann Arbor, Michigan, USA, 4-8 Aug 2015*. 2015. arXiv:1511.00105.

[55] Y. K. Hsiao and C. Q. Geng, "*Determinations of $|V_{cb}|$ and $|V_{ub}|$ from baryonic Λ_b decays*," Eur. Phys. J. **C77** (2017) no. 10, 714, arXiv:1705.00948.

[56] R. M. Woloshyn, "*Semileptonic decay of the Λ_b baryon*," PoS **Hadron2013** (2013) 203.

[57] W. Wu, "*Semi-leptonic Decay of Lambda-b in the Standard Model and with New Physics*," Master's thesis, Mississippi U., 2015. http://search.proquest.com/docview/1697862095.

[58] S. Shivashankara, W. Wu, and A. Datta, "*$\Lambda_b \to \Lambda_c \tau \bar{\nu}_\tau$ Decay in the Standard Model and with New Physics*," Phys. Rev. **D91** (2015) no. 11, 115003, arXiv:1502.07230.

[59] T. Gutsche, M. A. Ivanov, J. G. Korner, V. E. Lyubovitskij, and P. Santorelli, "*Semileptonic decays $\Lambda_c^+ \to \Lambda \ell^+ \nu_\ell$ ($\ell = e, \mu$) in the covariant quark model and comparison with the new absolute branching fraction measurements of Belle and BESIII*," Phys. Rev. **D93** (2016) no. 3, 034008, arXiv:1512.02168.

[60] T. Gutsche, M. A. Ivanov, J. G. Krner, V. E. Lyubovitskij, P. Santorelli, and N. Habyl, "*Semileptonic decay $\Lambda_b \to \Lambda_c + \tau^- + \bar{\nu_\tau}$ in the covariant confined quark model*," Phys. Rev. **D91** (2015) no. 7, 074001, arXiv:1502.04864. [Erratum: Phys. Rev.D91,no.11,119907(2015)].

[61] W. Detmold, C. Lehner, and S. Meinel, "*$\Lambda_b \to p \ell^- \bar{\nu}_\ell$ and $\Lambda_b \to \Lambda_c \ell^- \bar{\nu}_\ell$ form factors from lattice QCD with relativistic heavy quarks*," Phys. Rev. **D92** (2015) no. 3, 034503, arXiv:1503.01421.

[62] R. Dutta, "*$\Lambda_b \to (\Lambda_c,\, p)\, \tau\, \nu$ decays within standard model and beyond*," Phys. Rev. **D93** (2016) no. 5, 054003, arXiv:1512.04034.

[63] M. Pervin, W. Roberts, and S. Capstick, "*Semileptonic decays of heavy lambda baryons in a quark model*," Phys. Rev. **C72** (2005) 035201, arXiv:nucl-th/0503030.

[64] R. N. Faustov and V. O. Galkin, "*Semileptonic decays of Λ_c baryons in the relativistic quark model*," Eur. Phys. J. **C76** (2016) no. 11, 628, arXiv:1610.00957.

[65] A. Datta, S. Kamali, S. Meinel, and A. Rashed, "*Phenomenology of $\Lambda_b \to \Lambda_c \tau \overline{\nu}_\tau$ using lattice QCD calculations*," JHEP **08** (2017) 131, arXiv:1702.02243.

[66] X.-Q. Li, Y.-D. Yang, and X. Zhang, "*$\Lambda_b \to \Lambda_c \tau \overline{\nu}_\tau$ decay in scalar and vector leptoquark scenarios*," JHEP **02** (2017) 068, arXiv:1611.01635.

[67] E. Di Salvo, F. Fontanelli, and Z. J. Ajaltouni, "*Detailed Study of the Decay $\Lambda_b \to \Lambda_c \tau \bar{\nu}_\tau$*," arXiv:1804.05592.

[68] F. U. Bernlochner, Z. Ligeti, D. J. Robinson, and W. L. Sutcliffe, "*New predictions for $\Lambda_b \to \Lambda_c$ semileptonic decays and tests of heavy quark symmetry*," arXiv:1808.09464.

[69] V. Cirigliano, J. Jenkins, and M. Gonzalez-Alonso, "*Semileptonic decays of light quarks beyond the Standard Model*," Nucl. Phys. **B830** (2010) 95–115, arXiv:0908.1754.

[70] **TWQCD**, T.-W. Chiu, T.-H. Hsieh, C.-H. Huang, and K. Ogawa, "*Beauty mesons in lattice QCD with exact chiral symmetry*," Phys. Lett. **B651** (2007) 171–176, arXiv:0705.2797.

[71] A. G. Akeroyd and C.-H. Chen, "*Constraint on the branching ratio of $B_c \to \tau \bar{\nu}$ from LEP1 and consequences for $R(D^{(*)})$ anomaly*," Phys. Rev. **D96** (2017) no. 7, 075011, arXiv:1708.04072.

[72] M. Tanaka and R. Watanabe, "*New physics in the weak interaction of $\bar{B} \to D^{(*)} \tau \bar{\nu}$*," Phys. Rev. **D87** (2013) no. 3, 034028, arXiv:1212.1878.

[73] C. Bourrely, I. Caprini, and L. Lellouch, "*Model-independent description of $B \to \pi l \nu$ decays and a determination of $|V_{ub}|$*," Phys. Rev. **D79** (2009) 013008, arXiv:0807.2722. [Erratum: Phys. Rev.D82,099902(2010)].

[74] C. G. Boyd, B. Grinstein, and R. F. Lebed, "*Constraints on form-factors for exclusive semileptonic heavy to light meson decays*," Phys. Rev. Lett. **74** (1995) 4603–4606, arXiv:hep-ph/9412324.

[75] S. Fajfer, J. F. Kamenik, I. Nisandzic, and J. Zupan, "*Implications of Lepton Flavor Universality Violations in B Decays*," Phys. Rev. Lett. **109** (2012) 161801, arXiv:1206.1872.

[76] M. A. Ivanov, J. G. Körner, and C.-T. Tran, "*Probing new physics in $\bar{B}^0 \to D^{(*)} \tau^- \bar{\nu}_\tau$ using the longitudinal, transverse, and normal polarization components of the tau lepton*," Phys. Rev. D **95** (2017) no. 3, 036021, arXiv:1701.02937.

[77] C.-T. Tran, M. A. Ivanov, J. G. Körner, and P. Santorelli, "*Implications of new physics in the decays $B_c \to (J/\psi, \eta_c)\tau\nu$*," Phys. Rev. D **97** (2018) no. 5, 054014, arXiv:1801.06927.

[78] M. A. Ivanov, J. G. Körner, and C.-T. Tran, "*Analyzing new physics in the decays $\bar{B}^0 \to D^{(*)}\tau^-\bar{\nu}_\tau$ with form factors obtained from the covariant quark model*," Phys. Rev. D **94** (2016) no. 9, 094028, arXiv:1607.02932.

[79] T. Feldmann and M. W. Y. Yip, "*Form Factors for $\Lambda_b \to \Lambda$ Transitions in SCET*," Phys. Rev. **D85** (2012) 014035, arXiv:1111.1844. [Erratum: Phys. Rev.D86,079901(2012)].

[80] C.-H. Chen and C. Q. Geng, "*Baryonic rare decays of Lambda(b) —¿ Lambda lepton+ lepton-*," Phys. Rev. **D64** (2001) 074001, arXiv:hep-ph/0106193.

[81] B. Grinstein and J. Martin Camalich, "*Weak Decays of Excited B Mesons*," Phys. Rev. Lett. **116** (2016) no. 14, 141801, arXiv:1509.05049.

[82] S. Sahoo and R. Mohanta, "*Study of the rare decays $B^*_{s,d} \to \mu^+\mu^-$*," J. Phys. G **44** (2017) no. 3, 035001, arXiv:1612.02543.

[83] D. Kumar, J. Saini, S. Gangal, and S. B. Das, "*Probing new physics through $B^*_s \to \mu^+\mu^-$ decay*," Phys. Rev. D **97** (2018) no. 3, 035007, arXiv:1711.01989.

[84] S. Kumbhakar and J. Saini, "*New physics effects in purely leptonic B^*_s decays*," Eur. Phys. J. C **79** (2019) no. 5, 394, arXiv:1807.04055.

[85] Q. Chang, J. Zhu, X.-L. Wang, J.-F. Sun, and Y.-L. Yang, "*Study of semileptonic $B^? \to Pl\nu_l$ decays*," Nucl. Phys. **B909** (2016) 921–933, arXiv:1606.09071.

[86] Q. Chang, J. Zhu, N. Wang, and R.-M. Wang, "*Probing the effects of new physics in $\bar{B}^* \to P\ell\bar{\nu}_\ell$ decays*," Adv. High Energy Phys. **2018** (2018) 7231354, arXiv:1808.02188.

[87] J. Zhang, Y. Zhang, Q. Zeng, and R. Sun, "*New physics effects of the vector leptoquark on $\bar{B}^* \to P\tau\bar{\nu}_\tau$ decays*," Eur. Phys. J. C **79** (2019) no. 2, 164. [Erratum: Eur.Phys.J.C 79, 423 (2019)].

[88] M. Wirbel, B. Stech, and M. Bauer, "*Exclusive Semileptonic Decays of Heavy Mesons*," Z. Phys. **C29** (1985) 637.

[89] M. Bauer, B. Stech, and M. Wirbel, "*Exclusive Nonleptonic Decays of D, D(s), and B Mesons*," Z. Phys. C **34** (1987) 103.

[90] A. Ray, S. Sahoo, and R. Mohanta, "*Probing new physics in semileptonic Λ_b decays*," Phys. Rev. D **99** (2019) no. 1, 015015, arXiv:1812.08314.

List of Publications

Thesis Publications

1. ***"Model independent investigation of rare semileptonic*** $b \to ul\bar{\nu}_l$ ***decay processes"***, **S. Sahoo**, A. Ray, and R. Mohanta, Phys. Rev. D **96**, 115017 (2017), [arXiv:1711.1024].

2. ***"Probing new physics in semileptonic*** Λ_b ***decays"***, **A. Ray**, S. Sahoo , and R. Mohanta, Phys. Rev. D **99**, 015015 (2019), [arXiv:1812.08314].

3. ***"Model independent analysis of*** $B^* \to P\ell\bar{\nu}_\ell$ ***decay processes"***, **A. Ray**, S. Sahoo, and R. Mohanta, Eur. Phys. J. C **79**, 670 (2019), [arXiv:1907.13586].

Other Publications

1. ***"Exploring the role of new physics in*** $b \to u\tau\bar{\nu}_\tau$ ***decays "***, A. Bhatta, **A. Ray**, and R. Mohanta, arXiv: 2009.03175 (Under review).

Conference Proceedings

1. ***"Probing new physics in semileptonic*** Λ_b ***decays"***, **A. Ray**,S. Sahoo, and R. Mohanta, Springer Proc. Phys. **234**, 483-487(2019).

2. ***"Effect of New Physics in*** $\bar{B} \to \rho\ell\bar{\nu}_\ell$ ***Decay Process"***, **A. Ray**, A. Bhatta, and R. Mohanta, Springer Proc. Phys. **248**, 431-437(2020).

Impact of new Physics on b-> (u,c) l \nu_l transitions

by Atasi Ray

Impact of new Physics on b->(u,c) l \nu_l transitions

ORIGINALITY REPORT

43%	22%	41%	2%
SIMILARITY INDEX	INTERNET SOURCES	PUBLICATIONS	STUDENT PAPERS

PRIMARY SOURCES

1	Atasi Ray, Suchismita Sahoo, Rukmani Mohanta. " Probing new physics in semileptonic decays ", Physical Review D, 2019 Publication	15%
2	Suchismita Sahoo, Atasi Ray, Rukmani Mohanta. " Model-independent investigation of rare semileptonic decay processes ", Physical Review D, 2017 Publication	12%
3	export.arxiv.org Internet Source	8%
4	link.springer.com Internet Source	2%
5	iopscience.iop.org Internet Source	1%
6	arxiv.org Internet Source	<1%
7	"Workshop on Frontiers in High Energy Physics 2019", Springer Science and Business Media	<1%

This is to certify that the thesis entitled "Impact of New Physics on $b \to (c,u)\ell\bar{\nu}_\ell$ transitions" has been screened by the Turnitin software at the library of University of Hyderabad. The software shows 43% similarity index, out of which 27% has come from the candidate's own research article related to this thesis and 8% (export.arxiv.org) came from her research articles in the arXiv (1711.10924, 1812.08314, 1907.13586). The major part of remaining 8% might have come from her other articles and the use of some scientific terms and equations, which have not been detected by the software. Therefore, this thesis is free from plagiarism.

Rukmani Mohanta

Prof. Rukmani Mohanta
(Thesis Supervisor)

Dr. Rukmani Mohanta
Professor
School of Physics
UNIVERSITY OF HYDERABAD
Central University P.O.
Hyderabad-500 046.